Discipline of Engineering and Energy

Operation and Control Strategy of Coupled Microgrid Clusters

S.M.Ferdous

This thesis is submitted in fulfilment of the requirements
for the Degree of
Doctor of Philosophy
at
Murdoch University
Perth, Australia

June 2021

Declaration

I declare that this thesis is my own account of my research and contains as its main content work, which has not previously been submitted for a degree at any tertiary education institution and all the relevant published works are duely cited.

S M Ferdous

S.M.Ferdous
June 2021

Dedication

the philosophers and the mentors of my life

MY PARENTS

Acknowledgement

I want to express my deepest gratitude to my principal supervisor Dr GM Shafiullah, for his kind advice, invaluable guidance, encouragement, and support. I found him by my side in every difficulty that I faced during PhD period. I have learned a lot from his personality and knowledge. I am indebted to him for all those long discussions and meetings, which played a significant role in my research. I am feeling very lucky to have such wonderful, dynamic, and supportive supervisors.

I wish to express gratitude to my fellow colleagues at Murdoch University for all the smiles, greetings, and tea-time chit-chats over the years. I would also like to thank my colleagues- Dag, Mohammet, Remember, Jinping, and Kethaki for those social, political and cultural discussions. I would also like to thank Zakir, Moktadir, Atiq, Nipu, Zakia, Reza, Adnan, Ehsan and Amir for all the support and company. I wish to express my special gratitude to Ishika, Iqbal, Hassan, Taskin, Shoeb, Pinky, Saif, Shawon, Sohela, Kamrul and Vida. They have been the family here; without them, life would be way too tricky.

I would also like to take this opportunity to express my gratefulness to my parents, sister Tamanna and my newborn niece Mehrima for their belief, admiration, support, and love.

Finally, all praise to almighty Allah, the Most merciful, and the controller of the universe, without His mercy nothing would have been possible.

Abstract

A standalone remote area microgrid may frequently experience overloading due to lack of sufficient power generation or excessive renewable-based generation that can cause unacceptable voltage and frequency deviation. This can lead the microgrid to operate with less resiliency and reliability. Such problems are conventionally alleviated by load-shedding or renewable curtailment. Alternatively, autonomously operating microgrids in a geographical area can be provisionally connected to each other to facilitate power exchange for addressing the problems of overloading or overgeneration. The power exchange link among the microgrids can be of different types such as a three-phase ac, a single-phase ac, or a dc-link. Power electronic converters are required to interconnect such power exchange networks to the three-phase ac microgrids and control the power-sharing amongst them. Such arrangement is also essential to interconnect microgrid clusters to each other with proper isolation while maintaining autonomy if they are operating in different standards. In this thesis, the topologies, and structures of various forms of power exchange links are investigated and appropriate operation and control frameworks are established under which power exchange can take place properly. A decentralised control mechanism is employed to facilitate power-sharing without any data communication. The dynamic performance of the control mechanism for all the topologies is illustrated through simulation studies in PSIM® while the stability and robustness of the operation are evaluated using numerical studies in MATLAB®.

Table of Contents

List of Figures

List of Tables

List of Abbreviations

BES	Battery Energy Storage
BFC	Battery Frequency Controller
BSC	Battery Storage Converter
CMG	Coupled Microgrid
DER	Distributed energy resource
DG	Distributed Generator
FFT	Fast Fourier Transform
FMG	Floating Microgrid
HMG	Healthy Microgrid
ICC	Interconnection Converter
IFC	Interconnection Frequency Controller
LPF	Low Pass Filter
LQR	Linear Quadratic Regulator
LSC	Line-Side Converter
MG	Microgrid
MSC	Microgrid Side Converter
OG	Over-generation
OGFC	Over-generation Frequency Controller
OL	Overload
OLFC	Overload Frequency Controller
PMG	Problem Microgrid
PCC	Point of Common Coupling
PI	Proportional-integral
PLL	Phase-Locked Loop
VSC	Voltage Source Converter

Chapter 1 Introduction

This chapter provides the background and motivation of the conducted research in this thesis. The key research objectives and contributions of the thesis are highlighted and summarised. Finally, the organisation of the thesis, concerning each following chapter, has been introduced.

1.1. Background

A microgrid is usually referred to as a small-scale interconnected network of multiple Distributed Generators (DG) that are predominantly renewable energy source-based and power electronic converter-interfaced, distributed loads, and energy storage [1-3]. Such a system can operate under a centralised, semi-centralised, or decentralised control scheme [2, 4-6], that may have two modes of grid-connected and autonomous (islanded). Where a utility grid is not feasible or unavailable due to cost and economic constraint, e.g., the edge-of-grid or remote/regional areas, the microgrids can operate under a decentralised control scheme and permanently autonomous, to minimise the cost by saving the requirement of communication technologies and thus facilitating to integrate a large number of renewable sources [4-7]. One or some DGs in such a scheme usually operates based on droop control to realise the desired power-sharing amongst them while also regulating the desired frequency and voltage [8-13]. Thus, the active and reactive powers are regulated at the output of each DG operating in droop control, and the microgrid's voltage and frequency are regulated within the acceptable limits and thus, the system's stability will be maintained [14-18].

To electrifying remote and regional areas, autonomous microgrids are a cost-effective solution and preferred over commissioning long transmission and distribution lines. Hence, microgrids operating permanently in the autonomous mode can be commissioned for such areas [19-24]. However, seasonal variation, intermittency, and

unpredictability in renewable sources and fuel transportation cost impose further challenges for the operation of autonomous microgrids, and hence the microgrid operators are more interested in employing renewable energy resources in places where wind or solar-based resources are plentiful and thus, reducing the dependency of the network on diesel or gas [25-30]. Consequently, for remote locations like this, microgrid projects are gaining attention and popularity [4, 22, 31-34]. Such microgrid projects can significantly reduce the levelised cost of energy as demonstrated in several studies [4-8]. Therefore, standalone autonomous microgrids are getting prioritised and preferred for the electrification of remote off-grid towns. Power Electronic converter interfaced renewable energy sources along with diesel/gas-driven synchronous generators mostly dominate such microgrids' power supply [13-15, 20, 31-34].

1.2. Motivation

Microgrids can always experience over-generation and overloading despite the design considerations due to the high intermittency and uncertainty of the renewable energy sources [10, 32, 35-39]. Overloading is defined as a temporary shortage in the microgrid's generation capability against its total load demand. Load-shedding is the simplest mechanism to alleviate the problem in such a scenario and return the frequency and voltage to the acceptable limits [40-41]. Conversely, over-generation is referred to as a state when the microgrid experiences excess power production through its non-dispatchable DGs [35-36, 42-45]. An easy solution in such a condition is to curtailing renewable energy source-based distributed generators. Though, both solutions are uneconomic, undesirable and reduces the resiliency and reliability of the microgrid. If not alleviated, such overloading or overgeneration scenario can cause unacceptable frequency and voltage deviation from its desired limits and eventually lead to system instability [46-47].

Careful planning and considerations are required for such autonomous microgrids to account for the seasonal dependency, unpredictability, and intermittency associated with renewable energy sources [4-7]. Risk-based planning can decrease the probability of facing power shortage in the system; however, such system planning will result in

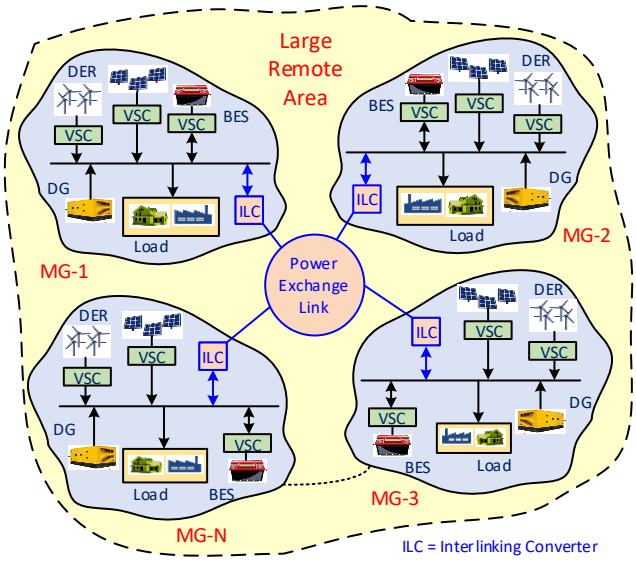

Figure 1.1 Microgrid interconnection through a common power exchange link.

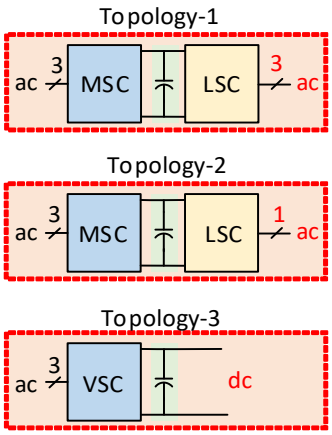

Figure 1.2 Topologies for Interlinking Converters used for power exchange links

a further increase in the projects' initial capital costs by either overdesigning and oversizing the distributed generators or installation of large-scale energy storage systems [4-6, 43-44, 48]. The problems of over-generation or overloading can be effectively alleviated using oversized energy storage systems, but it will increase the installation and operational costs of the microgrids [44-48]. Regardless of its cost, floating Battery Energy Storage (BES) units are used conventionally and are considered the most practical approach to support microgrids [49]. Such battery units, controller through power electronics-based converters, can play an essential role during peak demand, power deficiency, or overloading as they can respond faster than

micro-turbines and diesel generators. Nonetheless, using large BES units to alleviate the problem of overloading or overgeneration, is cost-ineffective as overloading or peak power demand or overgeneration through renewable sources are either temporary or intermittent, causing oversizing and overdesign of both BES unit and its converter [31-32, 44-49].

A third operation mode can be assumed to address these problems in which the neighbouring autonomous microgrids interconnect temporarily to exchange power with one another in such situations [50-53]. The purpose of such an interconnection is that the microgrids support each other to retain the voltage and frequency within the acceptable limits and thus, system stability will be maintained. Such a provisional interconnection of neighbouring microgrids to form a cluster that can facilitate power exchange amongst them also enhances and improves system reliability and resiliency [35-36, 49, 54-57]. A generic arrangement of forming such a structure and the three possible interlinking topologies are shown in Figure 1.1 and 1.2 respectively.

Properly coordinating and efficiently managing the power transaction from one microgrid to another through the Voltage Source Converters (VSC) and lines, is the key operational challenge that requires to be addressed. This thesis has focused on developing an appropriate power transaction management strategy among the microgrid clusters along with the proper structure and control techniques for the power electronic converters. The main objective is to control the power flow from a microgrid with sufficient generation to a neighbouring microgrid when it experiences power deficiency and hence, considerable frequency and/or voltage drop. In this regard, the VSC does not require to continuously exchange power but would only do so when a microgrid needs support. Similarly, if a renewable source-dominated microgrid suddenly experiences excessive generation, and thereby, leads to unacceptable voltage or frequency rise, a neighbouring microgrid can absorb this surplus power. In this thesis, an appropriate energy transaction management scheme is discussed with three different structures for Coupled Microgrid (CMG) formation and control principle for the converters to realise such operations. The exchange of power through an interconnected system of microgrid networks or cluster requires a suitable protocol and electrical framework along with a definite power exchange strategy.

1.3. Research Objectives

The main research objective is to develop suitable operational and control techniques for exchanging power amongst coupled microgrids because of the uncertainties of renewable energy resources and the loads. Various structures and thus control techniques have been proposed and developed to facilitate a smooth operation for the microgrid cluster irrespective of any unknown and sudden changes in these uncertain quantities. The major points can be summarised as

- Develop a technique to couple neighbouring microgrids via three different power electronics converter-based topologies.
- Develop a decentralised and scalable control mechanism to exchange power amongst any number of microgrids with different voltage, frequency, and operational standards using only local frequency measurement couple.
- Develop a mechanism to realise the desired power-sharing amongst the microgrids when exchanging power.
- Develop a mechanism to coordinate power-sharing among local BES and the interconnected microgrid network

1.4. Outline of Research Contributions

The main contributions of this thesis can be summarised as:

- Proposing three structures for the power exchange in the form of
    - a three-phase line connected to each microgrid via a three-phase back-to-back power electronics converter.
    - a single-phase line connected to each microgrid via a three-phase/single-phase back-to-back power electronics converter.
    - a dc line connected to each microgrid via a three-phase power electronics converter.
- Developing the suitable decentralised control techniques for each of the power electronics converters to distinguish the need and amount of the required power exchange,
- Developing a technique to coordinate the internal and external power exchange support amongst a local BES within a microgrid and the other neighbouring

microgrids,

- Validating the robustness of the proposed power exchange topologies and control techniques through stability and sensitivity analysis.

1.5. Organisation of the Thesis

The remainder of the thesis is organised as follows:

Chapter 2 surveys the relevant literature and critically analyses them to demonstrate the research problems and possible solutions. **Chapter 3** introduces suitable topologies and presents the developed decentralised control mechanisms to realise power exchange amongst the interconnected neighbouring microgrids. **Chapter 4** presents sample time-domain analysis results using the PSIM® simulation tool to demonstrate and validate the proposed power exchange mechanism for all introduced topologies. **Chapter 5** discusses the stability of the proposed controllers while **Chapter 6** evaluates the sensitivity and robustness of the proposals. Finally, **Chapter 7** highlights the key research findings and summarises the significant contributions of the thesis. This chapter also proposes probable future directions in this research field.

Chapter 2 Literature review

In this chapter, the operation and control principles of the interconnected microgrids have been discussed and reviewed, and the different techniques suggested and employed in the literature are surveyed. The chapter has first discussed the problems associated with autonomous remote area microgrids and hence the coupling of such neighbouring microgrids are proposed as a solution. Then, existing works on the control and coupling of such microgrids as well as their architecture and stability, are critically reviewed. This chapter also identifies the research gaps and suggests possible techniques to address those research problems.

2.1. Operation of an Autonomous Microgrid

In the autonomous or islanded mode, microgrids are usually operated under droop control to realise the desired power-sharing amongst the Distributed Energy Resources (DER) while the voltage and frequency are regulated. by one or more of the DERs. Thus, the active and reactive power must be continuously controlled at the output of each droop-controlled DER to regulate the MG's frequency and voltage within the desired (acceptable) limits to ensure system stability [4-5].

Let us consider a network of Figure 1.1 where N autonomous microgrids, each consisting of several DERs, distributed generators, loads, and one interlinking converter coupled to a power exchange link. The interlinking converter can be any one of the three topologies shown in Figure 1.2. The DERs are connected to the microgrid through VSCs which are controlled in different operating modes to regulate the power and frequency of each microgrid. The DERs are assumed to be operating in the $P - f$ and $Q - V$ droop control mode, where the voltage and frequency at the output of each DER is determined from [8-10]

$$f_{\mathrm{MG}} = f_{\max} - m_i P_i \tag{2.1}$$

$$V = V_{\mathrm{rated}} - n_i Q_i \tag{2.2}$$

where m_i and n_i are the droop coefficients of the ith DER of the microgrid, and can be obtained from

$$m_i = \frac{f_{\max} - f_{\min}}{P_i^{\max}} \tag{2.3}$$

$$n_i = \frac{V_{\max} - V_{\min}}{2Q_i^{\max}} \tag{2.4}$$

where subscript $_{\max}$, $_{\min}$, and $_{\mathrm{rated}}$ represent the maximum, minimum, and rated limits for frequency and voltage of the microgrids while P_i and Q_i are active and reactive powers injected by each DER to the microgrid. All DERs within a microgrid are assumed to have the same $\Delta f = f_{\max} - f_{\min}$ and $\Delta V = V_{\max} - V_{\min}$; V_{rated} is the rated voltage of the DER's point of common coupling, i.e., one per unit. However, these parameters can be different in each neighbouring microgrid. Each DER is provided with its own local energy storage and thus it can be assumed as a dispatchable DER. The structure and operation of the DERs are discussed in [11, 16, 54]. Lastly, each microgrid is connected to a common power exchange link via its interlinking converter to exchange power with the other microgrids in the event of power deficiency or over-generation. Each microgrid can operate independently at any predefined frequency and voltage level without affecting the operation of other neighbouring microgrids.

A microgrid central controller (MGCC) is employed for a higher level control approach to supervise and monitor the entire microgrid and respond to the voltage and frequency deviations, which has slower dynamics compared to the local controller [14-15]. Ref [16] proposes an analytical approach to determine the set-points for the droop parameters of the DERs to maintain the voltage and frequency of the microgrid, within acceptable limits. Another scheme is proposed in [17-20], in which the droop coefficients of the DERs are optimised by MGCC, based on load demand, to minimise the fuel cost and the power loss of the microgrid. On the other hand, the charging and discharging of the BESs [21-23], load-shedding [40-41], demand response [25-27], and curtailment of renewable sources [28-32] have also been suggested, to alleviate the voltage and frequency problem in the microgrids. Finally, [33-36] have proposed the concept of provisional coupling of neighbouring microgrid(s) or a utility feeder, if available to address the voltage and frequency problems.

2.2. Overloading and Excessive Generation in Microgrids

The trend of an islanded microgrid in remote localities or the regional edge-of-the-grid network is gaining popularity due to its economical aspects and advantages. Several studies have shown that employing autonomous microgrids is a feasible solution for the electrification of remote areas as it can significantly reduce the levelised cost of power generation [4-8, 37-38]. microgrids are cost-effective solutions than lengthy transmission and distribution lines when it comes to the electrification of remote and regional areas. Hence, a microgrid operating permanently in the autonomous mode can be considered for such areas. Such microgrids will be mostly dominated by renewable energy sources along with some diesel/gas-driven synchronous generators. High on-going fuel cost and its transportation impose further challenges for the operation of such MGs. At the same time, due to high intermittency and variability issues associated with renewable energy sources, phenomena such as overloading and over-generation can be seen in such microgrids, regardless of the considerations at the design stage [38-44]. Overloading refers to the provisional deficiency in the microgrid's generation capability compared to its total demand, following which, load-shedding is the most common and simple mechanism to alleviate the problem and return the voltage and frequency to the acceptable limits. On the other hand, over-generation refers to the situation in which the microgrid experiences high generation and an excess of power through one or more of its non-dispatchable DERs [38-41]. Curtailing such renewable energy resources is a solution to such conditions. However, both load-shedding and curtailing renewable sources are uneconomical and undesirable which reduces the reliability and resiliency of the system [42-44]. Proper risk-based planning can help to prevent such scenarios by overdesigning and oversizing the DGs and/or using large-scale energy storage systems to effectively mitigate the overloading and over-generation problems and the corresponding voltage and frequency issues. However, this will incur large installation and operational costs [3-4, 45-48]. Hence, the third mode of operation has been proposed for microgrids in [35-36, 49-55] in which the neighbouring microgrids can temporarily interconnect with each other during such situations to support each other and to retain the frequency and voltage within the desired limits and ensure the system stability. Note that, this interconnection is not to a grid but to another neighbouring MG, which is also operating autonomously. This system of interconnected autonomous microgrids is referred to as coupled microgrids

(CMGs) in the remainder of this paper. Connecting a microgrid to its neighbouring microgrids through a physical link is an effective operational strategy during power deficiency or surplus [51-53]. Thus, the provision of forming CMGs improves and enhances system reliability [22-24, 54-55].

2.3. Coupling of Autonomous Microgrids

In the future, it is expected that a remote locality will consist of several neighbouring microgrids within a geographical area. Under the above assumptions, the overloading or over-generation management strategy can be realised by properly interconnecting two or more of those neighbouring microgrids. a suitable power deficiency or surplus mitigation strategy can be instigated by suitably coupling two or more of those microgrids [34-35, 49-55]. The CMG model and its operation based on the availability of communication infrastructure and the concept of the power market is discussed in ref [50, 56-57]. According to this concept, a common power exchange link (i.e., distribution lines) that enables a physical connection among the microgrids will be introduced to interconnect the neighbouring microgrids. Such an interconnecting link can be in either form of ac or dc [49, 55, 61-64]. A direct ac-ac connection between a microgrid and the power exchange line can be easily realised through a conventional circuit breaker or an interconnecting static switch which is very economical to a large extent [60]. However, the structure and control mechanism of each microgrid can be different from its neighbouring microgrids and such a direct ac-ac connection will reduce the autonomy of their operations. In order to add proper isolation amongst the microgrids to retain the autonomy in their operation, the power electronic converter-based interlinking structure [65-66] will enable every microgrid to function independently and autonomously, as well as facilitate power exchange with the neighbouring microgrids [36, 60-62]. Power-sharing between two islanded microgrids during mutual contingency is studied in [54, 59], whereas an autonomous control approach to sharing power with neighbouring microgrids through a back-to-back converter in the presence of a utility grid is proposed in [36, 61]. Neighbouring microgrids can also interconnect to support each other during the occurrence of fault leading to the outage of a section [67] or during normal conditions to minimise the levelised cost of electricity [68]. If one of the microgrids temporarily observes a high-

power generation by one of its DERs, the other neighbouring microgrid(s) can get interconnected to one another to import power and thus offers electricity at a lower price. A transformative architecture is proposed for coupling the nearby microgrids is to improve the system resiliency during faults [69]. Ref [70-71] analyses the reliability aspects of a CMG, while the voltage and current controllability in CMGs is analysed in [72]. The dynamic operation of DERs within CMGs is investigated in [73] whereas [74] examines the dynamic security of the CMGs. Several structures to form such CMG, as well as its control mechanism are proposed in literature.

2.4. Structure and Control of Coupled Microgrids

Detailed analysis of different topologies and architectures of forming CMGs is shown in [56-57, 75]. Optimal control of a utility grid-connected CMG is studied in [36, 66], while an interactive control method to share the load in a CMG ensuring a wide range of system stability is shown in [76-82]. An optimization-based technique is developed in [83-85] to ensure optimal power exchange between the microgrids. A decision-making-based approach is proposed to determine the most suitable microgrid(s) to connect with an overloaded microgrid, based on different criteria such as available surplus power, electricity cost, reliability and the distance of the neighbouring microgrids as well as the voltage/frequency deviation in the CMG [86-88]. The ultimate objective is that a microgrid can be coupled to any other microgrid (and not necessarily an adjacent microgrid) if a general link is available to act as a power exchange highway [55-56, 75, 89]. Figure 2.1 shows some of the possible interconnection topologies of CMGs where the dashed lines mark the boundary of the microgrids and solid lines represent the interconnecting links amongst them. Back-to-back power electronic converter-based interface has been proposed in [35, 54, 90-91] that can be used between each microgrid and the interconnecting three-phase ac line to ensure autonomy in its operation. Such a scheme is comparatively expensive as two voltage source converters (VSCs) are employed for every microgrid. However, the main objective of such a connection is to provide isolation between the microgrids and thus, microgrids with different operational regulations can exchange power while being isolated through the dc-links within the back-to-back converters [35, 91]. Furthermore, such an interconnecting link can also be realised through a single-phase

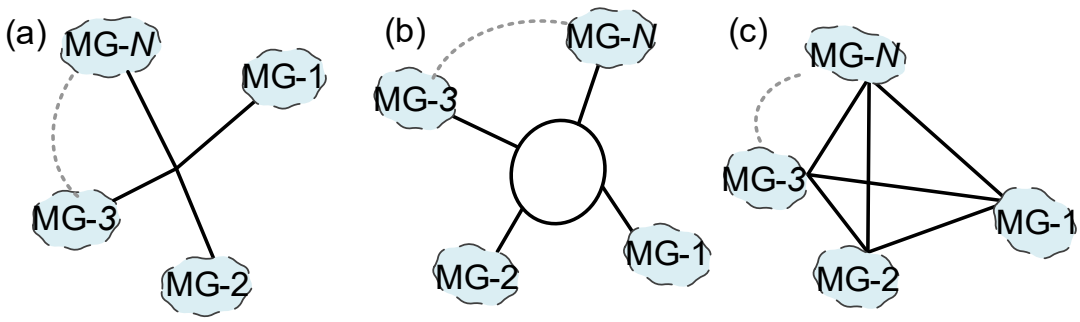

Figure 2.1 Possible topologies for the formation of coupled microgrid network

ac power line instead of a three-phase ac power line [91] to reduce the cost while fulfilling the requirements of the power transfer during overloading and/or overgeneration. It should be noted that such an interconnecting line is only operational during contingency of overloading or overgeneration and the total power exchanged through the links is comparatively smaller (around 10-20% of the microgrid maximum capacity). Therefore, such an alternative single-phase ac line over the three-phase ac lines can be more economical as the number of lines and the power electronic filter components will be less. However, the use of the back-to-back converter is limited to a couple of two microgrids and not scalable to a couple more than two microgrids. To couple multiple microgrids, the control technique and coordination among the converters will be complex as it involves a $2N$ number of converters to interconnect N microgrids and a common interlinking link that operates in a predefined frequency and voltage [35, 90]. At the same time, a communication network is necessary to coordinate such ac power exchange link as proper synchronization among the microgrids is necessary for power exchange which is not possible unless a suitable data communication link is established [90]. Hence, commissioning a dc-link rather than the ac links proves to be a better and effective operational strategy and, in such topology, only one converter is adequate for connecting each microgrid to the dc power exchange link [49, 89]. Thus, such a dc interconnecting link practically costs half of the price of the two previous ac topologies in terms of the power electronic converters. Even though the power loss in the interconnecting lines appears to be smaller; however, most of the commercial power line infrastructure, equipment, and accessories are based on ac systems. Besides, the network operators are usually more familiar with ac distribution systems as compare to dc systems. Moreover, the control and protection equipment and schemes for ac systems are more economical than dc

systems to some extent. Properly coordinating and efficiently managing the power transaction from one microgrid to another through the VSCs and lines, is the main challenge that requires to be addressed. transaction management scheme is discussed with three different structures for CMG
formation and control principle for the converters to realise such operations. The exchange of power through an interconnected system of microgrid networks requires a suitable protocol and electrical framework along with a definite power exchange strategy. At the same time, stability of the CMG network must be ensured as, such an interconnection may lead to system oscillation which may cause shut down of entire network due to instability.

2.5. Stability of Coupled Microgrids

Prior to form a coupled microgrid network, the stability of the newly formed network needs to be examined to avoid any instability of the system. For this purpose, eigenvalue based small signal stability analysis is proposed in [47-48, 76]. It has been shown in [77] that, the number of inertial and non-inertial DGs, their ratings, loads need to be evaluated to ensure the stability of the CMG. Ref [78] further expands and investigates the influence of the number of microgrids as well as the length and X/R ratio of lines. Ref [79] suggests a decision-making function along with a small signal stability evaluation prior to any transformation in the architecture of the CMG.
If properly designed, it is shown in [78-79] that, loci of the eigenvalue of the new CMG network, is approximately within the same operating point eigenvalues of each microgrid, when operating independently. Also, a sensitivity analysis is performed along with stability analysis in [80] which reveals that microgrid with smaller stability margins can cause a drop in the overall system stability margins of the other microgrids after they are coupled.
It has also been reported that stability margins of the CMG can be strongly affected by the DER nominal power while no significant effect was observed for the load demand and power factor. Also, it is observed that the length and X/R ratio of the lines of the microgrids can affect stability. However, no impact was observed whether the microgrids had a loop or radial configuration. It is also recommended that developing a general stability guideline is not straightforward as the operation of CMG depends

on the conditions of the newly created system. Ref [79, 81-82] used Monte Carlo simulations, to examine the network characteristics and the topology that can affect the small-signal stability of a converter-dominated microgrid. It is found that simple radial topologies are the most stable, though it is less resilient to faults and reduces the network reliability. As the level of meshing is increased, the less stable the network becomes. Hence it is recommended to keep the network topology as simple as possible and operate the CMG in a ring configuration with a tie-open point. The study also demonstrates that if the two adjacent converters tied with a smaller impedance line can adversely affect the stability margin. As a result, it is recommended to connect adjacent converters with enough electrical decoupling or isolation from each other to avoid unstable interactions. Also, it was revealed that the length of the lines of the adjacent microgrid can affect the stability margins of the CMG [80]. Based on stability studies, the most optimum and robust topology to form the CMG can be selected.

2.6. Topology Comparison for Coupled Microgrids

Realising power exchange among multiple microgrids requires a predefined coordinated control mechanism. It is possible to couple multiple microgrids to form CMG using single-phase ac lines. The purpose of using a single-phase power exchange link is to reduce the number of converter components and transmission lines in the CMG network to make the system more economical. However, the line power loss is higher in a single-phase link than that of a three-phase link for the same operating conditions and power. Also, the power quality is poorer as single-phase instantaneous power is oscillatory in nature. Hence, the three-phase power exchange link is superior in every aspect as compared to the single-phase link unless a very small amount of power is required to be exchanged within the CMG network through short interconnecting lines. Though the number of components and power lines require for the three-phase link are more, the power quality and performance are superior and produce significantly lower line loss and thus, makes the system more efficient. At the same time, the three-phase network exhibits larger system damping and hence, a better stability margin as can be seen from the stability analysis [91-92].

On the other hand, CMG formed using dc interconnecting lines outperform any types of ac links in terms of technical and economic aspects. However, there are several

critical issues with dc power exchange links such as lack of proper standard and guidelines for protection scheme, expensive protection equipment, larger fault current level, arching during fault current interruption as no natural zero current crossings, lower fault ride-through capability [91-93], circulating current in the network due to unequal line resistance [94-95] and inaccurate and less efficient power-sharing based on droop control technique [91-92]. On the other hand, the standard and infrastructure for ac power transmission and distribution systems are well established and most of the commercially available equipment are ac network-based which makes most of the network operators prefer ac transmission systems over dc. Considering the cost and complexity of the protection scheme, dc interconnecting link is more suitable when the distance among the microgrids is longer. But as the distance among the microgrids are increased (i.e. the line resistance is increased), the property of power-sharing based on the droop control technique deteriorates and eventually diminishes. At the same time, the increased value of line resistance makes the CMG network's performance highly sluggish [91]. Also, unequal line resistances can cause circulating current inside the CMG network [94]. However, these problems can be addressed using the technique discussed in [95], but the performance is not as satisfactory as the ac droop control technique. In this paper where a three-phase ac interconnecting link is proposed to form the CMG network, a modified virtual impedance-based angle-active power, and voltage-reactive power droop control technique is employed that can successfully address all the above-mentioned problems and the relevant results are shown in the sensitivity analysis section of the paper. Hence, it can be concluded that the performance of a CMG network formed using three-phase ac or dc interconnecting lines, are comparable in terms of different technical and economic aspects and thus, a proper techno-economical evaluation and optimization is required before selecting the most suitable topology based on the type of microgrids to be interconnected, amount of exchanged power, the duration and intervals at which power is going to be exchanged, protection scheme and finally, the distance among them. A comparative review of ac and dc technology used in microgrid application can be found in [91-92]. It was discussed in [91] that, though in theory dc systems are more advantageous in several aspects, however, considering the present power transmission infrastructure, commercially available protection equipment, technical constraints, network standards, and guidelines, ac systems are still more economical

To address the above research gaps, this thesis presents a fully decentralised approach

Table 2.1 Comparison of different CMG features.

CMG Features	[35]	[36]	[49]	[54]	[55]	[60]	[61]	[62]	[89]	Top-1	Top-2	Top-3
Communication Links	×	✓	×	✓	✓	✓	✓	×	✓	×	×	×
OL prevention	✓	✓	✓	✓	✓	✓	✓	×	×	✓	✓	✓
OG prevention	✓	✓	×	×	✓	×	×	×	×	✓	✓	✓
Multiple microgrids	✓	×	×	×	✓	×	×	×	✓	✓	✓	✓
Type of interconnecting link	CAC	CDC	CDC	CDC	CDC	DAC	CDC	CDC	CDC	CAC (3-ph)	CAC (1-ph)	CDC
Utility grid connection	×	✓	×	×	×	×	✓	✓	×	×	×	×
Energy storage	×	×	✓	×	×	✓	×	✓	×	×	×	×
Scalability	✓	×	✓	×	✓	×	×	×	✓	✓	✓	✓
Level of implementation	P	P	P	P	P/S	P/S	P	P	P/S	P	P	P
Control type	D	Dist.	D	C	C	C/D	Dist.	Dist.	Dist.	D	D	D
Unbalanced microgrid	×	×	×	×	×	×	×	×	×	✓	✓	✓
Desired power-sharing using droop control	✓	×	×	×	✓	×	×	×	×	✓	✓	✓

DAC = Direct ac coupling; **CDC =** Converter-based dc coupling; **CAC =** Converter-based ac coupling; **P=**Primary level; **S =** Secondary Level; **Mod. =** Moderate; **Med. =** Medium; **D** = Decentralized; **C**= Centralized; **Dist.** = Distributed.

to alleviate both over-generation and overload problems by coupling the neighbouring microgrids which are fully scalable to couple N autonomous microgrids in order to exchange power among them using any one of the above-mentioned three topologies. This approach does not need any data communication among the microgrids and their controller; thus, operates only based on local measurements at the terminals of the converter at the point of common coupling which offers the additional advantage of eliminating the requirement as well as the cost of communication infrastructure. Thus, it enhances the resiliency and self-healing capability of each microgrid while ensuring autonomy in the operation of individual microgrids enabling them to operate at any frequency and voltage level. Besides, this mechanism can also work as a backup for coupled microgrid (CMG) networks that are operating under a centralised control scheme, in the event of a communication link failure or any contingency, and hence, offering further reliability. The efficacy of this mechanism is evaluated by numerous examples with various scenarios in microgrids. To demonstrate its robustness and applicability for all three topologies, the technique is further validated with stability and sensitivity analysis of the CMG network against the key design and operational factors. A comparison of the implemented control technique and features of the three topologies against other approaches, available in the literature, has been summarised and provided in Table 2.1.

2.7. Summary

This chapter has surveyed different control techniques proposed in the literature to alleviate the overloading and excessive generation in an autonomous microgrid. The research gaps in the field and several proposed techniques to address those gaps are identified. Based on this literature review, suitable topologies are chosen, and proper control mechanisms have been developed and formulated, which are introduced and discussed in the next chapter. These methods can alleviate the overloading and excessive generation in autonomous microgrids and thus can improve the voltage and frequency quality by coupling a microgrid in problem to one or more of its neighbouring microgrids and coordinate power-sharing within its local BES. The proposed techniques overcome the limitations of the existing similar techniques in the literature and more generalised to couple any number of microgrids.

Chapter 3 Operational and Control Technique

This chapter presents the four proposed decentralised power exchange techniques and topologies for CMG operation. The proposed techniques and topologies are (a) Topology-1: three-phase ac power exchange link, (b) Topology-2: single-phase ac power exchange link, (c) Topology-3: dc power exchange link, and (d) Coordinated control and power-sharing mechanism among BES and CMGs.

3.1 Microgrid Classification

This provisional power exchange mechanism can be realised by interconnecting the neighbouring microgrids to a common power exchange link to facilitate power exchange among the microgrids during an overload/excess generation. Thus, the neighbouring microgrids can be coupled via a power electronic converter-based interface and ac/dc interconnecting power lines to form a CMG. Such a strategy is attained by monitoring and controlling the frequency of each microgrid. It is obvious that autonomous microgrids are conventionally operating under droop control to share power amongst their DERs and in such a control scheme, as the total load demand of a microgrid increases, its frequency decreases, and vice versa. Such a distinct behaviour can be used as an indication of the microgrid's power shortage or surplus, and hence, the approach eliminates the necessity of any sort of data communication link or a centralised controller. The key benefit of this approach is that it eliminates the necessity of installing and operating a communication infrastructure to enable the microgrids to exchange power. It should be mentioned here, even in the presence of a central controller with communication links to monitor and regulate the power exchange, this approach can be implemented as the backup system that is activated in

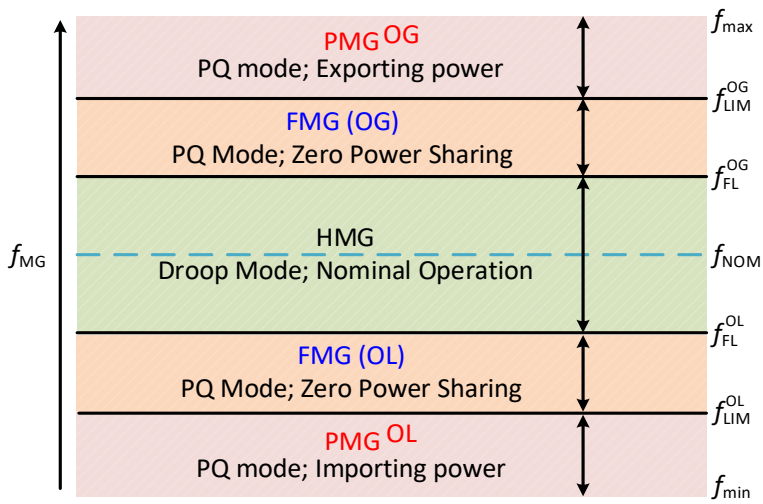

Figure 3.1. Microgrid classification based on its frequency level.

the event of communication failure or during any contingency. Thus, a fully decentralised mechanism to exchange power amongst the microgrids dynamically is introduced for effective overload/over-generation power management based on a predefined framework. Such provisional power exchange facility amongst the neighbouring microgrids increases the reliability and resiliency of the overall system.

Based on the above-mentioned framework, the microgrids can participate in forming the CMG based on a predefined set of standards, as permitting all (or many) microgrids to participate in the CMG network formation may lead to system instability [76-79, 81-82, 96]. Hence, the formation of a CMG would be allowed or denied based on the microgrids' existing loading level, which is identified by measuring their frequencies. Based on their loading level, every microgrid is classified and flagged in either of the three categories of a healthy, problem, or floating microgrid (respectively denoted by HMG, PMG, and FMG), as introduced below:

- An HMG refers to the status of a microgrid when it is operating within its nominal frequency and voltage range and can support the other neighbouring microgrids by exchanging power.
- A PMG refers to an operating condition when the microgrid experiences over-generation or overloading. Any PMG within the CMG network is expected to connect to one or more neighbouring HMGs and exchange power to retain their frequency and voltage within acceptable limits.

Table 3.1 Classification of microgrids based on their frequency

Frequency levels	MG Status	Mode of operation
$f_{\mathrm{FL}}^{\mathrm{OL}} < f_{\mathrm{MG}} < f_{\mathrm{FL}}^{\mathrm{OG}}$	HMG (nominal operation)	Droop Control
$f_{\mathrm{LIM}}^{\mathrm{OL}} < f_{\mathrm{MG}} < f_{\mathrm{FL}}^{\mathrm{OL}}$	FMG (boundary of overloading)	PQ mode (zero power exchange)
$f_{\mathrm{FL}}^{\mathrm{OG}} < f_{\mathrm{MG}} < f_{\mathrm{LIM}}^{\mathrm{OG}}$	FMG (boundary of excess generation)	PQ mode (zero power exchange)
$f_{\mathrm{MG}} \leq f_{\mathrm{LIM}}^{\mathrm{OL}}$	PMG (overloading)	PQ mode (importing power)
$f_{\mathrm{MG}} \geq f_{\mathrm{LIM}}^{\mathrm{OG}}$	PMG (over-generation)	PQ mode (exporting power)

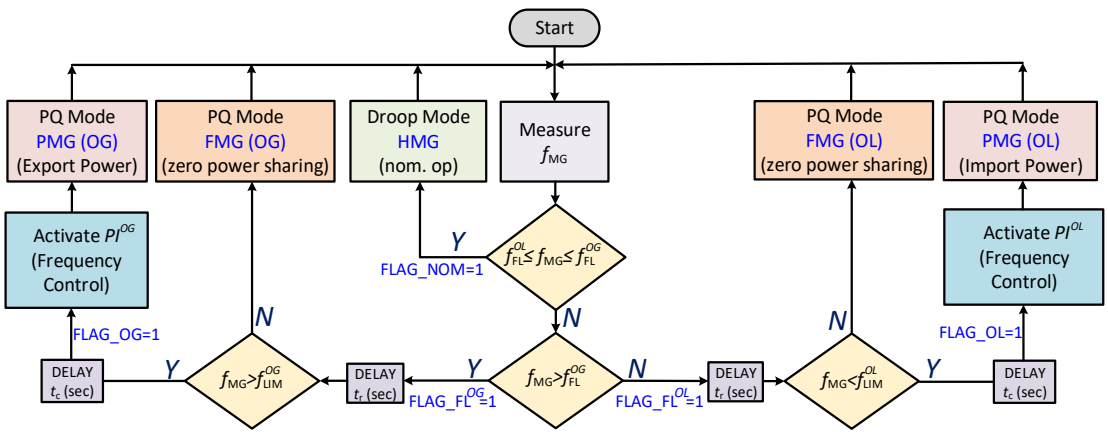

Figure 3.2. Flowchart of the microgrid's different modes of operation for power exchange.

- An FMG refers to a microgrid's loading condition that is in the boundary of becoming a PMG. In other words, the microgrid's frequency or voltage is in the boundary of maximum or minimum acceptable limits, and hence, should not be allowed to participate in power exchange within the CMG.

This classification of microgrids is shown in Figure 3.1 and their corresponding mode of operation based on frequency level is tabulated in Table 3.1.

To explain the operation of such a system, let us consider Figure 3.1 in which f_{MG} is the operating frequency of the microgrid while $f_{\mathrm{FL}}^{\mathrm{OL}}$ and $f_{\mathrm{FL}}^{\mathrm{OG}}$ are the two frequency limits, beyond which the overloading and over-generation begin in the microgrid, respectively. Parameters $f_{\mathrm{LIM}}^{\mathrm{OG}}$ and $f_{\mathrm{LIM}}^{\mathrm{OL}}$ are the microgrid's maximum and minimum

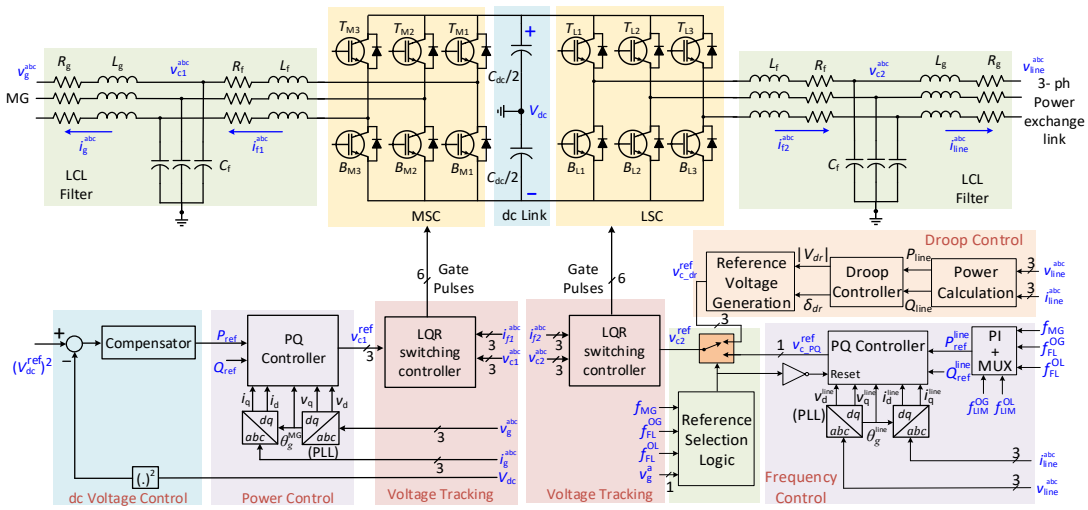

Figure 3.3. Assumed structure and close loop control mechanism of the MSC and LSC for topology-1.

permissible frequency to operate within the acceptable limit, while $f_{\max}$ is the no-load frequency and $f_{\min}$ is the frequency where the microgrid becomes unstable due to excessive loading. Referring to Figure 3.1 and Table 3.1, the microgrid's operating status can be denoted as:

- The microgrid is defined as HMG when $f_{\mathrm{FL}}^{\mathrm{OL}} < f_{\mathrm{MG}} < f_{\mathrm{FL}}^{\mathrm{OG}}$.
- FMG can be attained in two conditions; i.e., when $f_{\mathrm{LIM}}^{\mathrm{OL}} < f_{\mathrm{MG}} < f_{\mathrm{FL}}^{\mathrm{OL}}$ (increasing load demand) or $f_{\mathrm{FL}}^{\mathrm{OG}} < f_{\mathrm{MG}} < f_{\mathrm{LIM}}^{\mathrm{OG}}$ (decreasing load demand).
- PMG can be attained in two conditions; i.e., when $f_{\min} < f_{\mathrm{MG}} < f_{\mathrm{LIM}}^{\mathrm{OL}}$ (overloading) or $f_{\mathrm{LIM}}^{\mathrm{OG}} < f_{\mathrm{MG}} < f_{\max}$ (over-generation).

Figure 3.2 demonstrates the steps of detecting the microgrid's status and the operation of the CMG to enable power exchange amongst the microgrids using a flowchart.

3.2 Various CMG structure and their control

The CMG formation among the neighbouring microgrids is achieved through power electronics converters and interconnecting power lines using the three different topologies. For topology-1 and 2, a back-to-back converter structure is employed whereas, a single-stage converter is enough for topology-3. The converter connected to the microgrid is labelled as the microgrid-side converter (MSC) while the other one

is labelled as the line-side converter (LSC). In topology-1 and 2, both MSC and LSC are voltage source converters (VSCs) connected back-to-back with each other via a common dc-link to provide the isolation which enables the microgrids to operate with full autonomy and no synchronization of MSC with LSC is required (see Figure 1.1). In such an arrangement, MSC enables bi-directional power flow between the microgrid and dc-link whereas, LSC enables bidirectional power flow between dc-link and the interconnecting lines. In this approach, the purpose of MSC is to regulate only the dc-link voltage; however, the mode of operation of LSC depends on the frequency (i.e., loading level) of the microgrid to which it is connected. On the other hand, in topology-3, a single-stage voltage source converter is used to connect the dc power lines to the microgrid and labelled as VSC (see Figure 1.2), which can operate either in dc droop control mode or constant PQ control mode depending on the status of the microgrid.

3.2.1 Three-phase AC interconnection (Topology-1)

Topology-1 is a three-phase ac interconnecting line with two back-to-back connected power electronic converters. In this topology, both the MSC and LSC are assumed to be three-phase, three-leg VSC using IGBTs or MOSFETs. Each VSC is connected to its point of common coupling through a three-phase LCL filter. The structures of MSC and LSC are shown schematically in Figure 3.3. However, any other three-phase topologies of VSCs can also be used instead of the considered topologies here.

3.2.1.1 Control of MSC

The main function of MSC is to regulate and maintain the dc-link voltage of V_{dc} at the desired reference level of $V_{\mathrm{dc}}^{\mathrm{ref}}$. This is valid for any status of the microgrid (i.e., HMG, PMG, FMG). The dc-link will exchange the appropriate amount of power with the microgrid through proper voltage regulation, such that the dc-link voltage remains constant. This can be realised through a closed-loop control mechanism (i.e., the outermost loop in the MSC part of Figure 3.3) to determine the reference active power (P_{ref}) that should be drawn from or injected into the microgrid to avoid a deviation in V_{dc}. The MSC is not likely to exchange any reactive power with the microgrid and hence, the reference for reactive power (Q_{ref}) is assumed to be zero. Based on these

two reference parameters, the PQ controller determines the three-phase reference voltage (v_c^{ref}) across the capacitor C_f of LCL filter of the MSC. The most inner control loop of MSC in Figure 3.3, is the voltage tracking and switching control block. To achieve robust and optimum performance, the linear quadratic regulator is used to track the sinusoidal reference voltage, as discussed in [73].

3.2.1.1.1 Voltage Tracking and Switching Control

The voltage tracking and switching control of the MSC is designed based on the dynamics of the filter inductance, L_f and filter capacitor, C_f of the LCL filter of the MSC that is connected at the point of common coupling on the microgrid side, which operates as the inner-most loop of the closed-loop control mechanism of MSC. The dynamics of the LCL filter can be represented in the state-space form by

$$\dot{\boldsymbol{x}} = \boldsymbol{A}\boldsymbol{x} + \boldsymbol{B_1}u_c + \boldsymbol{B_2}i_g \tag{3.1}$$

where

$\boldsymbol{A} = \begin{bmatrix} 0 & 1/C_f \\ -1/L_f & -R_f/L_f \end{bmatrix}$, $\boldsymbol{B_1} = \begin{bmatrix} 0 \\ V_{dc}/2L_f \end{bmatrix}$, $\boldsymbol{B_2} = \begin{bmatrix} -1/C_f \\ 0 \end{bmatrix}$ and $\boldsymbol{x} = [v_c \quad i_f]^T$ while u_c is the control switching function and i_g is the current flowing through the coupling inductor and ^{T} is the transpose operator. The current, i_f is desired to have only a low-frequency component (i.e., 50Hz) and all high-frequency switching components are needed to be filtered out. Hence, a high-pass filter (with a cut-off frequency of ω_c) is introduced in the feedback control structure to extract the high-frequency components of i_f as denoted by $\tilde{i}_f$. Hence, Equation. (3.1) can be rewritten as

$$\dot{\boldsymbol{x}}_c = \boldsymbol{A}_c\boldsymbol{x}_c + \boldsymbol{B}_c u_c \tag{3.2}$$

where $\boldsymbol{A}_c = \begin{bmatrix} 0 & 1/C_f & 0 \\ -1/L_f & -R_f/L_f & 0 \\ -1/L_f & -R_f/L_f & -\omega_c \end{bmatrix}$, $\boldsymbol{B}_c = \begin{bmatrix} 0 \\ V_{dc}/2L_f \\ V_{dc}/2L_f \end{bmatrix}$ and $\boldsymbol{x}_c = [v_c \quad i_f \quad \tilde{i}_f]^T$.

An appropriate full state-feedback control law along with a reference input (which, in this case, is the reference filter capacitor voltage, v_c^{ref}) can be expressed in the form of

$$u_c = k_1\left(v_c^{ref} - v_c\right) - k_2 i_f - k_3 \tilde{i}_f = -\boldsymbol{K}\dot{\boldsymbol{x}}_c + k_1 v_c^{ref} \tag{3.3}$$

where $\boldsymbol{K} = [k_1 \quad k_2 \quad k_2]$ is the state-feedback gain matrix in which k_1, k_2 and k_3 are optimally determined by minimizing an appropriate cost function using a linear

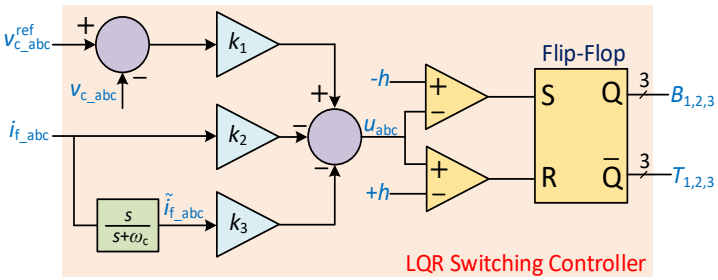

Figure 3.4. Linear Quadratic Regulator based switching and voltage tracking.

quadratic regulator [73]. Based on this optimization method, a highly robust switching controller can be designed with a bandwidth large enough to accurately track the low-frequency sinusoidal signal (i.e., 50 Hz) with zero phase delay and steady-state error. Therefore, Equation (3.2) can be rewritten as

$$\dot{\boldsymbol{x}}_{\mathrm{c}} = \boldsymbol{A}_{\mathrm{cl}}\boldsymbol{x}_{\mathrm{c}} + \boldsymbol{B}_{\mathrm{cl}}v_{\mathrm{c}}^{\mathrm{ref}} \tag{3.4}$$

where $\boldsymbol{A}_{\mathrm{cl}} = \boldsymbol{A}_{\mathrm{c}} - \boldsymbol{B}_{\mathrm{c}}\boldsymbol{K}$ and $\boldsymbol{B}_{\mathrm{cl}} = k_1\boldsymbol{B}_{\mathrm{c}}$. The implemented controller offers infinite gain and phase margin, and thus, robustly stable. The switching control of the MOSFET/IGBT can be implemented through a hysteresis function [97] with an adequately small band (e.g., $h = \pm 10^{-4}$). The control block diagram of such an LQR switching controller is shown in Figure 3.4.

3.2.1.1.2 Power Control

The next control loop is to determine the appropriate reference voltage across the capacitor, C_{f} of LCL filter by regulating the active and reactive power. For this purpose, the conventional direct-quadrature (dq) axis close loop power controller (i.e., PQ controller) is implemented. The PQ controller is the first of two outer control loops. The benefit of the PQ controller is that the active and reactive powers are decoupled and can be controlled independently. The active and reactive power are regulated by controlling the d-axis current i_{d} and q-axis current i_{q}, respectively. Hence, the PQ controller is also known as the current controller. The controller is made of two proportional-integral (PI) controllers that are responsible for producing the required d and q axis reference voltages of $v_{\mathrm{d}}^{\mathrm{ref}}$ and $v_{\mathrm{q}}^{\mathrm{ref}}$. Then, these two voltages are converted into three-phase ac reference voltage, $v_{\mathrm{c}}^{\mathrm{ref}}$ across the filter capacitor, C_{f} using the grid angle $\theta_{\mathrm{g}}^{\mathrm{MG}}$ as obtained through a synchronous reference frame phase-locked loop

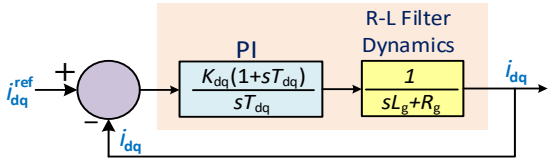

Figure 3.5. Block diagram of d and q axis current controller.

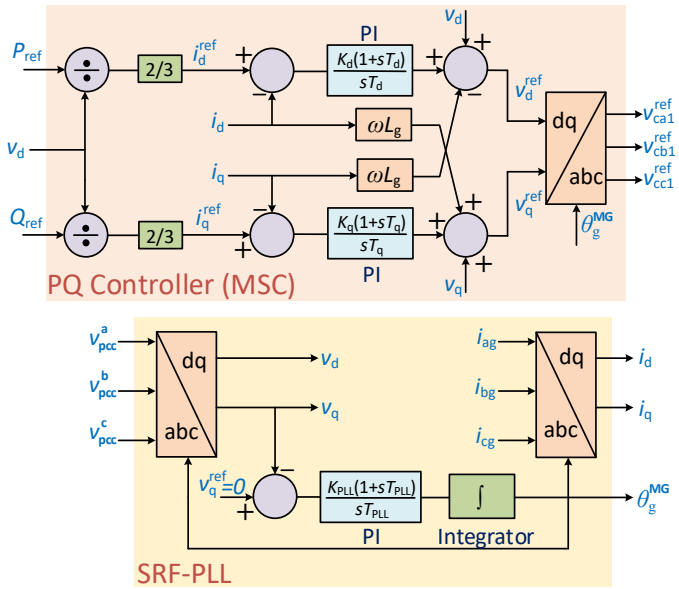

Figure 3.6. Block diagram of PQ controller for MSC.

(SRF-PLL) system. The dynamics of the output R-L branch of the LCL filter, comprised of coupling inductance, L_g, and resistance, R_g, are considered to design and tune the two PI controllers using the pole-zero cancellation method [98-99]. The transfer function of the PI controller is given by

$$C_{PI}(s) = \frac{K_c(sT_c + 1)}{sT_c} \tag{3.5}$$

where $T_c = L_g/R_g$ and $K_c = 2\pi f_{BW} L_g$ where f_{BW} is the closed-loop bandwidth of the controller that conventionally, requires to be at least 10 times smaller than the bandwidth of the inner voltage tracking loop, and hence, the inner loop can be assumed as a unity gain block while tuning the PI controllers of the PQ controller. In this design, f_{BW} is chosen to be 1000 times faster than the voltage tracking loop to ensure no overlap in the bandwidth of the control loops and proper sinusoidal voltage tracking at 50Hz. The closed-loop transfer function of the PQ controller is then given by

$$G_c(s) = \frac{i_{dq}^{ref}}{i_{dq}} = \frac{1}{s\tau_c + 1} = \frac{P_{ref}}{P_s} \tag{3.6}$$

where $\tau_c = L_g/K_c$ is the time constant of the current controller, P_{ref} is the reference power and P_s is the active power output of the converter. It should be noted here, P_{ref} is generated through the outermost control loop i.e., the dc-link voltage controller. The assumed close loop control block diagram of d and q axis current controller is shown in Figure 3.5 while the PQ controller for MSC is shown in Figure 3.6.

3.2.1.1.3 DC-link Voltage Control

The outermost loop of the control structure is the dc-link voltage controller. The dynamics of the voltage across the dc-link capacitor, V_{dc}, with respect to converter output power, P_s, can be described in terms of a transfer function as [98, 100]

$$G_{dc}(s) = \frac{V_{dc}^2}{P_s} = \left(\frac{-2}{C_{dc}}\right)\frac{(s\tau_{dc} + 1)}{s} \tag{3.7}$$

where $\tau_{dc} = 2(L_f + L_g)P_{so}/3V_{do}^2$. The transfer function of $G_{dc}(s)$ is a linearised small-signal model where P_{so} is the steady-state power output of the converter and V_{do} is the d-axis steady-state voltage at the point of common coupling of the converter to the microgrid. It is a non-minimum phase system with a right half plane zero, whose location depends on the steady-state value of P_{so} and V_{do}. If these two parameters are varied, then the controller needs to be redesigned to ensure the required stability margin. In other words, the controllers are designed to exchange rated power at a specific voltage level, and hence the exchanged power through the dc-link should not exceed its maximum limit. In order to design a controller that regulates the dc-link voltage with the required gain and phase margin to ensure satisfactory performance, a type-2 controller can be designed. The generic transfer function of a type- 2 controller can be written as

$$C_{dc}(s) = \frac{K_{dc}(s + \omega_z)}{s(s + \omega_p)} \tag{3.8}$$

Such type of controller can be designed using the *K*-factor method, as described in [102]. The closed-loop control system of the dc-link voltage can be realised by the block diagram of Figure 3.7. It should be noted here that, while regulating the dc-link

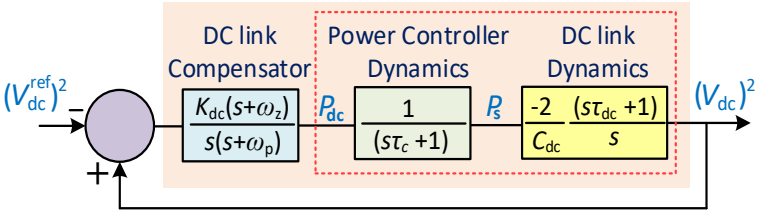

Figure 3.7. Block diagram of dc-link voltage controller for MSC.

voltage the reference power of P_{ref} in Equation (3.6) is P_{dc} (i.e., the power that needs to be exchanged bi-directionally to keep the dc-link voltage fixed to its reference value) as can be seen from Figure 3.7. As the voltage tracking loop is made almost 1000 times faster than the power control loop, the overall system dynamics of the dc-link voltage can be assumed as

$$G_{\text{OL}}(s) = G_{\text{c}}(s)G_{\text{dc}}(s) = \left(\frac{-2}{C_{\text{dc}}}\right)\frac{(s\tau_{\text{dc}}+1)}{s(s\tau_{\text{c}}+1)} \tag{3.9}$$

Hence, $G_{\text{OL}}(s)$ is the open-loop transfer function assumed to apply the K-factor method. The steps of designing the controller using this method are discussed in detail in [100-101]. The close loop frequency responses of all the three control loops are shown in Figure 3.8. The close loop bandwidths of voltage tracking, power, and dc-link controller are 318kHz, 300Hz, and 20Hz, respectively.

3.2.1.2 Control of LSC

Two separate modes of operation for the LSC are considered that depend on the status of the microgrid. It has been proposed that to form a CMG, the LSC of all HMGs should operate under droop control mode to enable power-sharing, whereas the LSC of the FMGs and PMGs should operate in constant power (PQ) control mode (Refer to the flowchart of Figure 3.2). The LSCs connected to HMGs, form the CMG and provide the required droop voltage and angle references that enable power-sharing among the HMGs within a CMG, whereas it will absorb or inject the desired amount of power from the interconnecting power lines to alleviate the overloading or over-generation situations respectively when a microgrid becomes PMG.

To realise the above objective, the frequencies of microgrids need to be continuously monitored. If the microgrid is overloaded, then a control mechanism should determine

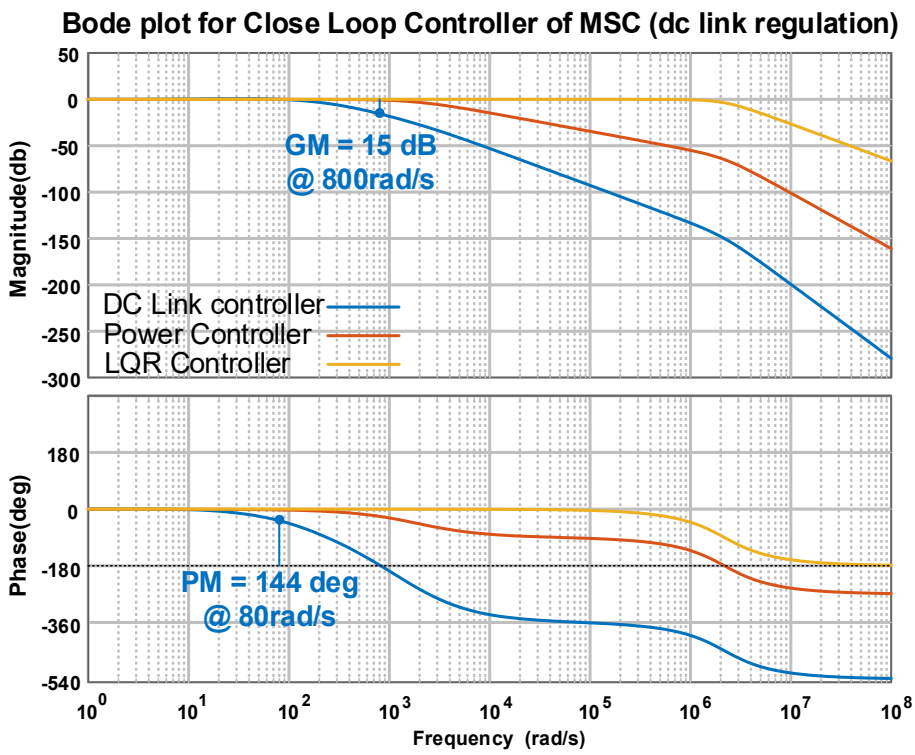

Figure 3.8. Frequency response plots of the control loops for the MSC.

the amount of power that needs to be absorbed from the interconnecting link by the PMG to return the frequency of the microgrid to the acceptable limit. The concept is equally applicable when the microgrid has surplus power generation and its frequency rises beyond the acceptable limit. Thus, the LSC of an overloaded or over-generating microgrid will start to operate in the constant PQ mode (see the flowchart of Figure 3.2). A frequency deviation-based control system determines the reference active power (P_{ref}), while the reactive power (Q_{ref}) reference is assumed to be zero. When the overloading or over-generation is alleviated, another frequency deviation-based controller determines the new status of the microgrid as HMG, and hence, the LSC of that microgrid changes its mode of operation from the constant PQ control to droop control, as can be realised by the flowchart of Figure 3.2.

During the idle operation of the CMG, (i.e., when all microgrids are HMGs and no power exchange is taking place), the LSCs of all the microgrids operate under the droop control mode. Also, during the nominal operation of an HMG within the CMG, the HMG should continue operating in droop mode to support the PMG and facilitate power exchange. The employed droop control is a virtual impedance technique-based angle-voltage droop. The LSC's mode of operation changes from droop to PQ and vice versa. This is done through a reference selection controller that switches between the

two modes of operation of LSC, by continuously monitoring the microgrid's frequency. Depending on the microgrid's status, the reference selection controller selects the appropriate voltage reference for voltage tracking and switching controller to enable the LSC to operate in either one of the modes, as seen from Figure 3.3.

3.2.1.2.1 LSC Control for HMG Operation

The LSC of an HMG operates under the angle-voltage droop control mode (on contrary to the conventional frequency-voltage droop that has been employed for the DERs within the microgrids). Employing such an angle-voltage droop instead of the frequency-voltage droop will set the frequency of the interconnecting lines at a fixed value (e.g., 50 Hz). The angle and voltage droop equations for the LSC of kth microgrid can be written as [102-105].

$$\delta_k = \delta_{\text{o}} - m_{\text{MG}-k} P_{\text{line}} \tag{3.10}$$

$$V_k = V_{\max} - n_{\text{MG}-k} Q_{\text{line}} \tag{3.11}$$

where $m_{\text{MG}-k}$ and $n_{\text{MG}-k}$ are the droop coefficients of the kth microgrid's LSC, and derived from

$$m_{\text{MG}-k} = (\delta_{\max} - \delta_{\min})/P_{\text{line}}^{\max} \tag{3.12}$$

$$n_{\text{MG}-k} = (V_{\max} - V_{\min})/2Q_{\text{line}}^{\max} \tag{3.13}$$

in which subscript $_{\min}$ and $_{\max}$ represents the minimum and maximum allowable limits for angle and voltage while $P_{\text{line}}^{\max}$ and $Q_{\text{line}}^{\max}$ are the maximum active and reactive powers injected/absorbed by each microgrid to the interconnecting lines. All the LSCs have similar $\Delta\delta = \delta_{\max} - \delta_{\min}$ and $\Delta V = V_{\max} - V_{\min}$. It should be mentioned here, that the transition from PQ to droop mode cannot be realised using the frequency-voltage droop because, when all the microgrids become HMG with no exchange of power through the interconnecting lines, the voltages at the output of the LSCs will be operating at the same frequency. Thus, the synchronization among the LSCs is not possible in this situation without having a centralised controller backed up by a data communication link. The decentralised control scheme would work only under the angle-voltage droop control technique. However, the conventional angle-voltage droop control technique cannot ensure the desired power-sharing among the HMGs unless a modified angle droop [102] mechanism is implemented using the virtual

impedance method. To implement the virtual impedance-based modified angle droop, Equation (3.10) and (3.11) needs to be transformed into the $\alpha\beta$ coordinates and the voltage across the virtual impedance needs to be subtracted. Hence, the reference angle and voltage equation can be modified and rewritten $\alpha\beta$ coordinates as

$$V_{\alpha-k}^{\mathrm{ref}} = V_k \cos\delta_k + X_{\mathrm{v}}^k I_{\mathrm{g}}^k \sin\theta_{\mathrm{g}}^k \tag{3.14}$$

$$V_{\beta-k}^{\mathrm{ref}} = V_k \sin\delta_k - X_{\mathrm{v}}^k I_{\mathrm{g}}^k \cos\theta_{\mathrm{g}}^k \tag{3.15}$$

where $X_{\mathrm{v}}^k = \omega_{\mathrm{ref}} L_{\mathrm{v}}^k$ and $i_{\mathrm{g}}^k = I_{\mathrm{g}}^k \angle\theta_{\mathrm{g}}^k$ are respectively the virtual impedance and current of the coupling inductance. Then, the reference voltage and phase angle for the LSC of microgrid-*k* operating under the modified droop control technique, are calculated as

$$V_{\mathrm{dr}}^k = \sqrt{(V_{\alpha-k}^{\mathrm{ref}})^2 + (V_{\beta-k}^{\mathrm{ref}})^2} \tag{3.16}$$

$$\delta_{\mathrm{dr}}^k = \tan^{-1}\left(\frac{V_{\beta-k}^{\mathrm{ref}}}{V_{\alpha-k}^{\mathrm{ref}}}\right) \tag{3.17}$$

From Equation (3.16) and (3.17), the instantaneous reference voltage for the LQR switching control block of the LSC in microgrid-*k* can be determined as

$$V_{\mathrm{a}-k}^{\mathrm{ref}} = V_{\mathrm{dr}}^k \sin(\omega_{\mathrm{ref}} t + \delta_{\mathrm{dr}}^k) \tag{3.18}$$

$$V_{\mathrm{b}-k}^{\mathrm{ref}} = V_{\mathrm{dr}}^k \sin(\omega_{\mathrm{ref}} t + \delta_{\mathrm{dr}}^k - 120°) \tag{3.19}$$

$$V_{\mathrm{c}-k}^{\mathrm{ref}} = V_{\mathrm{dr}}^k \sin(\omega_{\mathrm{ref}} t + \delta_{\mathrm{dr}}^k - 240°) \tag{3.20}$$

where ω_{ref} is selected based on the desired frequency level in the three-phase ac power lines (e.g., 50 Hz). The virtual impedances to share power between microgrid-*i* and *j* can be calculated based on their droop coefficients as [103, 105-106]

$$\frac{m_{\mathrm{MG}-i}}{m_{\mathrm{MG}-j}} = \frac{L_{\mathrm{g}} + L_{\mathrm{v}}^i}{L_{\mathrm{g}} + L_{\mathrm{v}}^j} \tag{3.21}$$

Figure 3.9 shows the block diagram of the modified angle-voltage droop control technique. It may be noted here that, the central controller of a microgrid determines the amount of power that is going to be shared by each HMG and it is governed by numerous factors such as distance among the microgrids, cost of power generation, line loss, willingness to participate in power exchange and so on [106-108]. Different types of optimization and decision-making techniques are proposed in ref [109-112]

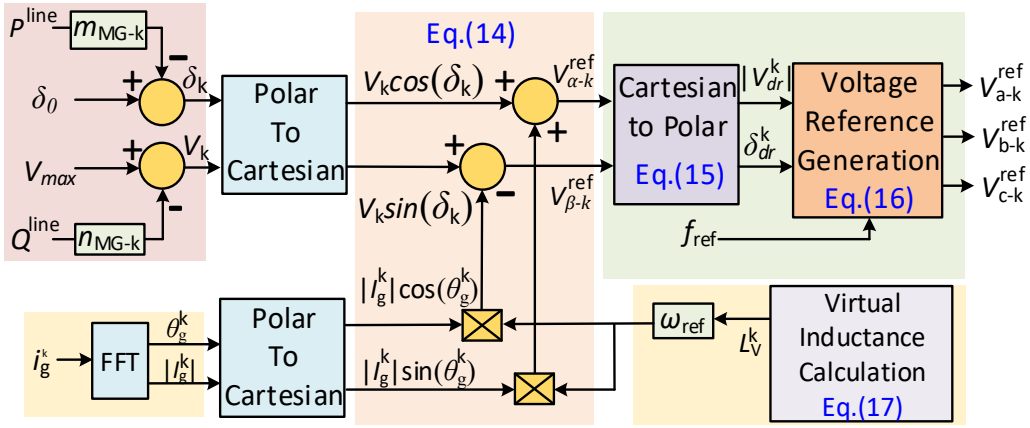

Figure 3.9. Modified angle-voltage droop control employed for the LSC during HMG operation.

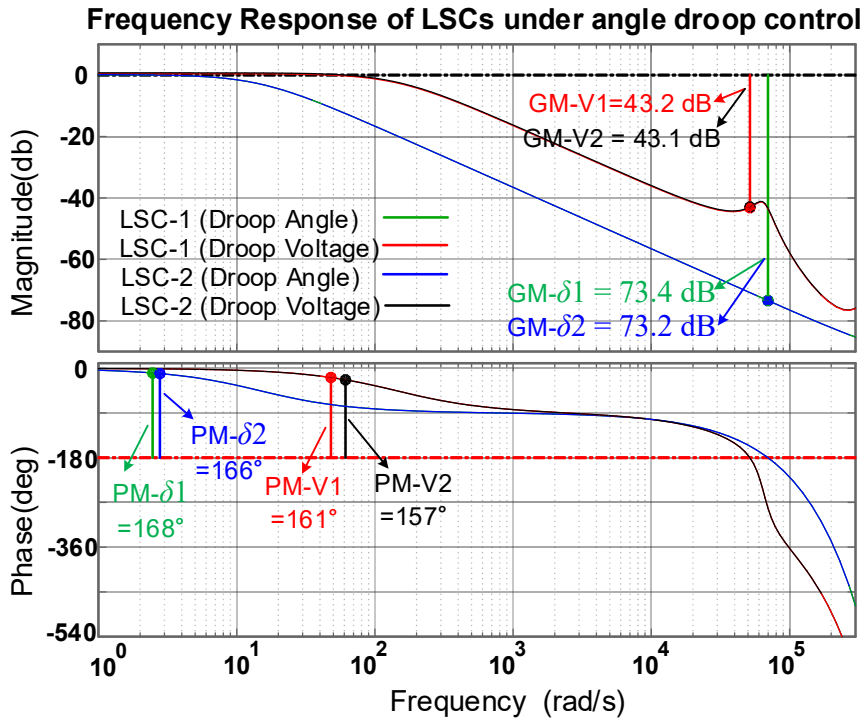

Figure 3.10. Frequency response plots of LSC operating under modified angle-voltage droop control.

that determine the optimum power-sharing and evaluates the desired droop coefficients. Thus, the droop coefficient of m_{MG} and n_{MG} will be modified based on Equation (3.21) to achieve the desired power-sharing.

The frequency response plot of LSCs of two HMGs operating under modified angle droop control, while supporting one PMG, is shown in Figure 3.10. The plot shows both the angle and voltage droop response of LSCs.

It may be mentioned here that, the power-sharing ratio of the two LSCs operating under droop mode is set to 2:1 in this example. Hence it can be seen from Figure 3.10 that, the LSC with the larger droop coefficients has a slightly smaller gain and phase margin compare to the other LSC with smaller droop coefficients.

3.2.1.2.2 LSC Control for PMG Operation

When a microgrid becomes PMG, the LSC of that particular microgrid switches its operation from droop control to frequency regulation mode, which is a constant PQ control mode where the active power reference is generated through an outer frequency control loop. This mode of operation of PMG through its LSC can be termed as frequency regulation or control mode. The PMG alleviates its overloading and/or over-generation situation through this mode of operation. If a microgrid becomes PMG by overloading, a frequency deviation-based control mechanism termed as overload frequency controller (OLFC) gets activated and determines the amount of power that should be absorbed from the neighbouring microgrids to retain the microgrid frequency within the acceptable limit. Likewise, during over-generation, the over-generation frequency controller (OGFC) gets activated to determine the required amount of power to inject into the neighbouring microgrids. Thus, the LSC will start to operate in the constant PQ mode when a microgrid becomes a PMG. Figure 3.11 shows an arrangement of such a control mechanism along with its control activation logic. The reference of the active power (P_{ref}) is determined by either OLFC or OGFC block while the reference of the reactive power (Q_{ref}) is assumed to be zero. Once the overloading or over-generation problem is alleviated, another frequency deviation-based control system determines the new status of the microgrid as an HMG that can resume its normal operation, and hence, the LSC of that microgrid should change its operation from the constant PQ mode to the droop control mode.

The desired active power reference is determined by the frequency controller that employs two separate proportional-integral (PI) controllers and the necessary control logic and circuitry. Then, the desired reference power during an overload or over-generation is obtained either by activating the OLFC or OGFC, respectively and is passed through a 4×1 multiplexer that selects the proper reference. The overall control block diagram of the frequency controller is shown in Figure 3.12.

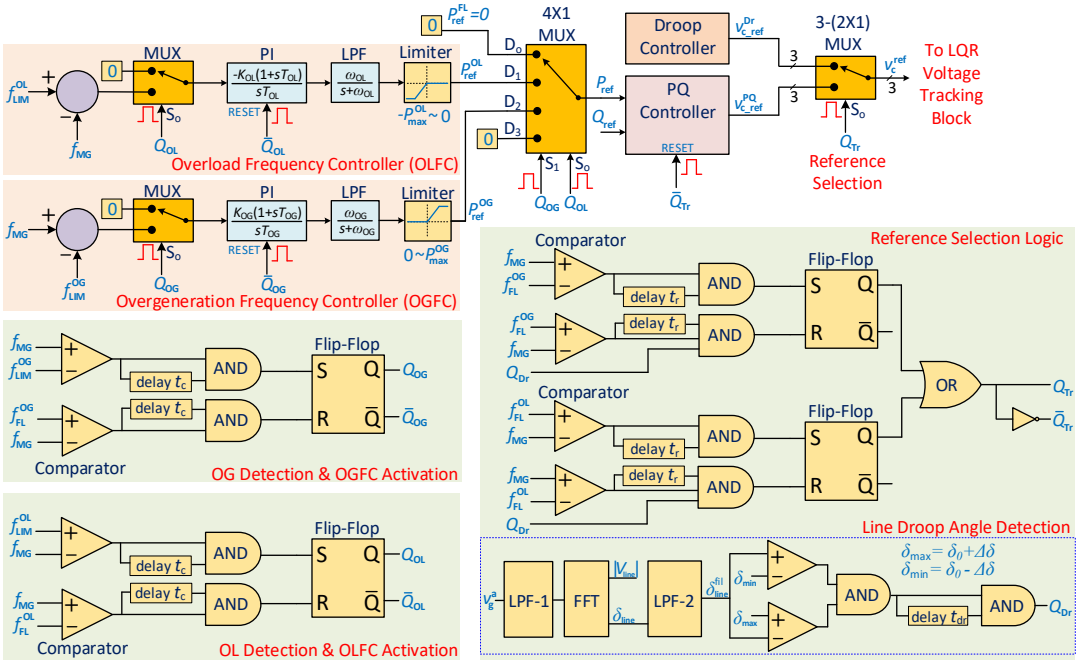

Figure 3.11. Frequency controller of LSC for PMG operation in topology-1.

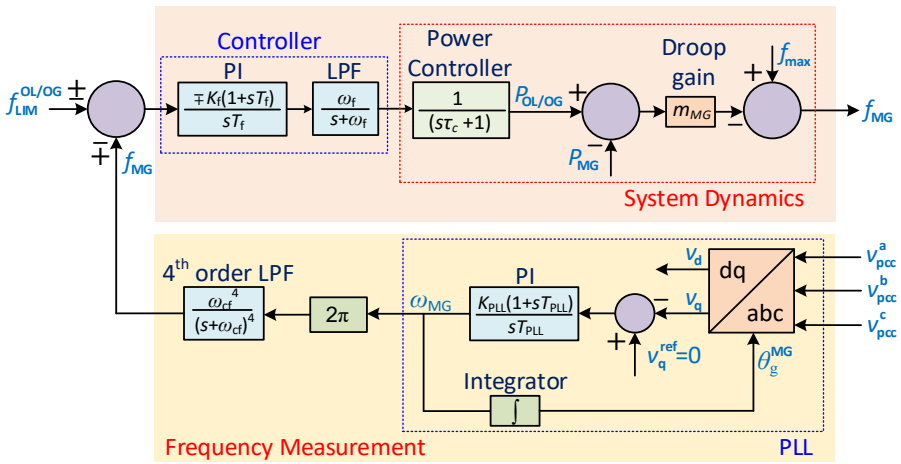

Figure 3.12. Frequency controller for overload and over-generation prevention.

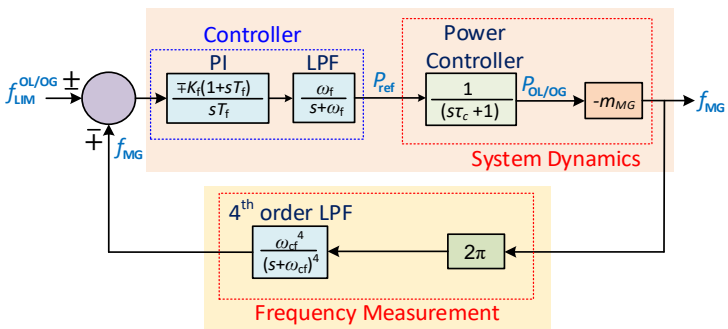

Figure 3.13. Assumed close loop control mechanism of frequency controller.

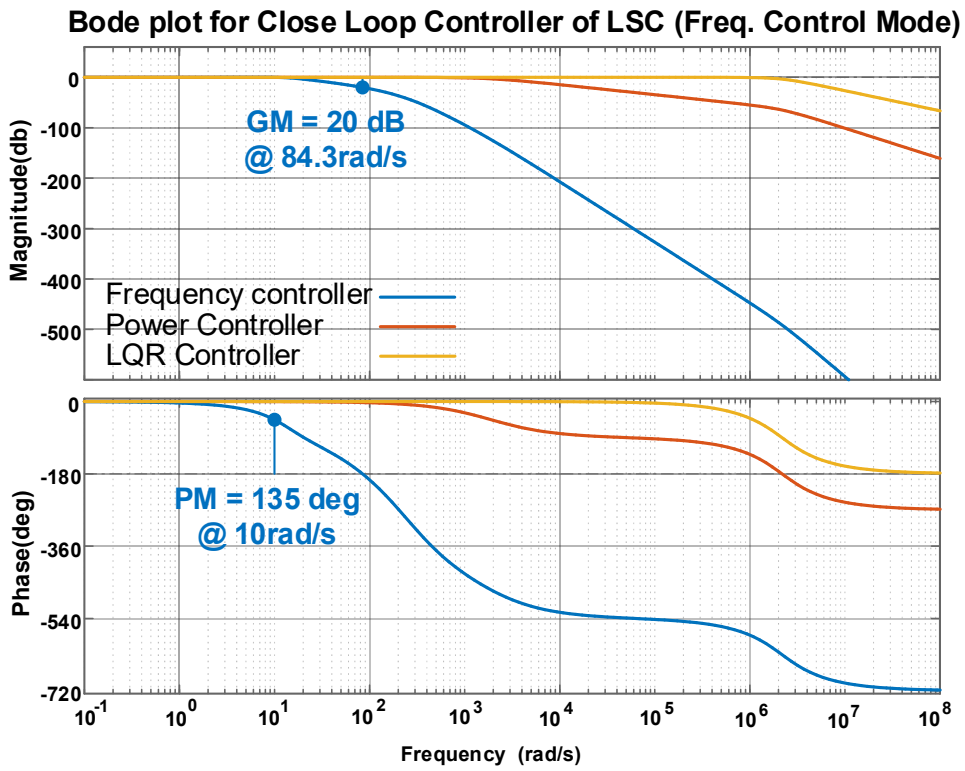

Figure 3.14. Frequency response plots of LSC operating under frequency regulation mode.

To design the frequency controller, P_{MG} and $f_{\max}$ can be considered as a disturbance to the system. The PI controller employed for the PLL is very fast compared to the overall system dynamics and LPF; hence, the PLL block can be assumed to be a unity gain block, and thus, the overall control block diagram of Figure 3.12 can be represented as shown in Figure 3.13. Based on the closed-loop control system of Figure 3.13, the PI controllers can be designed based on the symmetrical optimum method as described in [99]. The bode plot of the closed-loop frequency regulation controller is shown in Figure 3.14.

A proper reference selection logic is required to facilitate a smooth transition between constant PQ control mode (for FMG and PMG) and droop control mode (for HMG) without causing unwanted transients, oscillations, and instability. Such an arrangement to change over between the operating modes of LSC is shown in Figure 3.11. The three-phase reference voltages are either selected from the droop control block or PQ controller block through three sets of 2×1 multiplexers using the reference selection logic employed in the mode transition controller. Then the appropriate reference voltages are passed to the LQR voltage tracking and switching control block. When

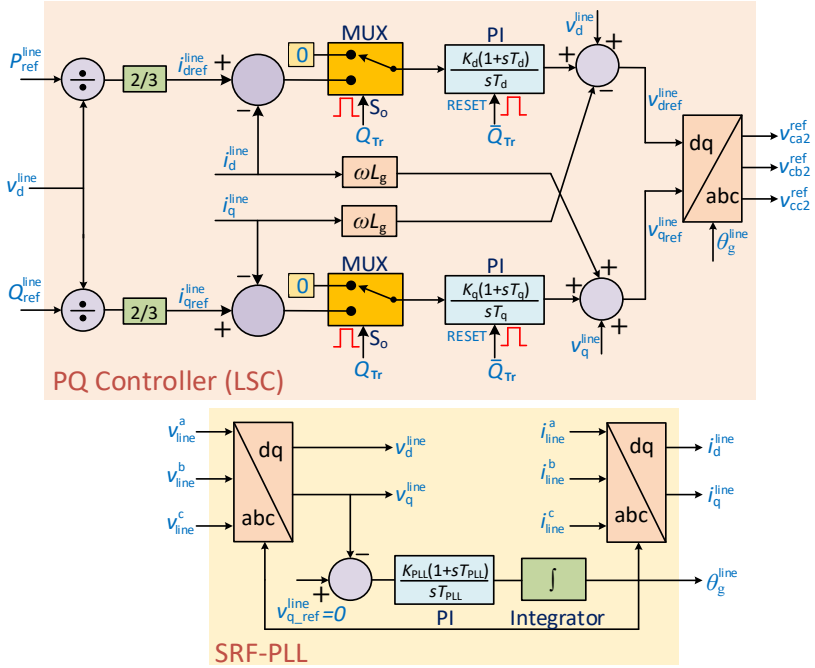

Figure 3.15. Block diagram of the PQ controller for LSC operation.

the voltage references are selected from the droop control block, the PI controllers of the PQ control block should be held into reset mode to avoid integrator drift, windup, and unwanted overshoot upon activation. The switchover from droop to constant PQ mode (i.e. an HMG becoming an FMG or PMG) is straightforward as only the reset signals need to be withdrawn and the PI controllers will be made operational. However, during switchover from constant PQ to droop control mode (i.e., an FMG or PMG becoming an HMG), an additional line angle detection logic is required. When overloading or over-generation problem is over, a PMG or FMG should not be allowed to switch back to droop mode unless all the remaining microgrids within the CMG network are HMG (i.e., no operational PMG) and operating in the same phase angle, δ_0, where δ_0 is the phase angle of the line voltage when there is zero or no power-sharing among the microgrids through the interconnecting lines (i.e., $P_{\text{line}} = 0$). For this purpose and to facilitate such mode transition, a line angle detection mechanism, consists of a fast Fourier transform (FFT) block and a window detector, is used to detect whether all the microgrids are HMGs or not, as shown in Figure 3.11. Hence, the PQ controller of the LSC needs to be modified as shown in Figure 3.15 to facilitate such switchover.

3.2.2 Single-phase AC interconnection (Topology-2)

Topology-2 is a single-phase ac interconnecting line with back-to-back power electronic converters. In this topology, the MSC is assumed to be a three-phase, three-leg VSC whereas, the LSC is assumed to be a single-phase H-bridge VSC using IGBTs or MOSFETs. Each VSC is connected to their point of common coupling through LCL filters (i.e., a three-phase LCL for the MSC and a single-phase LCL for the LSC). The structures of MSC and LSC are shown schematically in Figure 3.16. Like topology- 1, any other type of three-phase and single-phase VSC topologies can also be used instead of the assumed topologies for the MSC and LSC, respectively.

3.2.2.1 Control of MSC

The control of MSC for this topology is identical to the technique as discussed in Section 3.2.1.1 for three-phase ac interconnection lines (topology-1). It should be noted here that, in this topology, the dc-link of the back-to-back converter is comprised of only one capacitor and should not be grounded, unlike the topology-1 where the dc-link is comprised of two split capacitors with the midpoint grounded.

3.2.2.2 Control of LSC

The control technique for LSC in this topology is similar to the methods discussed for the topology- 1. However, some modifications in the control technique are required to implement them for single-phase VSC. Similar to topology-1, the LSCs in this topology are operating in two modes – droop control and constant PQ mode, depending on the microgrid's status. The conditions of their operation and transition between the modes based on the microgrid's status are identical to topology-1 and will not be repeated here. Only the modifications adopted to incorporate the control mechanism will be discussed here.

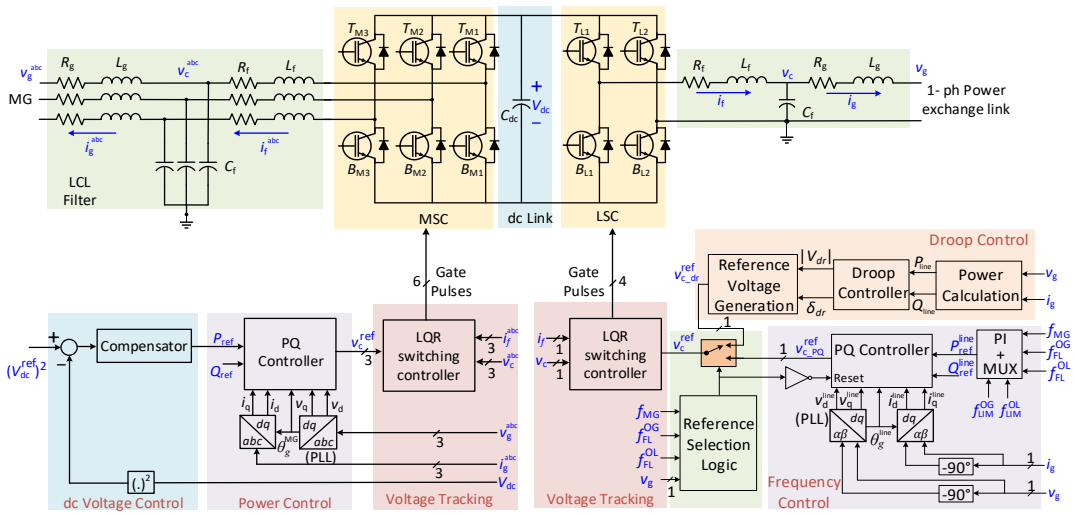

Figure 3.16. Assumed structure and close loop control mechanism of the MSC and LSC for topology-2.

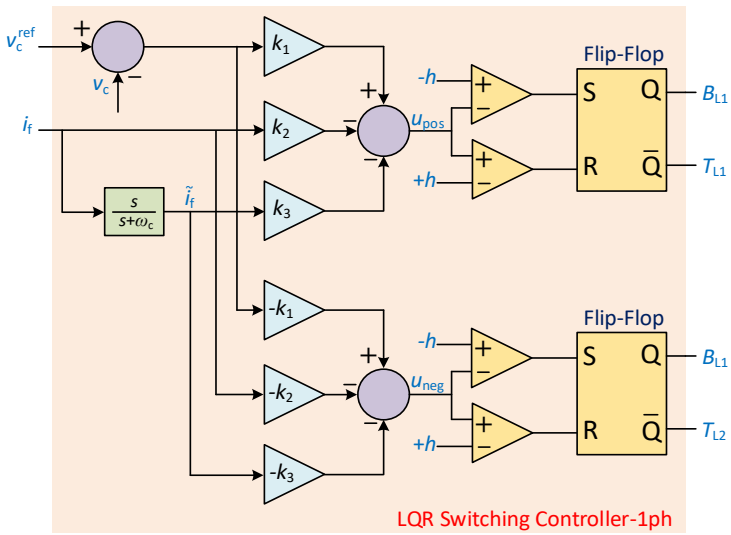

Figure 3.17. Linear Quadratic Regulator based switching and voltage tracking for single-phase VSC.

The first key difference is reference voltage generation for the single-phase VSC while operating in droop mode (i.e., HMG operation). In this regard, based on Equation (3.16) and (3.17), the instantaneous reference voltage for single-phase VSC can be expressed as

$$V_{\mathrm{a}-k}^{\mathrm{ref}} = V_{\mathrm{dr}}^{k} \sin(\omega_{\mathrm{ref}} t + \delta_{\mathrm{dr}}^{k}) \tag{3.22}$$

$$V_{\mathrm{b}-k}^{\mathrm{ref}} = V_{\mathrm{dr}}^{k} \sin(\omega_{\mathrm{ref}} t + \delta_{\mathrm{dr}}^{k} - 180°) \tag{3.23}$$

which are the reference voltages, $v_{\mathrm{c}}^{\mathrm{ref}}$ for the single-phase LSC and applied to the LQR voltage tracking and switching block. Thus, the LQR switching controller needs to be

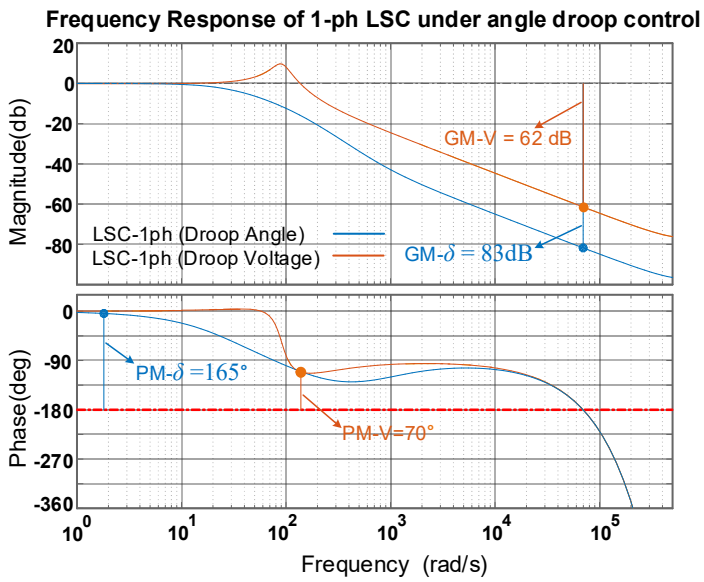

Figure 3.18. Frequency response of single-phase LSC operating under modified angle-voltage droop control.

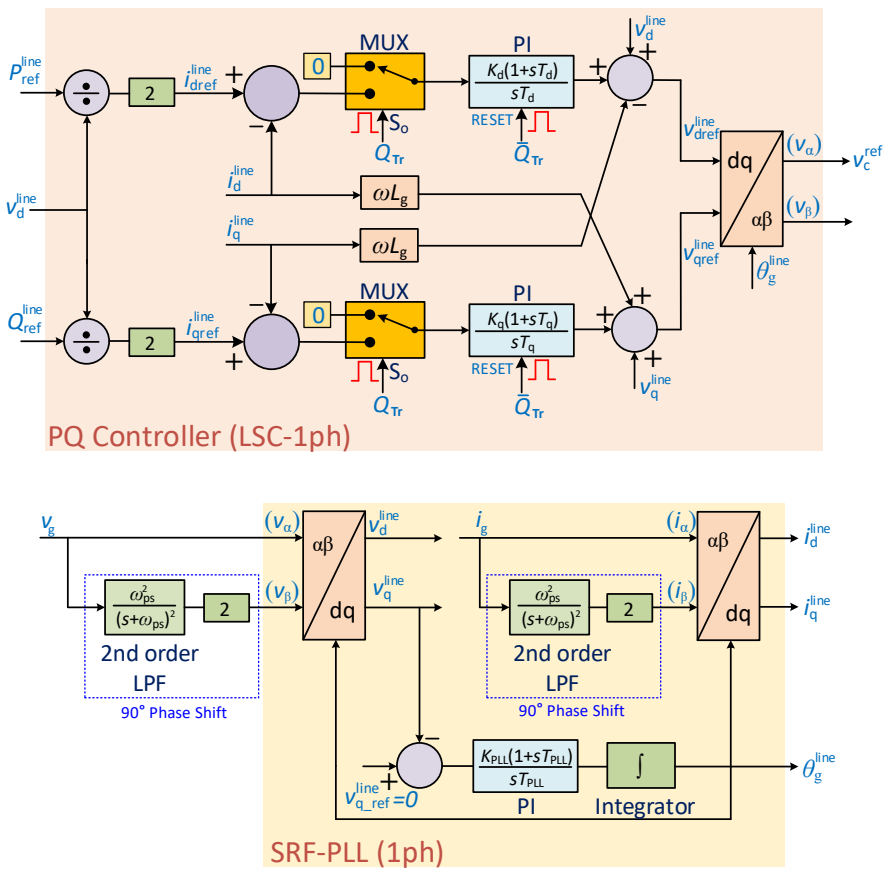

Figure 3.19. Block diagram of the PQ controller for single-phase LSC.

modified as shown in Figure 3.17. The bode plots for single-phase LSC operating under droop control are shown in Figure 3.18. It can be observed from Figure 3.18

that, the single-phase LSC has a relatively smaller phase and gain margin as compared to the three-phase LSC. In other words, the three-phase LSC operating in droop mode appears to be more stable than the single-phase LSC.

Finally, the PQ controller for the LSC needs to be modified and implemented for single-phase topology. The single-phase PQ controller implemented in dq frame for LSC is shown in Figure 3.19 along with its reset and control signals. To implement the PQ controller in dq frame for a single-phase converter, $\alpha\beta$ to dq transformation (Clark transformation) is used where the measured line voltage v_{g} and current i_{g} are the α components for voltage and current respectively, whereas a 90° phase-shifted version of v_{g} and i_{g} are the β components for voltage and current. The phase shift in voltage and current are introduced by a critically damped second order low pass filter that operates with a gain of 0.5 and phase shift of 90° at its cross over frequency, ω_{ps} (which is 50Hz or 314.16rad/s in this case). To compensate for this gain of 0.5, the signal needs to be amplified with a gain of 2. To determine the angle of the interconnection line, $\theta_{\mathrm{g}}^{\mathrm{line}}$, a synchronous reference frame PLL is used as before.

3.2.3 DC interconnection (Topology-3)

Topology-3 is a dc interconnecting line with a single VSC. It is connected to the microgrid's three-phase ac lines and facilitates bi-directional power flow between the microgrid and the dc-link. The dc-links are directly connected to the dc interconnecting lines that form the CMG network. In this topology, a single VSC serves the functions of both the MSC and LSC of the previous two topologies. The VSC connected to each HMG within the CMG regulates the dc voltage across the dc-link capacitor. As the HMGs will share the power injected/absorbed by the PMGs of the CMG, an active power-dc voltage droop technique is employed that determines the reference dc voltage such that the power shared by the HMGs is as defined by the ratios of the droop coefficients. On the other hand, the VSC connected to each PMG operates in constant PQ mode and facilitates absorption or injection of the required active power to retain and regulate the frequency of the PMG within its acceptable limits. The structure and control mechanism of the VSC are discussed in the following subsections:

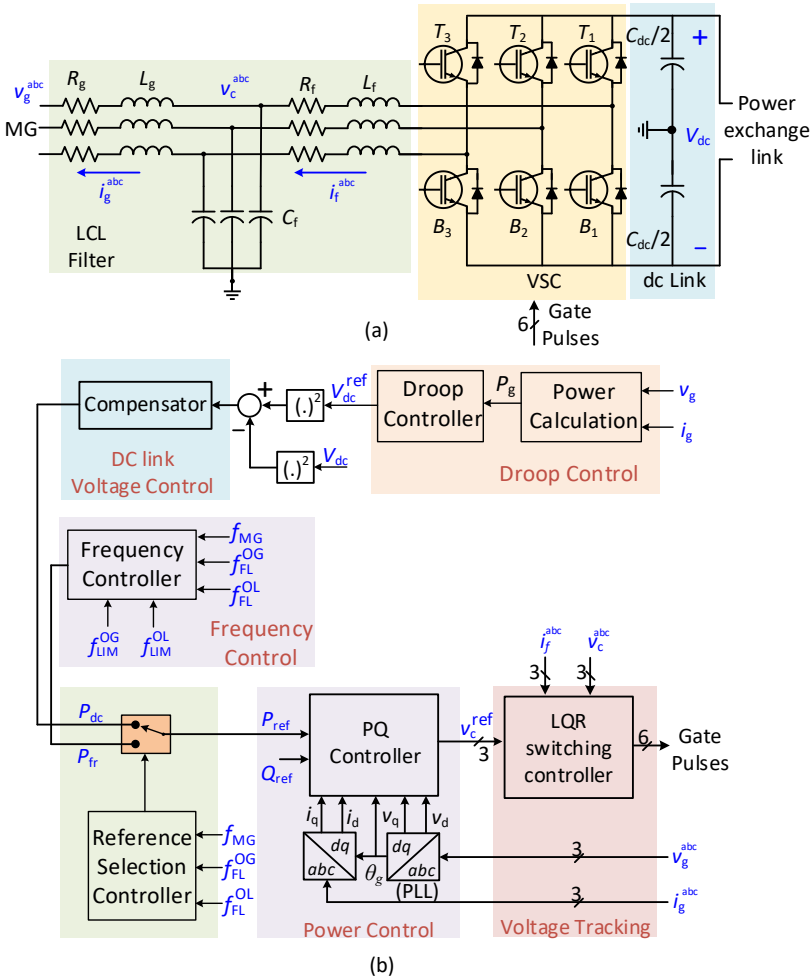

Figure 3.20. VSC operation for topology-3 (a) VSC structure, (b) Closed-loop control system.

3.2.3.1 VSC Structure

The assumed VSC structure is a three-phase, three-leg topology using MOSFETs or IGBTs. The VSC is connected to the microgrid through an LCL filter while the dc-link is formed with two series-connected dc capacitors with midpoint grounded. The schematic of the VSC structure is shown in Figure 3.20(a). It may be noted that any other three-phase VSC topology can also be used.

3.2.3.2 VSC Control

The overall close loop control system of the VSC is shown in Figure 3.20(b). The detailed operation and design steps of the LQR Switching controller, PQ controller,

and dc-link voltage controller are identical to the MSC control of topology-1 as discussed in Section 3.2.1.1. The only difference is that, in this topology, the reference voltage of the dc power exchange link (i.e., the voltage across the dc capacitor) should be generated through dc droop control block whereas, in topology-1 the dc-link voltage was fixed and predefined. The VSC operates in two different modes, depending on the status of the microgrid, i.e. when it is connected to an HMG or a PMG. Each of these modes is discussed separately below.

3.2.3.2.1 VSC of an HMG

The VSC connected to an HMG is operating in droop mode and primarily responsible for regulating the dc-link voltage across the dc capacitor V_{dc}, to the desired level of $V_{\mathrm{dc}}^{\mathrm{ref}}$. The desired voltage level is not constant as the value depends on the total power that the HMG should absorb from the link or supply to that. If the CMG network includes multiple HMGs, then they can share the power supplied to the PMGs or received from them at any desired ratio. This can be easily realised by using an active power - dc voltage droop control mechanism for the output dc-link voltage of each VSC. This is schematically illustrated by the dc droop control block in Figure 3.20(b) and can be mathematically represented as

$$\left(V_{\mathrm{dc}}^{\mathrm{ref}}\right)_{\mathrm{MG}\text{-}i} = V_{\mathrm{nom}} - m_{\mathrm{MG}\text{-}i} P_{\mathrm{MG}\text{-}i} \tag{3.24}$$

where m_{MG} and P_{MG} denote the dc droop coefficient and the active power absorbed/injected by the VSC respectively and V_{nom} is the nominal voltage of the dc-link (e.g., 1 pu). It should be noted that an active power absorption will be considered as negative whereas, active power injection by the VSC is considered as positive. According to Equation (3.24), the ratio of the power absorbed (or injected) by HMG i and j will be the reciprocal of the ratio of their droop coefficients, i.e.,

$$m_{\mathrm{MG}\text{-}i} P_{\mathrm{MG}\text{-}i} = m_{\mathrm{MG}\text{-}j} P_{\mathrm{MG}\text{-}j} \tag{3.25}$$

3.2.3.2.2 VSC of a PMG

The VSCs of a PMG should absorb the required amount of power from the dc-link into the PMG when it is overloaded. Likewise, if the PMG experiences over-generation,

the VSC should inject the required amount of power from the PMG to its dc-link. Thus, the frequency of the PMG will be retained to the acceptable range through such power exchange. To facilitate such power exchange, the VSC is required to operate in the constant PQ mode. As the key objective of power exchange mechanism in CMG network is to control the active power flow, the reference of the reactive power (Q_{ref}) is set to be zero. The reference for the active power (P_{ref}) is determined through the deviation of the PMG's frequency from the acceptable limit. Such a frequency regulation controller is schematically shown in Figure 3.21.

The switchover in the mode of operation from droop to PQ and vice versa is achieved through a reference selection controller which monitors the microgrid's frequency continuously. Depending on the status of the microgrid, the appropriate P_{ref} will be selected, as schematically illustrated in Figure 3.21.

When a microgrid becomes a PMG, the frequency controller gets activated. During overloading, a control mechanism termed as overload frequency controller (OLFC), determines the total amount of power that should be received by that particular PMG from the neighbouring microgrids to return the microgrid frequency to the acceptable limits. Similarly, during over-generation, the over-generation frequency controller (OGFC) gets activated and determines the required power that should be delivered to the neighbouring microgrids. Thus, when a microgrid becomes a PMG, its VSC should change its operation from droop control to the constant PQ mode. Such a control mechanism can be realised using a hysteresis controller implemented with the reference selection logic and schematically shown in Figure 3.21. The active power reference (P_{ref}) is determined by a frequency deviation-based overload or over-generation control mechanism while the reactive power reference (Q_{ref}) is set to be zero. Once the overloading or over-generation situation is mitigated, another frequency deviation-based control mechanism will determine the new status of the microgrid. After the detection of the microgrid's status and certain predefined time delay as set by the controller, the VSC of that particular microgrid will change from the constant PQ mode to the droop control mode and hence, deactivates the frequency controller.

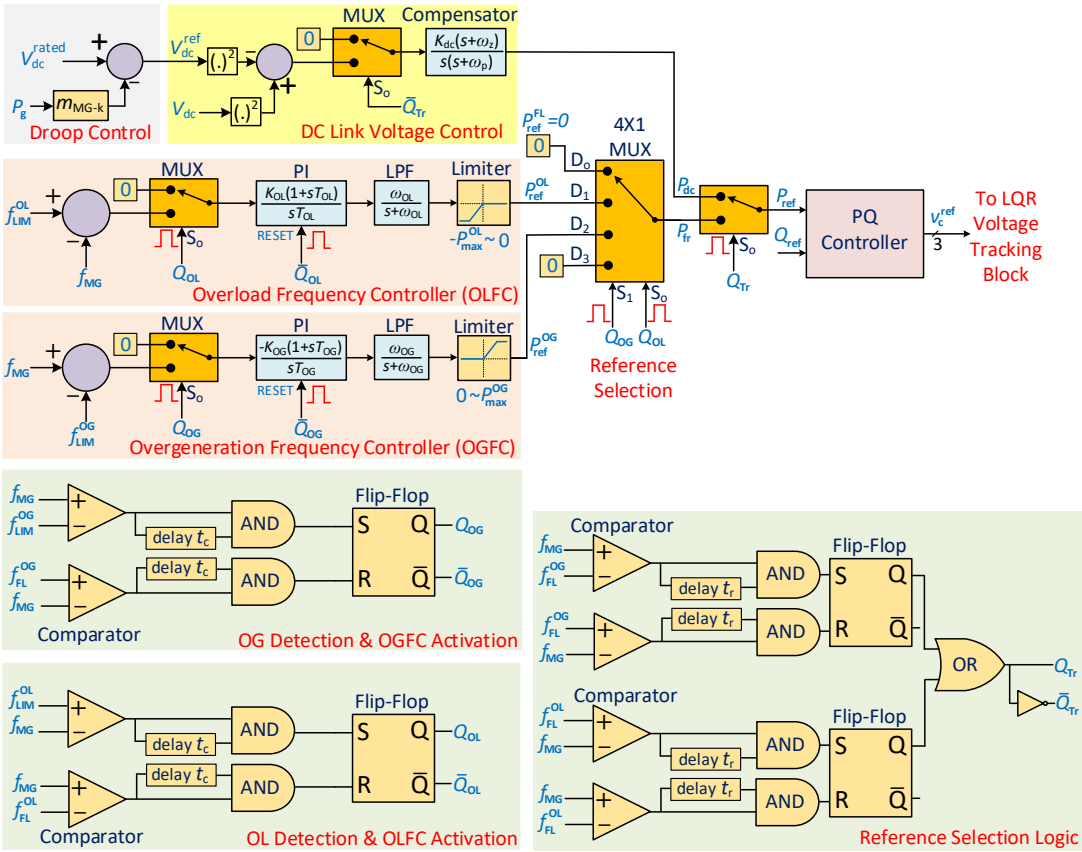

Figure 3.21. Frequency regulation controller of VSC for PMG operation in topology- 3.

The frequency controller determines the desired power reference through two different PI-based closed-loop control systems along with its necessary control logic and circuitry. Then, the desired power reference is selected through a 4×1 Multiplexer circuit that selects the proper power reference during the overload or excess-generation situation respectively by activating the OLFC or OGFC. To coordinate between droop control mode (for HMG) and constant PQ control mode (for the FMG and PMG), a proper reference selection logic is needed to switch over between the modes smoothly without causing unwanted transients, oscillations, and instability. The reference selector will select proper active power reference either from the droop control-based dc-link controller block or frequency controller block through a 2×1 multiplexer and pass it to the PQ control block. Once a PMG becomes an HMG, the reference selector will enable the VSC to switch back to droop-based dc-link voltage control mode.

3.3 Coordinated Power Sharing among BES and CMG

This study proposes a two-stage, coordinated power-sharing strategy among BES and coupled microgrids for overload management in autonomous microgrids, through dynamic frequency control. Both local BES and the neighbouring microgrids can work in conjunction or individually to supply the required overload power demand. For this, BES' state of charge should be above a minimum level and extra power generation capacity needs to be available in the neighbouring microgrids. A predefined framework with appropriate constraints and conditions, under which the power exchange will take place, is defined and formulated. For this purpose, two different self-healing agents, functioning in a decentralised (communication free) manner. This is realised by continuously monitoring the microgrid frequency and its BES unit's SoC. This information is then used to cooperatively activate or deactivate two developed self-healing agents, namely, battery frequency controller (BFC) for BES unit, and interconnection frequency controller (IFC) for the coupling of microgrids. These self-healing agents dynamically modify the amount of internal and external power exchange levels based on the BES units' SoC and the microgrids' loading condition.

3.3.1 Network Structure

Let us consider a system of Figure 3.22 where N autonomous microgrids, each consisting of multiple DERs, DGs, loads, one BES and one inter-connection converter (ICC). Each microgrid is monitored, supervised, and controlled through its microgrid central controller, termed as MGCC. The DERs and BES are connected to the microgrid through VSCs. Different VSCs are controlled in different operating modes to regulate the power and frequency of each microgrid. The VSCs of DERs are assumed to be operating in the $P - f$ and $Q - V$ droop control mode [73]. It is assumed that each DER is provided with its local energy storage and thus they can be represented as a dispatchable DER. The structure and operation of the DERs are discussed in [11-12, 73] and is not repeated here. It should be noted that these local storages are independent and different from the BES of each microgrid as the BESs are assigned to support the microgrids in the event of power deficiency and

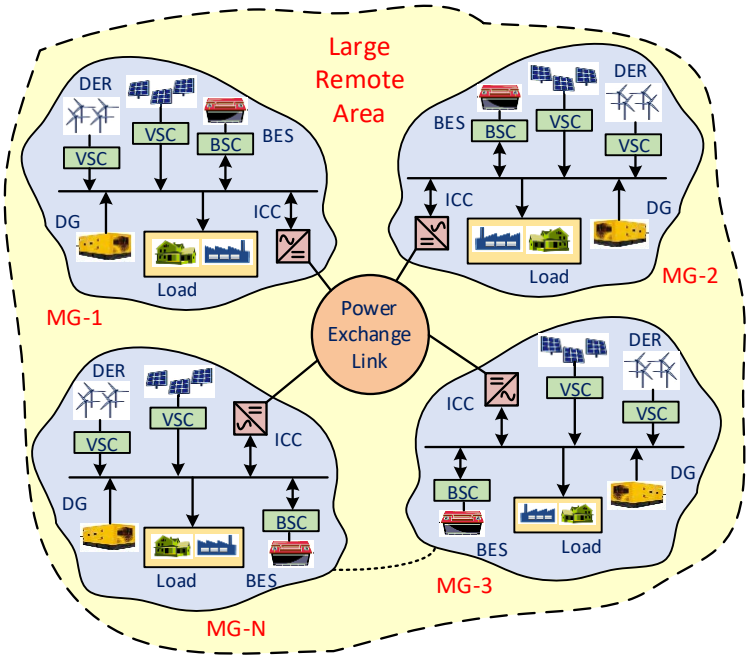

Figure 3.22. Autonomous CMG network with BES to coordinate power-sharing

dynamically regulate the frequency within the acceptable limit. The BES is connected to the microgrid through a separate VSC termed as Battery Energy Storage converter (BSC) that operates in constant PQ mode. The charging or discharging mode of the BES is determined by the MGCC, based on the MG's loading condition. Finally, each microgrid is connected to a common dc power exchange link through its ICC to exchange power with the other microgrids in the event of overloading or power deficiency. Each microgrid can operate independently at any predefined voltage and frequency level without affecting the operation of other neighbouring microgrids.

3.3.2 Control of Converters

The structure of the BSC and ICC are assumed identical and their overall control block diagram is shown in Figure 3.23. Both BSC and ICC are VSCs connected to their respective MG, which enable bi-directional power flow with BES and the dc power exchange link, respectively. Each converter is working in constant PQ mode and has three cascaded feedback control loops, namely, voltage tracking, power control and reference power generation loop, as can be seen from Figure 3.23. The voltage tracking and power control loop are identical for both converters, whereas, the reference power generation loop, which is the most outer loop, is different and depends on the mode of operation of the microgrid and converter.

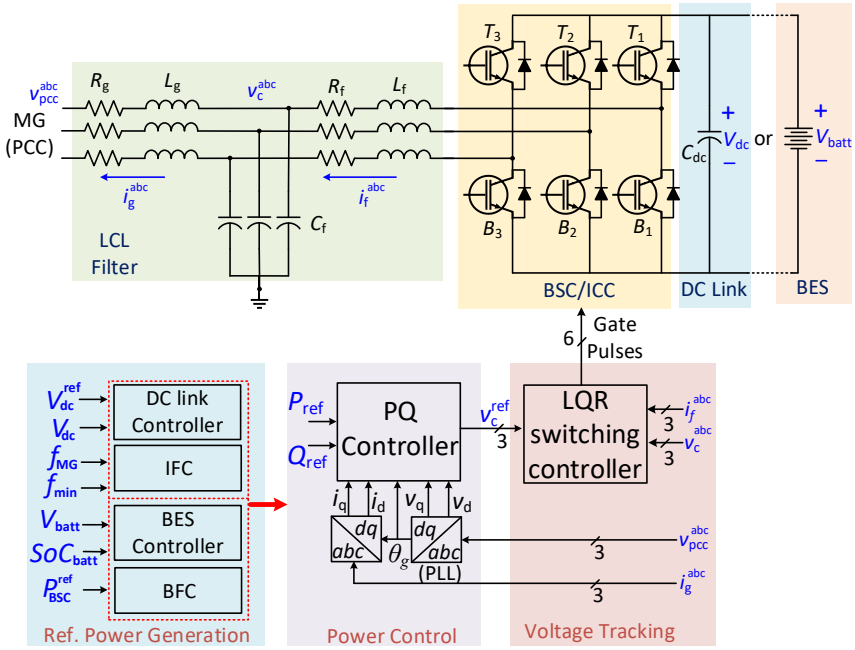

Figure 3.23. Assumed structure and closed-loop control block diagram of VSC and filter system for BSC/ICC

3.3.2.1 Converters Structure

The BSC and ICC structure is assumed to be a three-phase, three-leg VSC using IGBTs or MOSFETs, as schematically shown in Figure 3.23. They are connected to the microgrid through an LCL filter to effectively filter out the undesired switching harmonics. The dc side of the BSC is connected to the BES while a dc capacitor is installed on the dc-link side of the ICC to interconnect it to the power exchange link. It is to be noted that, any other three-phase VSC topology can also be used for BSC and ICC.

3.3.2.2 Converter Control Technique

Both converters are operating in constant PQ mode irrespective of the loading condition of the MG. Only the respective VSC's output power reference varies depending on the MG's loading condition and the outermost control loop which is active during that time. The BSC is primarily controlled by the MGCC through the BES controller block, operating as the outermost loop. The BFC gets activated and operates in conjunction with the BES controller during an overloading situation. On

the other, during the normal operating condition, each ICC maintains the dc-link voltage of the point at which it is connected to the power exchange link. In the event of overloading and if the BES capacity is not enough to alleviate the overloading situation; IFC gets activated to import the required amount of power from the neighbouring MG. The effective operation of both BSC and ICC are achieved through coordinated control among the three cascaded control loops, namely, linear quadratic regulator (LQR) based voltage tracking and switching control, power control and dc-link voltage control. The description of these control loops is given in Section 3.2.1.1.

3.3.3 Proposed Power Exchange Strategy

The proposed power exchange strategy is a two-stage coordinated overload prevention mechanism for a group of coupled autonomous microgrids. Let us consider each microgrid with the two introduced self-healing agents of BFC and IFC. All the neighbouring microgrids are interconnected to each other through the power exchange link and their ICCs while each microgrid has its own BES connected, and controlled through its BSC and MGCC respectively. To facilitate the proposed power exchange mechanism, the two self-healing agents continuously monitor the SoC of the BES and the frequency of the MG. The SoC is a measure of the stored energy of BES, and hence, its capability to support the microgrid [102, 113]. On the other hand, the loading status of an individual microgrid can be determined by monitoring its frequency. As the demand of a microgrid increases, its frequency decreases, and vice versa. Such characteristic is due to the droop control technique employed for the DERs, as the grid-forming units of the microgrid and can be used as the indicator of power deficiency or overloading in an MG. Hence, there is no need for any communication link or a central controller to regulate the power flow. Furthermore, even in the presence of a central controller, the proposed power exchange mechanism can be assigned as the backup system in the event of communication failure or during any contingency. For effective power-sharing among all the entities, a predefined framework needs to be introduced to identify different system parameters and their boundaries. Whether an entity (BSC/ICC) can participate in power exchange or not, must be determined by the predefined framework as their participation without proper coordination and control may lead to system instability. In general, such coordination among the entities can be

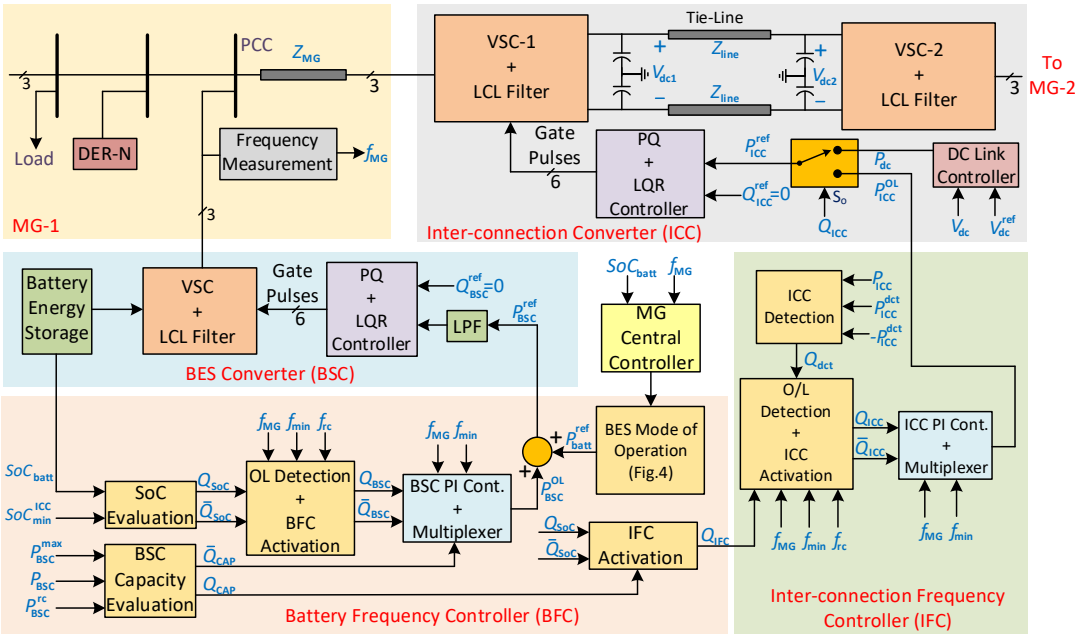

Figure 3.24. Overall block diagram of the proposed coordinated power exchange mechanism among BES and CMG network

done by the self-healing agents, by monitoring the MG's loading level and BES's stored energy level through frequency and SoC measurements, respectively.

During normal operation, the MGCC decides the BES's operation mode (i.e., charging/discharging) based on the MG's power generation, loading level and its frequency, f_{MG}. During overloading, if f_{MG} falls beyond the minimum value of $f_{\min}$, then first the BFC would respond to alleviate the overload situation and will work in conjunction with the BES controller. The BFC would determine the amount of excess power that needs to be provided by the BES to return the MG's frequency back to $f_{\min}$. The operation of BFC is dictated by the SoC of BES and the maximum power that can be handled by the BSC, $P_{\mathrm{BSC}}^{\max}$. In case of severe overloading, the BES may not be capable enough to alleviate the situation just by itself due to reasons such as, the BSC reaching the maximum limit of its rated capacity and/or the SoC level not being large enough to provide the required power. Hence, the self-healing agent of IFC will then get activated to import power from the neighbouring microgrids. The exchange of power through interconnection can be achieved in two ways- first, a portion of the overload power demand is mitigated by the BES and the rest is provided by the neighbouring microgrids; second, the total overload power demand is mitigated by the power imported from the neighbouring microgrids assuming that they have excess power generation available. The overall block diagram of the proposed power

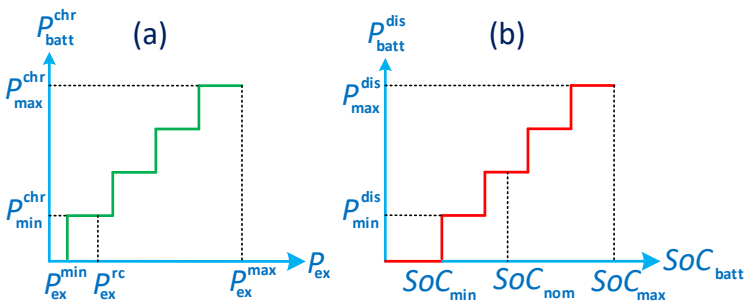

Figure 3.25. BES nominal operation scheme- (a) charging mode (b) discharging mode

exchange mechanism is shown in Figure 3.24.

3.3.3.1 BES Control

The control mechanism of BES during charging and discharging mode is developed based on its SoC level, $SoC_{\text{batt}}(t)$, and excess available power of the MG, $P_{\text{ex}}(t)$, respectively. Both parameters are instantaneous and vary with respect to time. Different methods of measuring $SoC_{\text{batt}}(t)$ are discussed in detail in [113]. On the other hand, $P_{ex}(t) = \sum P_{DER}(t) - \sum P_L(t)$ where $\sum P_{DER}(t)$ is the instantaneous total generated power of all DERs in microgrid and $\sum P_L(t)$ is the MG's total instantaneous demand. Since the stored energy of a BES system reduces overtime during discharging mode, it is a more practical approach to set the BES discharge power as a function of SoC instead of its ratings [102-104]. Hence, a BES system with a lower SoC level can be expected to inject less power to prevent its fast discharging. Thus, the output reference power, $P_{\text{batt}}^{\text{dis}}$, of the BES unit during discharge mode, can vary proportionally to its SoC level in discrete steps (e.g., in steps of 5-10% as SoC level varies dynamically) [102-103]. It may be noted that the BES system will stop discharging if the SoC level drops to its minimum value of SoC_{min}. The BES cannot discharge further unless it is charged up to a value of SoC_{nom}. Such a control mechanism can be implemented using a hysteresis controller.

Similarly, the charging power of the BES unit can be varied proportionally to P_{ex} in discrete steps of 5-10%. The higher is the surplus power available through the excess generation of DERs in the MG, the larger is the charging power for the BES unit, and vice versa. A graphical illustration of charging and discharging power variation in

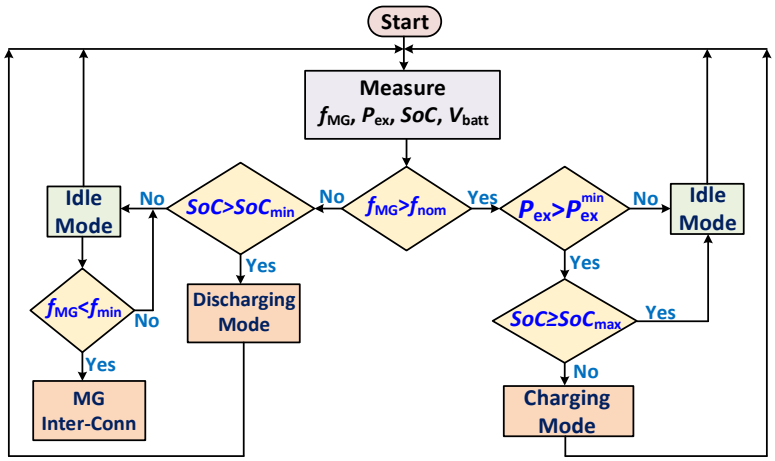

Figure 3.26. Different mode of operation of BES.

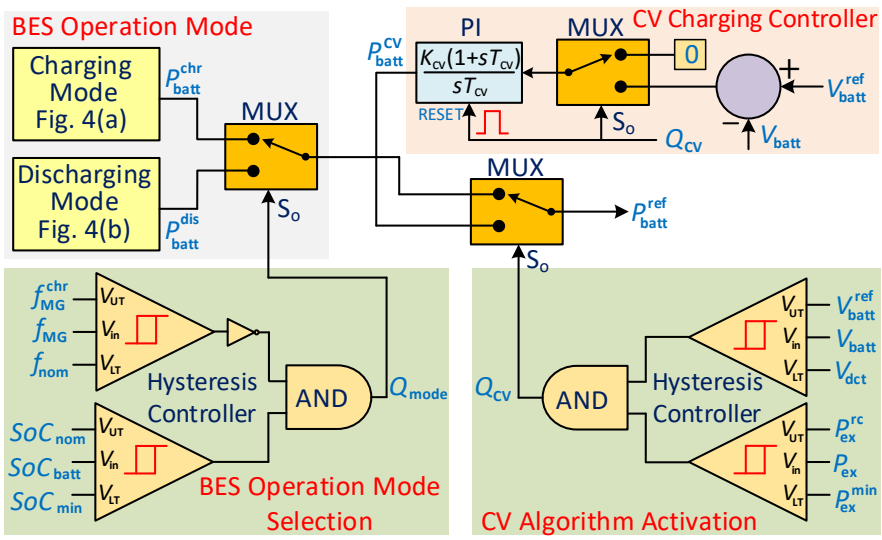

Figure 3.27 Control of BES different operation modes

discrete steps as a function of MG's surplus power and BES' SoC level respectively is shown in Figure 3.25. It is to be noted that, the BES charging and discharging mode is selected based on the microgrid's nominal frequency of f_{nom}. The charging mode is enabled when $f_{\mathrm{MG}} > f_{\mathrm{nom}}$ as this indicates the availability of surplus power generation in microgrid whereas the discharging mode is enabled when $f_{\mathrm{MG}} < f_{\mathrm{nom}}$ as this condition characterises the loading level where the microgrid needs support from the BES unit. The flowchart of Figure 3.26 shows the steps of operation of BES during its different operating modes while the schematic of the BES controller is shown in Figure 3.27.

A distinctive feature of the proposed method is that the BES is operating in grid-following mode (constant PQ control) instead of the typical grid-forming mode (droop control) to provide the necessary support for the MG. Hence, it is controlled and

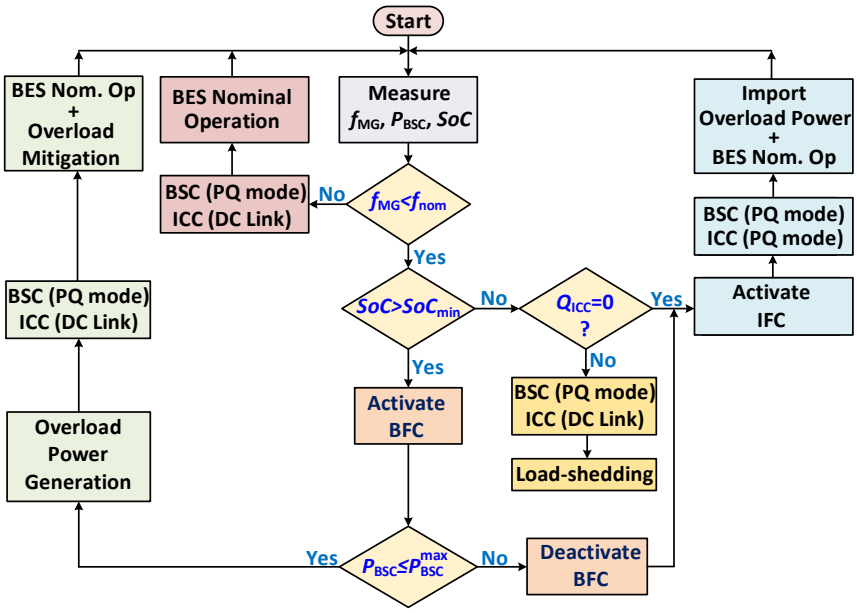

Figure 3.28. Proposed overload management scheme and its different modes of operation

monitored through the MGCC. This proposed mechanism offers better control and more flexibility in power-sharing via BES units. Also, the stability issues associated with droop control are eliminated; as in the droop control technique, it is important to select the proper droop coefficients to ensure system stability [102]. Most of the commercially available batteries are needed to be charged in constant current-constant voltage mode for optimum performance and longer lifecycle, also known as healthy charging [114]. Such a CC-CV charging approach is not realizable in the droop control technique. But with the proposed BES control mechanism, constant-voltage healthy charging mode can be easily implemented as shown in Figure 3.27.

3.3.3.2 Operation of BFC and BSC

The BFC is the outermost control loop that gets activated and operates in conjunction with the BES controller and regulates the output power of BSC during overload situation. To better understand the operation of BFC and BSC, let us consider the flowchart of Figure 3.28. During the nominal operating condition of the MG, the BSC will receive the power reference from the BES controller and the charging/discharging mode will be decided based on the developed logic. The BFC will only get activated during discharge mode when there is no surplus power generation available in MG. Thus, the activation and operation of BFC is governed by f_{MG}, SoC_{batt} and $P_{\mathrm{BSC}}^{\mathrm{max}}$. The

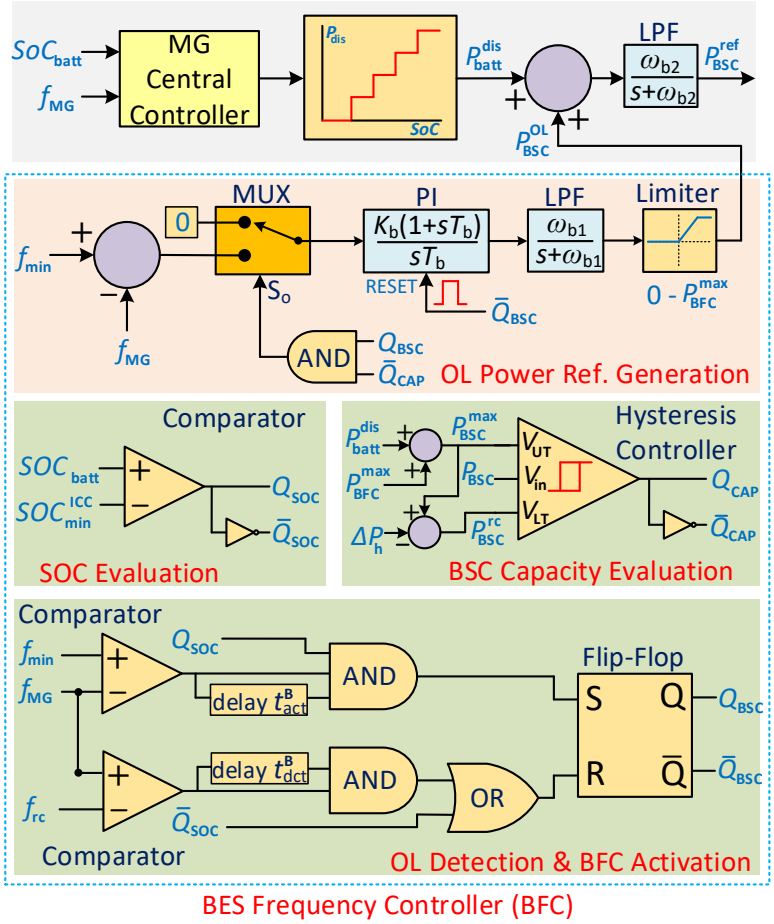

Figure 3.29. Control mechanism of BSC for overload management

functional block diagram of BFC is shown in Figure 3.29. In the event of overloading, if f_{MG} drops below f_{min}, the BFC will get activated through the control signal of Q_{BSC} after a certain time delay of t_{act}^{B}, if the BES SoC level is greater than the minimum value of $SOC_{\mathrm{min}}^{\mathrm{ICC}}$. If not, then BFC will not get activated as the SoC level of the BES unit is not enough to alleviate the overload, and hence, power needs to be imported from neighbouring microgrids via the ICC. Similarly, when the overloading period of the microgrid is over, the BFC will get deactivated and the proportional-integral (PI) controller is reset after a certain delay of t_{dct}^{B}. The input signal fed to the PI controller is controlled through a multiplexer to ensure proper operation and to avoid drift in PI controller. A low pass filter (LPF) is added to introduce a certain delay to match the battery response time. It is to be noted that, the delays are essential to allow a reasonable time for the system transients to settle down. Without a proper delay, it is highly possible that the self-healing agents are activated even during transients which will result in redundant and unnecessary power-sharing. The selection of time delays are based on the converter and controller dynamics, response time and band width.

Another mode of operation of BFC is possible when the SoC level can only alleviate a portion of the total overload. Hence, the total overload power demand needs to be shared by the BES systems of the overloaded microgrid and its neighbouring microgrids. This is realised by the BSC capacity evaluation block of the BFC and dynamically varying the parameter, $P_{\mathrm{BSC}}^{\mathrm{max}}$ as a function of the SoC. The arrangement is shown in Figure 3.29. $P_{\mathrm{BFC}}^{\mathrm{max}}$ is the maximum reference power generated by the PI controller of BFC and P_{BSC} is the measured output power of BSC. When P_{BSC} reaches its maximum limit of $P_{\mathrm{BSC}}^{\mathrm{max}}$, the input of PI controller should be set to zero. The reset command of PI controller should not be activated at this instant as the controller must retain the value at its output. The output power reference produced by the PI controller is the portion of overload power demand that can be supplied by the BES unit as per its SoC level. The rest of the overload power demand must be supplied by the neighbouring microgrids. Hence, an activation command for the ICC must be produced to initiate the power-sharing through the power exchange link.

3.3.3.3 Operation of IFC and ICC

The second self-healing agent of the microgrid is IFC which is responsible for importing power from the neighbouring microgrids through the power exchange link. The IFC is one of the outermost control loops for ICC. The activation of IFC depends on two specific conditions. First, when the SoC level of BES is less than $SoC_{\mathrm{min}}^{\mathrm{ICC}}$, i.e., the SoC level is not large enough to supply the required overload power demand. In this case, the entire overload power demand is supplied by the ICC from the neighbouring microgrids. Second, when the BSC reaches its maximum power limit while supplying overload demand as explained in the previous section. Hence, the rest of the overload power demand must be imported from the neighbouring microgrid through the ICC. These two conditions are used to derive the activation logic, Q_{IFC}, to activate the IFC which enables the ICC to import the required power for the overloaded MG. The functional block diagram of the IFC is shown in Figure 3.30. The structure and function of the controller are similar to BFC. During nominal operation of the microgrid or while a healthy microgrid supporting a neighbouring overloaded MG, the ICC should operate in the dc-link voltage control mode while the IFC must remain

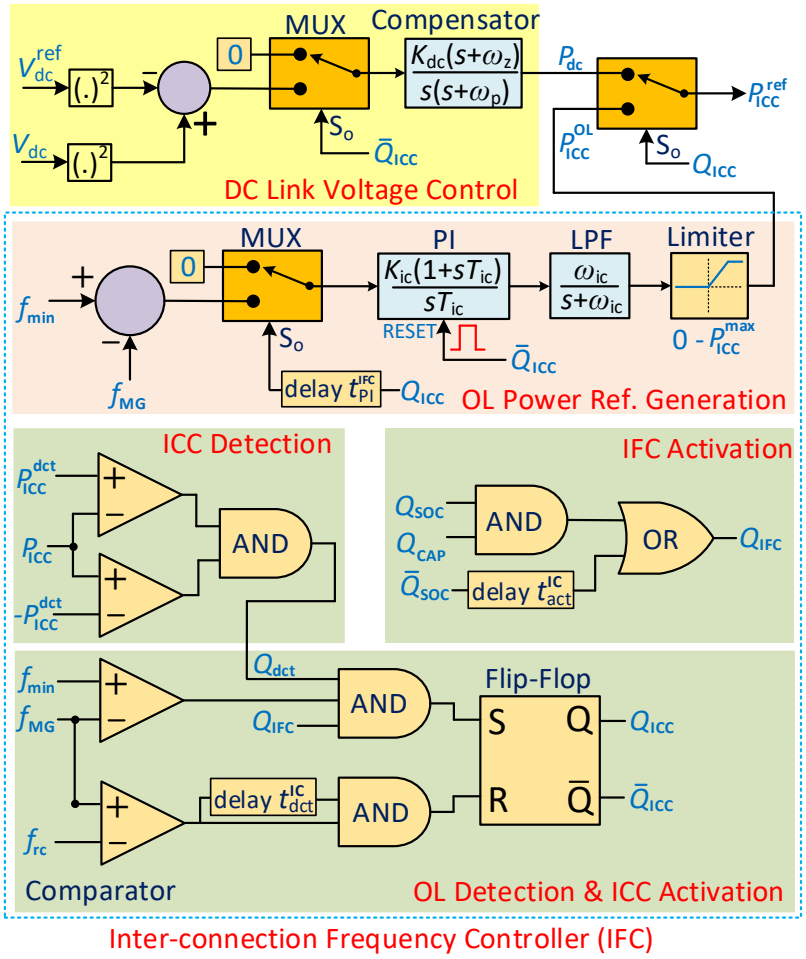

Figure 3.30. Control mechanism of ICC for overload management

deactivated. However, if the healthy microgrid that was supporting an overloaded MG, becomes overloaded too, the local BES system of the healthy microgrid and its BFC should get activated to alleviate the overload situation as long as the overload power is less than $P_{\mathrm{BSC}}^{\max}$ of that particular MG. If the overload power exceeds $P_{\mathrm{BSC}}^{\max}$, then there is no alternative other than to initiate load-shedding. This is achieved by the activation logic of Q_{ICC}, as can be seen from Figure 3.30. A logic low value of Q_{ICC} indicates that, the microgrid is already supporting another neighbouring overloaded microgrid and the ICC must operate in the dc-link voltage control mode, while IFC should remain deactivated. The steps of operation of the control approach in such a case can be interpreted from the flowchart of Figure 3.28. The sequence of the control logic is necessary to implement the developed decentralised control approach. Otherwise, the interconnection among the microgrids will lead to instability throughout the entire system.

3.4 Comparison among the three topologies

In this study, it has been established that the power exchange amongst the microgrids can be realised through any of the three topologies where each topology has its own advantages or drawbacks. However, it should be noted that such links only enable power exchange among the microgrids provisionally and during any contingency that requires to exchange 10-20% of the total generation capacity of each microgrid. To realise such interconnecting links that only carry a small amount of power for a short duration, proper economical, feasible and most optimal option needs to be selected. It is obvious that based on the distance among the microgrids and the amount of power that is going to be shared will play the most important role in selecting the most optimal topology for such interconnection. For microgrid clusters located in close proximity, ac interconnection may be more suitable and economical whereas, if the distance is large, then dc interconnection will be preferred. Furthermore, when selecting an ac interconnecting link based on the above-mentioned criteria, a single-phase link can be more suitable over a three-phase link or vice versa. A single-phase ac link of topology-2, and a single-phase power electronics converter requires fewer components than a three-phase ac link of topology-3. Also, the required number of current and voltage sensors, closed-loop controllers, and signal processing circuitry is less. Nevertheless, the computational effort for signal processing in a single-phase voltage source converter is smaller compared to the three-phase converter. On the other hand, employing a dc interconnection reduces the number of the required interlinking converter by 50% and thus reducing the number of components required as well as the computational effort of signal processing. Applying dc-link also eliminates the complexity of synchronization of the converters to power exchange lines and the operation of the power exchange link is more versatile, robust, and flexible. This distinctive feature of the dc-link can be explained with the help of the presented simulation results discussed in the time domain case studies of the three topologies.

A comparison among the three topologies is given in Table 3.2. In topology- 3, as the number of switching devices, LCL filters, and conductors is less, the power losses in these components will also be the minimum among all the three topologies, and a better converter efficiency can be achieved. At the same time, the number of sensors and LCL filters (the most expensive components of the converter) required for a dc-link is 50% less than that of the three-phase link and 40% less than that of the single-

Table 3.2 Comparison of different topologies employed for power exchange link

Parameters	single-phase link	three-phase link	dc-link
No. of switching devices	10	12	6
No. of LCL filters	4	6	3
No. of current sensors	8	12	6
No. of voltage sensors	8	12	6
Number of lines	1	3	2

phase link, and thus offers a substantial reduction in cost and size of the converter. Finally, the number of conductors required in the single-phase link is one (assuming earth neutral), whereas two and three conductors are required for dc and three-phase ac link, respectively. However, the total power that can be exchanged in a single-phase link is one-third of the three-phase link, whereas the maximum power that can be exchanged for a given voltage level, is through the dc-link. If the same amount of power needs to be transferred through a single-phase link, either the reference voltage across the filter capacitor of C_{f} needs to be increased or the size of the conductors needs to be increased to minimise the line impedance (approximately, one-third than that of three-phase lines). Also, the coupling inductance L_{g} needs to be reduced to accommodate the desired power flow. Each one of these solutions has its own limitation. First, the voltage reference across C_{f} cannot be made very large as it may produce excess stress over the switching devices and the other components and thus may incur an additional cost. Also, the voltage across C_{f} is related to the dc-link voltage of the converter as its value should be less than half of the dc-link voltage to avoid saturation. Second, using conductors with a larger cross-section area would make the system and its transmission structures more expensive. Third, L_{g} cannot be made very small as the switching harmonics may not get properly filtered out and can cause harmonic distortion in the output voltage waveform. At the same time, the modified angle droop with virtual impedance is employed to ensure the desired power-sharing among the HMGs. To implement such a droop control scheme, L_{g} needs to be large enough to decouple the active and reactive power-sharing and needs to be larger than a certain minimum value. Otherwise, it may deteriorate the property of power-sharing based on droop coefficients.

The main purpose of using a single-phase ac link over a three-phase link to couple microgrids is to reduce the cost as the number of equipment and interconnecting lines will be less. However, this is valid in the case of autonomous microgrids which are

located close to each other in a certain geographical area. If the distance among the microgrids is large, then the benefits of the single-phase links over three-phase links may not be applicable anymore. Using dc-link to couple microgrids can be more feasible but, the protection equipment for dc system are expensive compare to ac system up to some extent. Also, the majority of the power distribution line infrastructure and commercially available equipment are based on ac systems. At the same time, the network operators are usually more accustomed to ac distribution systems as compared to dc systems. Moreover, dc systems would be more economical or cost-effective if the distance among the microgrids is long.

3.5 Summary

This chapter presented the technique and control mechanism of coupling neighbouring microgrids to exchange power amongst them. The designed controller and its frequency response characteristics are discussed. A detailed explanation of coordinating between different mode of operation of the converters and their controllers are presented. The performances of each of these techniques are validated through time-domain simulation and numerical analyses in the following chapters.

Chapter 4 Time Domain Analysis

This chapter presents the time domain simulation used for demonstrating and validating the performance of the proposed control mechanism. Several case studies have been developed for a sample network made up individually using the three proposed topologies in which uncertainties in the generation of the renewable sources or load demand result in overloading or over-generation leading to unacceptable frequency and voltage deviation. It has been demonstrated in this chapter that the proposed control mechanism can successfully alleviate the overloading and over-generation problems and retain the voltage and frequency. The chapter also presents a comparative analysis of the performance of the three proposed topologies.

4.1 Network Under Consideration

Let Consider a network of Figure 1.1 where *3* autonomous microgrids, each consisting of several DERs, distributed generators, loads, and one interlinking converter coupled to a power exchange link. The interlinking converter can be any one of the three topologies shown in Figure 1.2. The DERs are connected to the microgrid through VSCs which are controlled in different operating modes to regulate the power and frequency of each microgrid. The DERs are assumed to be operating in the $P - f$ and $Q - V$ droop control modes, where the voltage and frequency at the output of each DER is determined from [73]

4.2 Performance Evaluation

To evaluate the dynamic performance of the proposed control technique for all the three topologies, let us consider the system of Fig. 1.1 with 3 microgrids that have formed a CMG through a common power exchange link and power electronic

converters where every individual microgrid is operating under the droop control technique mentioned in Section 2.1. The power exchange link can be any one of the three proposed topologies as discussed in chapter 3. The performance of such a system with every topology has been evaluated under various conditions, i.e., the normal, overloaded, and over-generating, using different case studies. Each microgrid is operating under a voltage and frequency droop while the technical parameters of the network under consideration and the controllers are provided in Table 4.1. The time-domain results of the study are presented in this chapter. The results show the frequency of each microgrid and the injected/absorbed power from/to one microgrid to the interconnecting lines (measured at the output of their corresponding LSCs). These figures also illustrate the dc-link voltage within the back-to-back converter (topology -1 and 2) or VSC (topology-3 and battery storage and CMG coordination), as well as the reference power and the voltage angle at the output of the LSCs. The transition of the control of the LSCs from droop to constant PQ mode and vice versa is also illustrated.

4.2.1 Topology-1 (Three-phase ac link)

The performance of proposed topology-1 is evaluated using two different case studies. In the first case study, the microgrids are overloaded or experiencing overgeneration separately whereas in the second case, overloading and overgeneration scenario are created simultaneously. The objective of these case studies is to validate the efficacy of the power exchange mechanism which demonstrates that, both overloading or over-generation problems can be addressed effectively, and the injected/absorbed power is shared based on the MG's droop ratio

4.2.1.1 Case Study-1 *(Separate overloaded and over-generating PMG)*

In this case study first MG-1 has become provisionally overloaded; thus, the other two HMGs (i.e., MG-2 and 3) successfully support MG-1 by supplying the required power demand under the proposed power exchange and control strategy. After a certain period, overloading in MG-1 is over and all the three microgrids operate as HMGs. Later, MG-3 starts experiencing over-generation, and hence, MG-1 and MG-2 start

Table 4.1 Technical data of network under consideration

Network	$V_{\text{rated}} = 415\text{V}$, $f_{\text{nom}} = 50\text{Hz}$, $f_{\text{min}} = 49.5\text{Hz}$, $f_{\text{max}} = 50.2\text{Hz}$, $P_{\text{max}} = 100\text{kW}$, $V_{\text{dc}} = 1.5\text{kV}$, $Z_{\text{MG}} = 0.1 + j0.5\Omega$, $Z_{\text{line}} = 0.1 + j0.08\Omega$
DER droop	$m = 0.01\text{Hz/kW}$, $n = 0.1\text{V/kVAR}$
Angle droop	$m_{\text{d}} = 0.002\ \text{rad/kW}$, $n_{\text{d}} = 0.004\text{V/kVAR}$
DC Droop Parameters	$m_{\text{MG}-1} = 2.5\text{V/kW}$, $m_{\text{MG}-2} = 5\text{V/kW}$, $m_{\text{MG}-3} = 5\text{V/kW}$
VSC and filters	$R_{\text{f}} = 0.1\Omega$, $L_{\text{f}} = 2\text{mH}$, $R_{\text{g}}(\text{MSC}) = 0.04\Omega$, $L_g(\text{MSC}) = 1.36\text{mH}$, $R_{\text{g}}(\text{LSC}) = 0.12\Omega$, $L_g(\text{LSC}) = 10\text{mH}$, $C_{\text{f}} = 25\mu\text{F}$, $C_{\text{dc}} = 4700\mu\text{F}$
Linear quadratic regulator gains	$k_1 = 58.63$, $k_2 = 97.18$, $k_3 = 1.2$, $\omega_c = 6283.2\ \text{rad/s}$
PI - PQ controller (MSC)	Proportional Gain, $K_{\text{c}} = 0.628$, Time Constant, $T_{\text{c}} = 0.034$ s, $f_{\text{BW}} = 73.5\text{Hz}$
PI - PQ controller (LSC)	Proportional Gain, $K_{\text{c}} = 0.628$, Time Constant, $T_{\text{c}} = 0.0834$ s, $f_{\text{BW}} = 10\text{Hz}$
Frequency controller	$K_{\text{OL}} = 15\text{k}$, $T_{\text{OL}} = 0.025$ s, $\omega_{\text{OL}} = 314$ rad/s, $K_{\text{OG}} = 20\text{k}$, $T_{\text{OG}} = 0.05$ s, $\omega_{\text{OG}} = 37.7$ krad/s $K_{\text{PLL}} = 5$, $T_{\text{PLL}} = 0.02$ s
Dc-link voltage controller	$K_{\text{dc}} = 222$, $\omega_{\text{z}} = 2.2\text{rad/s}$, $\omega_{\text{p}} = 1000\text{rad/s}$, $\tau_{\text{dc}} = 392.2\text{ms}$, $P_{\text{so}} = 100\text{kW}$, $V_{\text{d}} = 380\text{V}$

absorbing the excess power from it to maintain its minimum or baseload power demand.

Initially, all microgrids are assumed to be operating at the steady-state condition and under the droop control mode with zero power exchange as all the microgrids are HMGs. At, $t = t_1$, MG-1 becomes overloaded by 20% (see Figure. 4.1a); hence, its frequency decreases from 49.8 to 49.3 Hz (see Figure. 4.1c). which is below the acceptable limit of 49.5 Hz and thus, MG-1 becomes a PMG. The frequency controller of MG-1 senses this situation and switches its mode of operation from droop to constant PQ control after a certain time delay (i.e., 0.6 s). Hence, the OLFC gets activated and determines the amount of power that needs to be supplied to MG-1 to retain its frequency back to the acceptable limit. Thus at $t = t_2$, MG-2 and MG-3 start injecting the required power of 0.155 and 0.076 pu as demanded by MG-1, respectively. The share of power between MG-2 and MG-3 is determined by the assumed (desired) droop ratio (i.e., 1: 2 in this case); thus, the power delivered by MG-2 is twice that of MG-3, as seen from Figure. 4.1b.

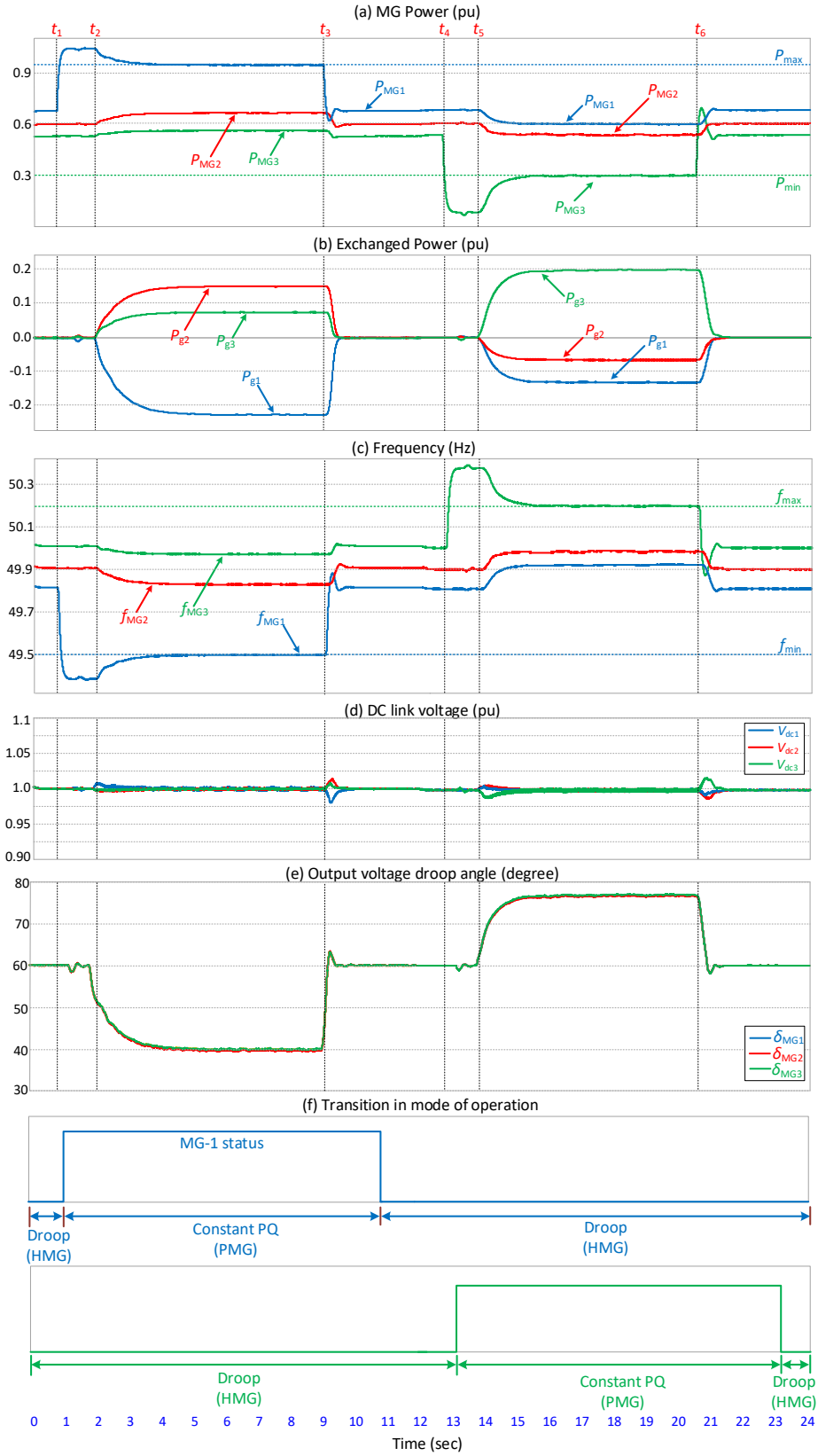

Figure 4.1 Simulation results of case study-1 for topology- 1.

The required power demand of MG-1 is 0.22 pu and the rest of the power is to overcome the line losses. This continues until $t = t_3$ in which the overloading situation

Table 4.2 Events applied to microgrids in Case study-1 at different intervals

Time Instant	MG Status MG-1	MG-2	MG-3	Action taken
t_1	**OL**	HMG	HMG	Normal operation for MG-2 and MG-3 while MG-1 is overloaded.
t_2	PMG	HMG	HMG	MG-1 is overloaded while MG-2 and MG-3 are supporting it by supplying the overload power.
t_3	HMG	HMG	HMG	Over-generation of MG-1 is over, and all MGs become HMG.
t_4	HMG	HMG	**OG**	Normal operation for MG-1 and MG-2 while MG-3 is over-generating.
t_5	HMG	HMG	PMG	MG-3 over-generating while MG-1 and MG-2 are supporting it by absorbing the excess power.
t_6	HMG	HMG	HMG	Over-generation of MG-3 is over, and all MGs become HMG.

is alleviated. At $t = t_3$ the overload is removed, and as soon as this occurs, the frequency of MG-1 increases to 49.8 Hz (i.e., above the level of minimum acceptable limit). Therefore, MG-1 goes back to its nominal operating condition and becomes an HMG. Hence, MG-2 and MG-3 cease to supply power to MG-1. After the MG-1 settles back as HMG and steady-state condition is reached, the frequency controller of MG-1 switches its mode of operation from constant PQ to droop control as can be seen from Figure. 4.1f. At $t = t_4$, MG-3 experiences an excessive power generation by 18% (see Figure. 4.1a), and its frequency increases from 49.94 to 50.36 Hz (see Figure. 4.1c). As the frequency has increased beyond the acceptable limit of 50.2 Hz, MG-3 becomes a PMG. Thus, the frequency controller of MG-3 senses the situation and switches its mode of operation from droop to constant PQ control after a certain predefined time delay (i.e., 0.6 s). Hence, the OGFC gets activated and determines the amount of power that needs to be exported from MG-3 to retain its frequency back to the acceptable limit. Thus at $t = t_5$, MG-1 and MG-2 start absorbing the required power of 0.121 and 0.062 pu, respectively. The power-sharing between MG-1 and MG-2 is maintained as 1: 2, as seen from Figure. 4.1b. The power delivered by MG-3 is 0.195 pu. This continues until $t = t_6$ in which the situation of excessive generation in MG-3 is alleviated and the frequency of MG-3 decreases to 49.94 Hz (i.e., below the level of the maximum acceptable limit of 50.2 Hz). Therefore, MG-3 goes back to its nominal operating condition and becomes an HMG. Hence, MG-1 and MG-2 cease to absorb power form MG-3. After MG-3 settles back as HMG and steady-state condition is attained, the frequency controller of MG-3 switches its mode of operation from constant PQ to droop control. Table 4.2 summarises the events applied to the

microgrids and the corresponding actions taken according to the proposed control mechanism for case study-1.

4.2.1.2 Case Study-2 *(Simultaneous overloaded and over-generating PMG)*

Now, let us assume that the system is at steady-state condition initially, and all microgrids are healthy and the LSCs operating under droop. At $t = t_1$, MG-1 becomes overloaded by 20% (see Figure. 4.2a), and hence, its frequency decreases to 49.3Hz (lower than the minimum frequency limit of 49.5Hz). Thus, after a predefined delay of 0.6s, MG-1 changes its mode from droop to constant PQ control and at $t = t_2$, MG-2 and 3 start to transfer power to MG-1 to retain its frequency back to the acceptable limit (see Figure. 4.2c). Note that, the power delivered by MG-2 is twice that of MG-3. This is determined by the employed 1: 2 droop ratios. At $t = t_3$, MG-3 experiences over-generation after an internal demand decrease. As such, it turns into an FMG and later a PMG after 0.6s of delay at $t = t_4$. In such a condition, MG-3 changes its mode from droop control to constant PQ control with zero power-sharing (i.e., the floating mode) as it is not participating in supplying MG-1. During this interval, MG-2 supplies all the excess demand of MG-1 alone. At $t = t_5$, MG-3 changes its mode of operation to constant PQ and feeds its excess power of 0.12 pu to MG-1. Hence, MG-2 only supplies the rest of the MG-1's excess demand. At $t = t_6$, MG-1's overloading is eased following the reduction in its internal demand by 20%. Thus, MG-1 becomes an HMG. However, it cannot be allowed to switch back to droop mode as it cannot be synchronised with the interconnecting link. So, it continues its operation under the constant PQ mode but with zero output power reference (as FMG).

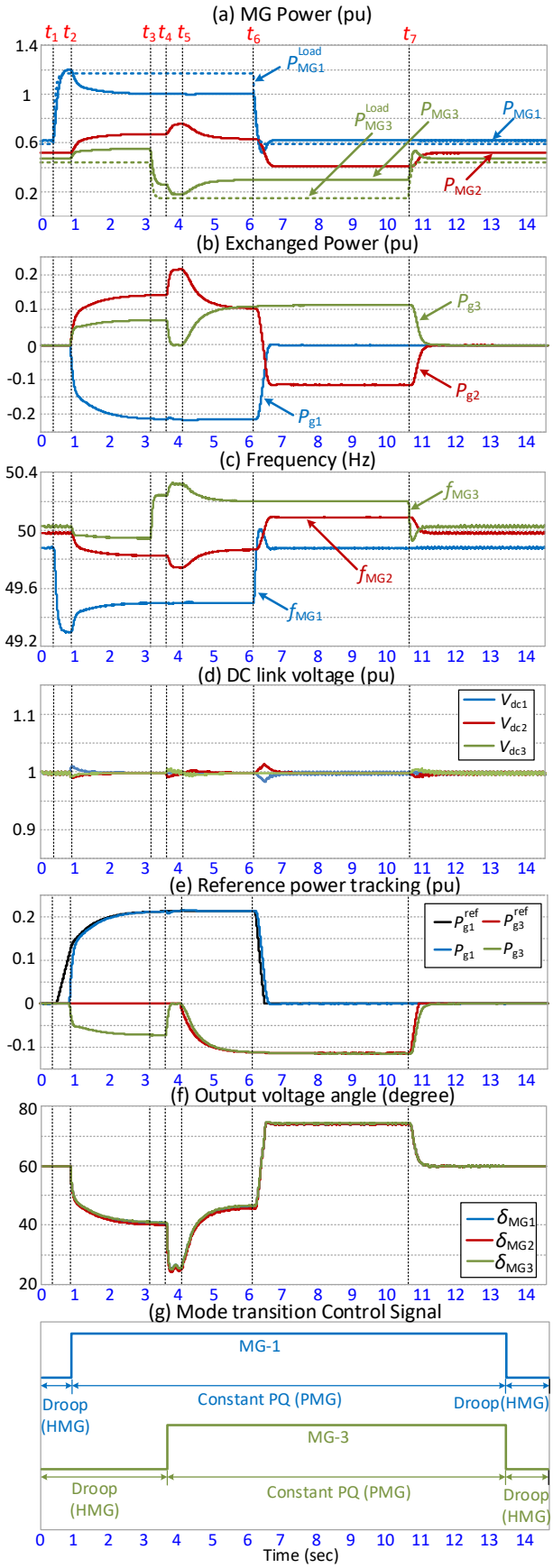

Figure 4.2 Simulation results of case study-2 for topology- 1.

Table 4.3 Overloading and over-generating events applied to microgrids in case study-2 at different intervals

Time Instant	MG Status MG-1	MG-2	MG-3	Action taken
t_1	**OL**	HMG	HMG	Normal operation for MG-2 and MG-3 while MG-1 is overloaded.
t_2	PMG	HMG	HMG	MG-1 becomes overloaded, and hence, MG-2 and 3 support it.
t_3	PMG	HMG	**OG**	MG-3 is over-generating.
t_4	PMG	HMG	FMG	MG-3 changes its operation mode from droop to PQ but shares zero power. MG-2 is supporting MG-1.
t_5	PMG	HMG	PMG	Both MG-1 and 3 are supported by MG-2.
t_6	FMG	HMG	PMG	MG-1 overload condition is removed while MG-2 is supporting MG-3.
t_7	HMG	HMG	HMG	All the MGs become HMG and all MGs switch to droop mode.

In this condition, the excess power of MG-3 is consumed by MG-2. Finally, at $t = t_7$, all the microgrids become HMGs. After a delay of 2s (determined by the mode transition controller), both MG-1 and 3 change back to droop mode and resumes operating under their normal condition. Table 4.3 summarises the events applied to the microgrids and the corresponding actions taken according to the proposed control mechanism for case study- 2.

4.2.2 Topology-2

The performance of proposed topology-2 is evaluated using three different case studies. In the first two case studies, there is one overloaded or over-generating PMG supported by two HMGs. The shared injected or absorbed power between two HMGs, is based on the preset droop coefficient values. The third case study demonstrates the ability of the proposed control mechanism to address the most extreme scenario, where two simultaneously overloaded and over-generating PMG are supported by a single HMG.

4.2.2.1 Case Study-1 *(Overloaded PMG)*

This study case assumes that MG-1 has become provisionally overloaded; thus, the other two HMGs (i.e., MG-2 and 3) successfully support MG-1 by injecting the required power demand under the proposed power exchange and control strategy.

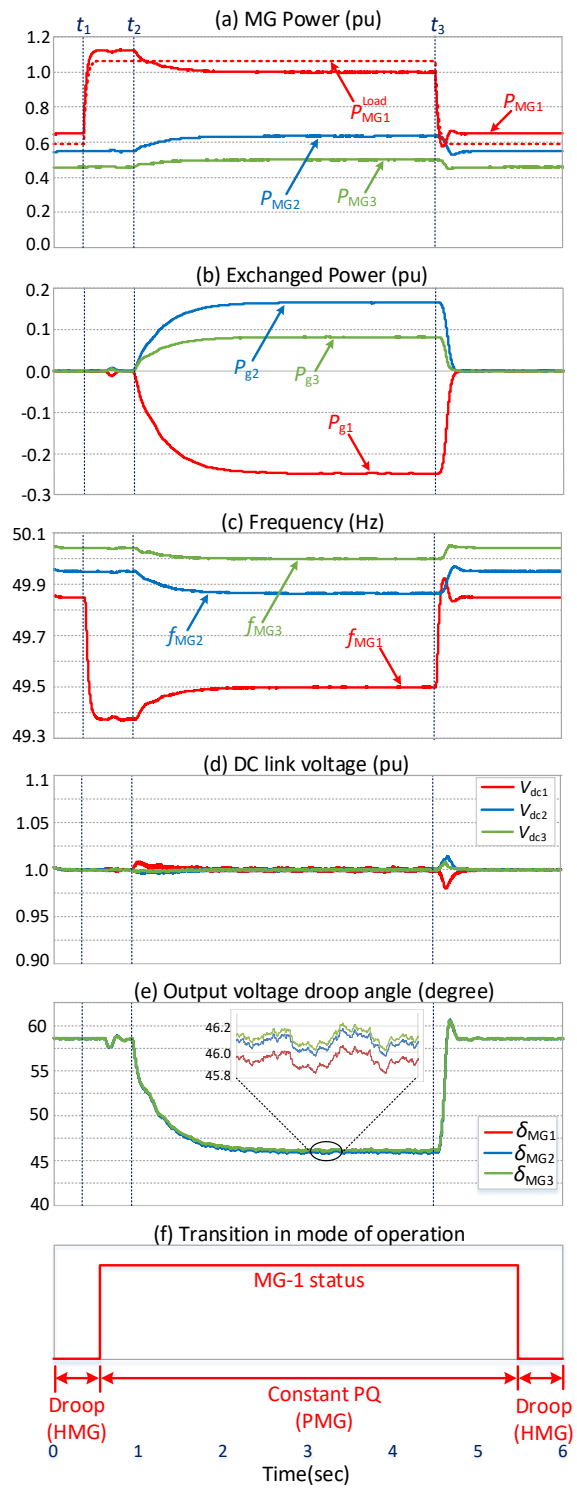

Figure 4.3 Simulation results of case study-1 for topology- 2.

Initially, all microgrids are assumed to be HMGs and operating at the steady-state condition and under droop control. At, $t = t_1$, MG-1 becomes overloaded by 18% (see Figure. 4.3a); hence, its frequency decreases from 49.85 to 49.38 Hz (see Figure. 4.3c). As the frequency has fallen beyond the acceptable limit of 49.5 Hz, MG-1

Table 4.4 Events applied to microgrids in case study-1 at different intervals for overloading scenario.

Time Instant	MG Status MG-1	MG-2	MG-3	Action taken
t_1	**OL**	HMG	HMG	Normal operation for MG-2 and 3 while MG-1 is overloaded.
t_2	PMG	HMG	HMG	MG-1 is overloaded while MG-2 and 3 are supporting it by supplying the overload power.
t_3	HMG	HMG	HMG	Over-generation of MG-1 is over, and all MGs become HMG.

becomes a PMG. Thus, the LSC controller of MG-1 senses this situation and switches its mode of operation from droop to constant PQ control after a certain time delay (i.e., 0.7 s). With this change, the frequency controller gets activated and determines the amount of power that needs to be transferred to MG-1 to retain its frequency back to the acceptable limit. Thus at $t = t_2$, MG-2 and MG-3 start injecting the required power of 0.174 and 0.086 pu as demanded by MG-1, respectively. The power-sharing between MG-2 and MG-3 is determined by the assumed (desired) droop ratio (i.e., 1: 2 in this case); thus, the power delivered by MG-2 is twice that of MG-3, as seen from Figure. 4.3b. The required power demand of MG-1 is 0.237 pu and the rest of the power is to overcome the line losses. This continues until $t = t_3$ in which the overloading situation is alleviated. At $t = t_3$ the overload is removed, and as soon as this occurs, the frequency of MG-1 increases to 49.86 Hz (i.e., above the level of minimum acceptable limit). Therefore, MG-1 goes back to its nominal operating condition and becomes an HMG. Hence, MG-2 and MG-3 cease to transfer power to MG-1. After the MG-1 settles back as HMG and steady-state condition is reached, the LSC controller of MG-1 switches its mode of operation from constant PQ to droop control. Table 4.4 summarises the events applied to the microgrids and the corresponding actions taken according to the proposed control mechanism for case study- 1.

4.2.2.2 Case Study-2 *(Over-generating PMG)*

This study case assumes that MG-1 experiences an excess power generation from its renewable-based DGs; thus, the other two HMGs (i.e., MG-2 and 3) successfully support MG-1 by absorbing the required amount of this excess power under the

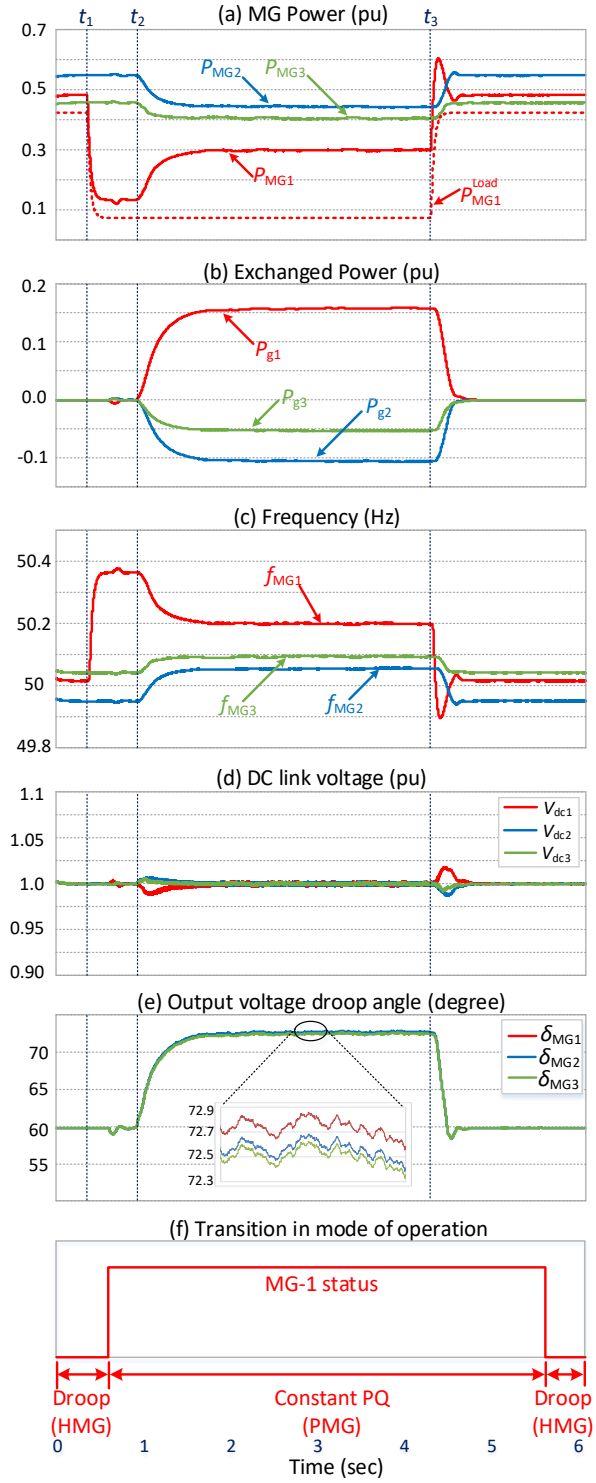

Figure 4.4 Simulation results of case study-2 for topology- 2.

proposed power exchange and control strategy.

Initially, all microgrids are assumed to be HMGs and operating at the steady-state condition and under droop control. At $t = t_1$, MG-1 experiences an excessive power generation of 17% (see Figure. 4.4a), and its frequency increases from 50.03 to

Table 4.5 Events applied to microgrids in case study-2 at different intervals for over-generation scenario.

Time Instant	MG Status			Action taken
	MG-1	MG-2	MG-3	
t_1	**OG**	HMG	HMG	Normal operation for MG-2 and 3 while MG-1 is over-generating.
t_2	PMG	HMG	HMG	MG-1 over-generating while MG-2 and 3 are supporting it by absorbing the excess power.
t_3	HMG	HMG	HMG	Over-generation of MG-1 is over, and all MGs become HMG.

50.36 Hz (see Figure. 4.4c). As the frequency has increased beyond the acceptable limit of 50.2 Hz, MG-1 becomes a PMG. Thus, the LSC controller of MG-1 senses the situation and switches its mode of operation from droop to constant PQ control after a certain time delay (i.e., 0.7 s). With this change, the frequency controller gets activated and determines the amount of power that needs to be exported from MG-1 to retain its frequency back to the acceptable limit. Thus at $t = t_2$, MG-2 and 3 starts absorbing the required power of 0.104 pu and 0.051 pu, respectively. The power-sharing between MG-2 and 3 is again maintained as 1:2, as seen from Figure. 4.4b. The power delivered by MG-1 is 0.16 pu. This continues until $t = t_3$ in which the situation of excessive generation in MG-1 is alleviated. As soon as this occurs, the frequency of MG-1 decreases to 50.02 Hz (i.e., below the level of maximum acceptable limit). Therefore, MG-1 goes back to its nominal operating condition and becomes an HMG. Hence, MG-2 and MG-3 cease to absorb power from MG-1. After MG-1 settles back as HMG and steady-state condition is attained, the LSC controller of MG-1 switches its mode of operation from constant PQ to droop control. Table 4.5 summarises the events applied to the microgrids and the corresponding actions taken according to the proposed control mechanism for case study- 2

4.2.2.3 Case Study-3 *(Two PMGs; one Overloaded and one Over-generating)*

Let us assume that the system is at steady-state condition initially, and all microgrids are healthy and the LSCs are operating under droop. At $t = t_1$, MG-3 experiences over-generation by 8% after an internal demand decrease (see Figure. 4.5a), and hence, its frequency rises to 50.28Hz (higher than the maximum frequency limit of 50.2Hz).

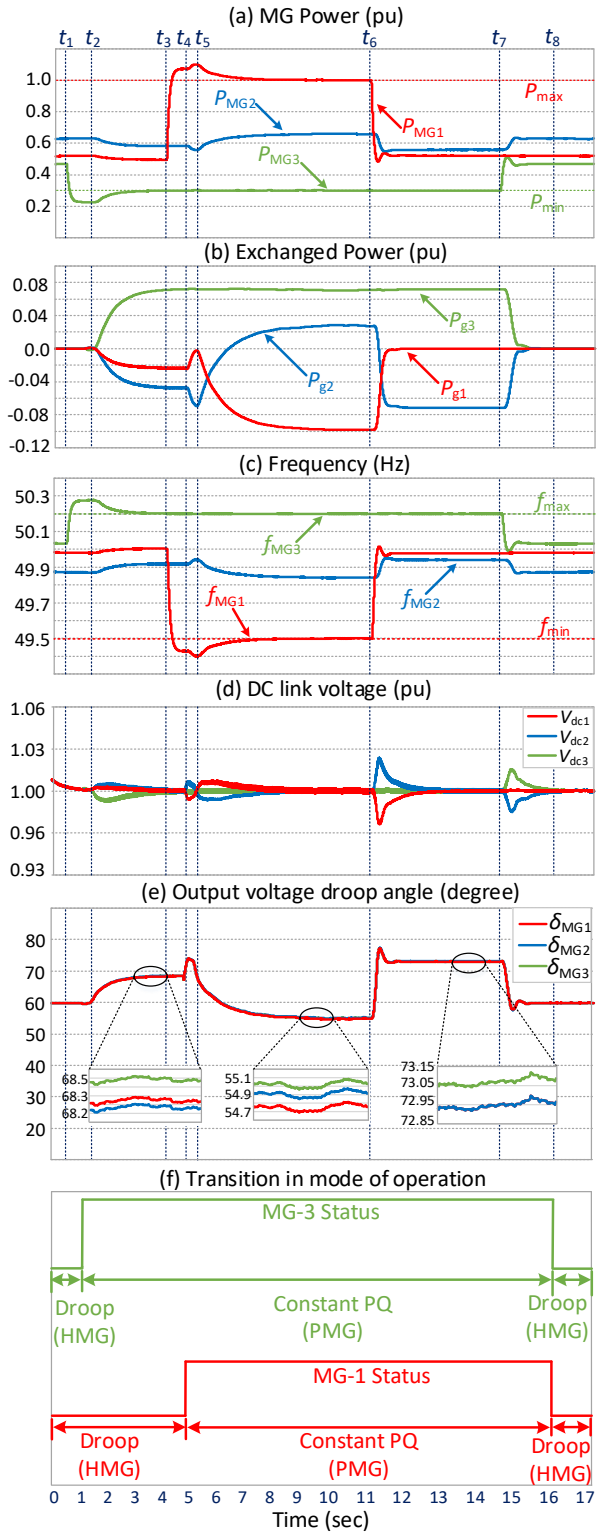

Figure 4.5 Simulation results of case study-3 for topology- 2.

Thus, after a predefined delay of 0.6s, MG-3 changes its operation mode from droop to constant PQ control, and at $t = t_2$, MG-1 and 2 start to absorb the excess power from MG-3 so that its frequency is retained back to the acceptable limit (see Figure.

Table 4.6 Overloading and over-generating events applied to microgrids in case study-3 at different intervals.

Time Instant	MG Status MG-1	MG-2	MG-3	Action taken
t_1	HMG	HMG	**OG**	Normal operation for MG-1 and MG-2 while MG-3 is over-generating.
t_2	HMG	HMG	PMG	MG-3 becomes over-generating, and hence, MG-1 and 2 support it.
t_3	**OL**	HMG	PMG	MG-1 is overloaded.
t_4	FMG	HMG	PMG	MG-1 changes its operation mode from droop to PQ but shares zero power. MG-2 is supporting MG-3.
t_5	PMG	HMG	PMG	Both MG-1 and 3 are supported by MG-2.
t_6	FMG	HMG	PMG	MG-1's overload condition is removed while MG-2 is supporting MG-3.
t_7	FMG	HMG	FMG	MG-3's over-generation is over and both MG-1 and MG-3 are in PQ mode with zero power-sharing
t_8	HMG	HMG	HMG	All MGs become HMG and all MGs switch to droop mode.

4.5c). Note that, the power delivered by MG-2 ($P_{g2} = -0.0474$ pu) is twice that of MG-1 ($P_{g1} = -0.024$ pu). This is determined by the employed 1: 2 droop ratios between these microgrids (see Figure. 4.5b). At $t = t_3$, MG-1 becomes overloaded by 10% and its frequency falls to 49.4 Hz. As such, it turns into an FMG and later a PMG after 0.6s of delay at $t = t_4$. In such a condition, MG-1 changes its operation mode from droop control to constant PQ control with zero power-sharing (i.e., the floating mode) as it is not participating in absorbing any excess power from MG-3. During this interval, MG-2 absorbs all excess power of MG-3 alone. At $t = t_5$, MG-1 starts to receive power from both over-generating PMG of MG-3 and HMG of MG-2. First, MG-1 absorbs the total over-generating power ($P_{g3} = 0.075$ pu) of MG-3 and the rest of the overload demand is supplied by MG-2 ($P_{g2} = 0.025$ pu) to retain MG-1's frequency back to the minimum limit of 49.5Hz. At $t = t_6$, MG-1's overloading is eased following the reduction in its internal demand by 10%. Thus, MG-1 becomes an HMG. However, it cannot be allowed to switch back to droop mode as it cannot be synchronised with the interconnecting link. So, it continues its operation under the constant PQ mode but with zero output power reference (as an FMG). In this condition, the excess power of MG-3 is consumed by MG-2 only. Finally, at $t = t_7$, the over-generation of MG-3 is over and all microgrids become HMGs, but both MG-1 and MG-3 will continue to operate as FMG until the droop angle of the interconnecting lines returns back to δ_o. Once the desired value of δ_o is attained, indicating that, there is no power exchange taking place in the link (i.e., all microgrids are HMGs), and after

a preset delay of 2s (determined by the mode transition controller), both MG-1 and 3 change their operation mode back to droop mode. All microgrids resume operating under their normal condition with no power flow in the power exchange link. Table 4.6 summarises the events applied to the microgrids and the corresponding actions taken according to the proposed control mechanism for study case- 3.

4.2.3 Topology-3

The performance of proposed topology-3 is evaluated using two different case studies under both balanced (case-1) and unbalanced (case-2) loading condition of CMG. In both case studies, two PMGs (one overloaded and one over-generating) are supported by one HMG. The purpose of this case study is to demonstrate the capability and efficacy of the proposed power exchange mechanism in alleviating overloading/over-generation scenario even when the microgrids are heavily unbalanced.

4.2.3.1 Case Study-1 (*Balanced CMG*)

Initially let us assume the system is at the steady-state condition and all the microgrids are at the HMG mode. Therefore, the VSCs of all HMGs are operating under the dc voltage droop control mode (i.e. their output power is zero and the voltage at their dc-link is 1 pu); thus, there is no power flow in the power exchange dc-link.
Referring to Figure 4.6, At $t = t_1$, MG-3 becomes overloaded by 17%, and hence, its frequency drops to 49.33 Hz (i.e., below the frequency limit of 49.5 Hz) while the other two microgrids are still at the mode of operation from dc voltage droop control to constant PQ mode, requesting an active power demand of 0.167 pu to alleviate the overloading situation. As a result, at $t = t_2$, the other two HMGs start to support MG-3 by injecting the required demand after a pre-defined delay of 0.6 s. MG-2 supplies 0.065 pu of power while MG-1 provides 0.122 pu which is twice that of MG-2 because of the preset ratio of droop coefficients ($m_{\text{MG-2}}/m_{\text{MG-1}} = 2:1$) and thus, the frequency of MG-3 is retained back to the desired limit of 49.5 Hz. This continues until $t = t_3$ at which MG-2 experiences excess-generation, and thus, its frequency rises and settles at 50.35 Hz (beyond the acceptable limit of 50.3 Hz in this particular

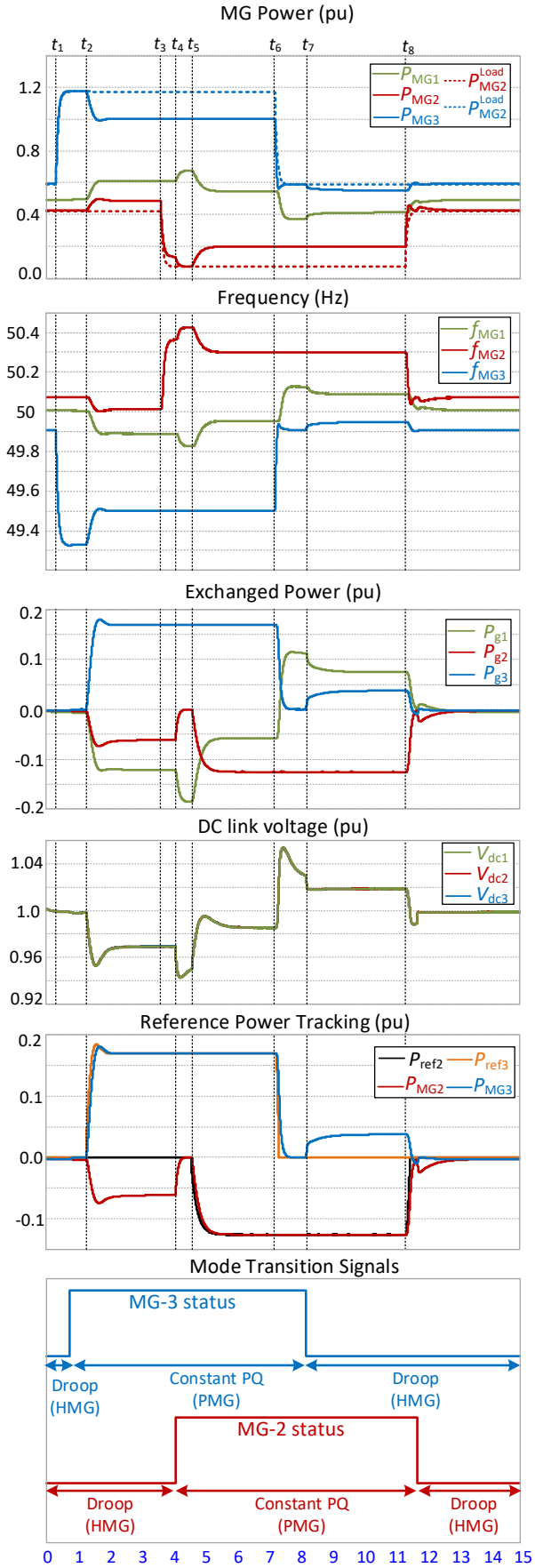

Figure 4.6 Simulation results of case study-1 for topology- 3.

Table 4.7 Events applied to microgrids in case study-1 at different intervals..

Time Instant	MG Status MG-1	MG-2	MG-3	Action taken
t_1	HMG	HMG	**OL**	Normal operation for MG-1 and 2 while MG-3 is overloaded.
t_2	HMG	HMG	PMG	MG-3 switches to PQ mode to absorb power and MG-1 and 2 are operating in droop to support it.
t_3	**OG**	HMG	PMG	MG-1 is over-generating.
t_4	FMG	HMG	PMG	MG-1 changes its operation mode from droop to PQ but shares zero power. MG-2 is supporting MG-3.
t_5	PMG	HMG	PMG	Both MG-1 and 3 are supported by MG-2.
t_6	PMG	HMG	FMG	MG-3's overload condition is removed while MG-2 is supporting MG-1.
t_7	PMG	HMG	HMG	MG-3 joins MG-2 in dc droop mode to support MG-1
t_8	HMG	HMG	HMG	MG-1's overgeneration is over. All the MGs become HMG and all MGs switch to droop mode.

case) at $t = t_4$. During this interval, the frequency controller of MG-2 is triggered and determines the amount of power that needs to be exported to the dc-link to regulate its frequency to the desired level. It changes its mode of operation from dc voltage droop control to constant PQ mode at $t = t_5$, and the VSC of MG-2 starts exporting power of 0.125 pu. This power is absorbed by the overloaded PMG of MG-3, as well as the HMG of MG-1. MG-3 only absorbs the amount of power needed to improve its overloading while the remainder of the excess power is absorbed by MG-1. This scenario continues until $t = t_6$ at which the overloading of MG-3 is removed and does not need external support. As a result, the VSC of MG-3 switches its mode of operation from constant PQ mode to the dc voltage droop control mode with zero power exchange. However, as the CMG still includes an over-generating PMG (i.e., MG-2), the HMG of MG-3 starts to absorb a portion of the excess power at $t = t_7$ in addition to MG-1. The amount of the power absorbed by MG-1 and MG-3 is again determined based on the ratio of their dc voltage droop coefficients (i.e., $P_{\text{MG-1}}: P_{\text{MG-3}} = m_{\text{MG-3}}: m_{\text{MG-1}} = 2 : 1$). At $t = t_8$, the situation of excess generation in MG-2 is alleviated and goes back to its nominal operating condition to become an HMG. Thus, the exchange of power is ceased and the VSC of MG-2 switches back to dc voltage droop. Table 4.7 summarises the events applied to the microgrids and the corresponding actions taken according to the proposed control mechanism for study case- 1

4.2.3.2 Case Study-2 (*Unbalanced CMG*)

Let us assume all the microgrids are HMG and hence, the VSC of all HMGs are operating under the dc voltage droop control mode with no power flow in the power exchange dc-link. Unlike, case- 1, all the microgrids are heavily unbalanced as can be seen from Figure 4.7. All the three MG's individual per phase load power and their variation over the simulation period are shown.

At $t = t_1$, MG-2 starts over-generation by 10% due to withdrawal of some connected loads (note that all the phases are underloaded nonuniformly and the underloaded microgrid is heavily unbalanced), and hence, its frequency rises to 50.4 Hz (i.e., over the maximum frequency limit of 50.3 Hz) while the other two microgrids are still at the healthy condition. Therefore, the VSC of MG-2 changes its mode of operation from dc voltage droop control to constant PQ mode and starts to deliver an active power of 0.1pu to alleviate the over-generation situation. As a result, at $t = t_2$, the other two HMGs start to support MG-2 by absorbing the excess power produced by it after a pre-defined delay of 0.6 s. MG-1 absorbs 0.062 pu of power while MG-3 absorbs 0.03 pu which is half of that of MG-1 because of the preset ratio of droop coefficients ($m_{\text{MG-3}}/m_{\text{MG-1}} = 2:1$) and thus, the frequency of MG-2 is regulated to the desired maximum limit of 50.3 Hz. It may be noted here that, the choice of droop coefficients to share power depends on the microgrid loading condition. As the connected load in MG-1 is higher than MG-3, the former is allowed to receive more power than the latter. This continues until $t = t_3$ at which MG-1 experiences overloading of 20% due to the addition of loads in phase-b and c, and thus, its frequency falls and settles at 49.35 Hz (beyond the acceptable minimum limit of 49.5 Hz in this particular case). During this interval, the frequency controller of MG-1 is triggered and determines the amount of power that needs to be imported from the dc-link to regulate its frequency to the desired level. It changes its mode of operation from dc voltage droop control to constant PQ mode and at $t = t_4$, the VSC of MG-1 starts absorbing power of 0.2 pu. This power is provided by the over-generating PMG of MG-2, as well as the HMG of MG-3. MG-1 only absorbs the amount of power needed to improve its overloading as a result MG-3 starts to deliver a power of 0.12pu in addition to the excess power of 0.1pu as provided by MG-2 which is also operating as a PMG. This scenario continues until $t = t_5$ at which the overloading of MG-1 is removed and does not need external

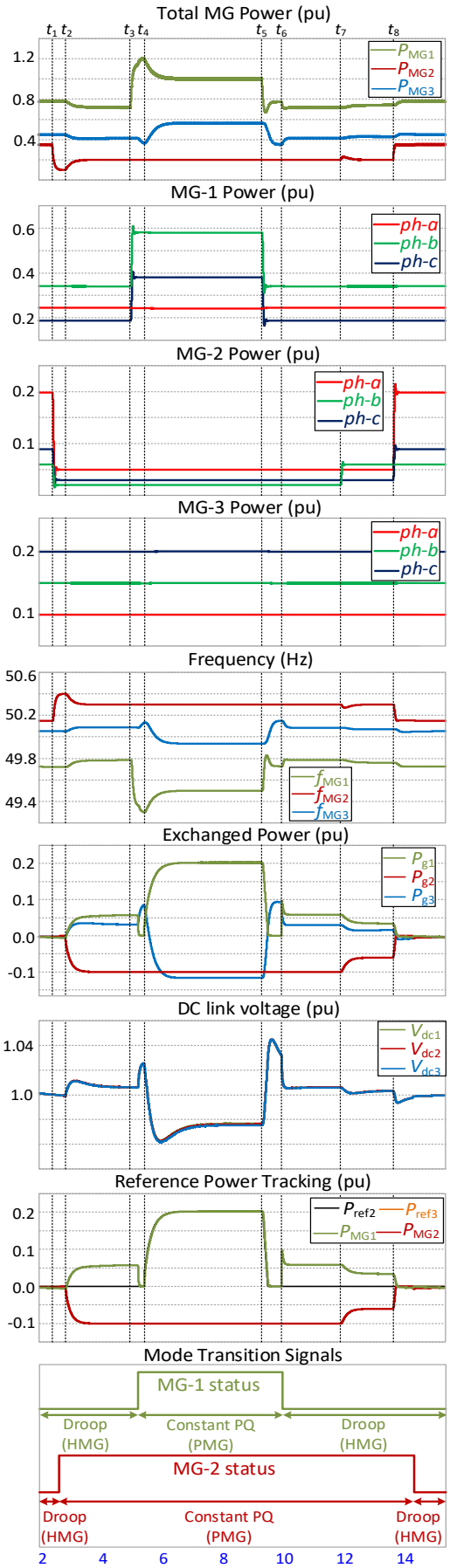

Figure 4.7 Simulation results of case study-2 for topology- 3.

Table 4.8 Over-generation and overloading events applied to microgrids in case study-2 at different intervals.

Time Instant	MG Status MG-1	MG-2	MG-3	Action taken
t_1	HMG	**OG**	HMG	Normal operation for MG-1 and 3 while MG-2 is over-generating.
t_2	HMG	PMG	HMG	MG-2 switches to PQ mode to deliver power and MG-1 and 3 are operating in droop to support it.
t_3	**OL**	PMG	HMG	MG-1 is over-loaded.
t_4	PMG	PMG	HMG	MG-1 changes its operation mode from droop to PQ to receive power. Both MG-1 and 2 are supported by MG-3.
t_5	FMG	PMG	HMG	MG-1's overload is removed while MG-3 was supporting MG-2. MG-1 exchanges zero power at this instant.
t_6	HMG	PMG	HMG	MG-1 switches to droop and joins MG-3 in supporting MG-2.
t_7	HMG	PMG	HMG	MG-2's over-generation is reduced but still remains overloaded. The absorbed power by HMGs is adjusted.
t_8	HMG	HMG	HMG	MG-2's overgeneration is over. All the MGs become HMG and all MGs switch to droop mode.

support. As a result, the VSC of MG-1 switches its mode of operation from constant PQ mode to the dc voltage droop control mode with zero power exchange. However, as the CMG still includes an over-generating PMG (i.e., MG-2), the HMG of MG-3 starts to absorb the excess power of MG-2. At $t = t_6$ MG-1 switches back in dc droop mode and starts absorbing excess power in addition to MG-3, based on their preset droop coefficient value as before. At $t = t_7$, some load is added back to phase-b of MG-2 and hence reduces the excess generation from 10% to 6%. The frequency controller of MG-2 adjusts the power reference to 0.06pu and thus the power absorbed by MG-1 and MG-3 are 0.038pu and 0.018pu respectively. At $t = t_8$, the situation of excess generation in MG-2 is alleviated and goes back to its nominal operating condition to become an HMG. Thus, the exchange of power is ceased and the VSC of MG-2 switches back to dc voltage droop. Table 4.8 summarises the events applied to the microgrids and the corresponding actions taken according to the proposed control mechanism for study case- 2

4.2.4 Coordinated Control Mechanism among BESs and CMGs

To evaluate the dynamic performance of the proposed coordinated control mechanism of power-sharing among BESs and CMGs, let us consider the system of Fig. 3.22 with

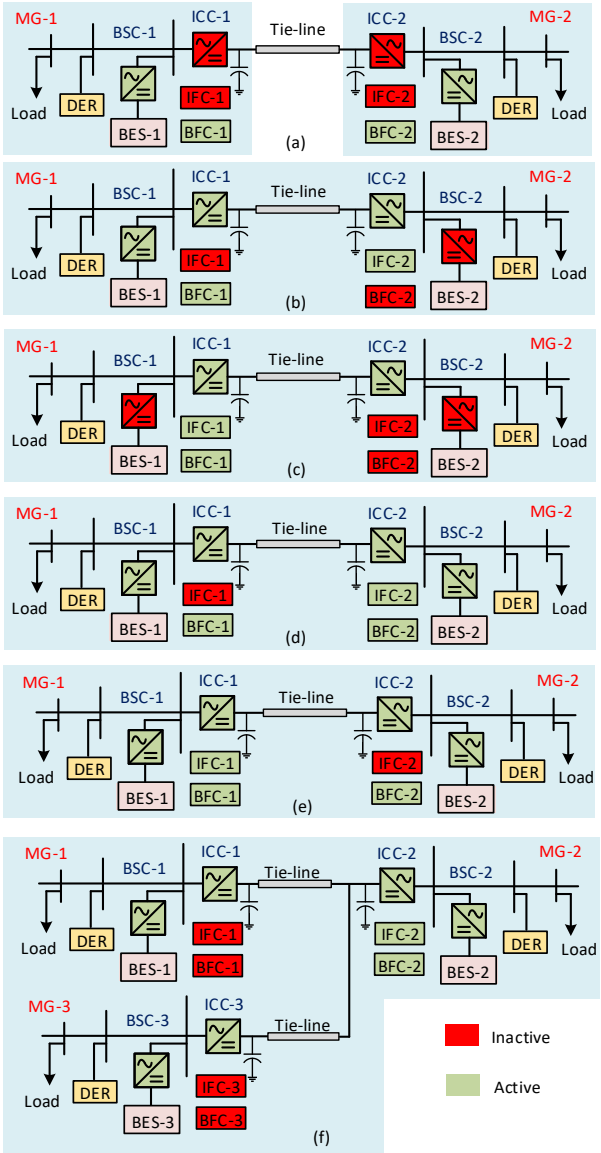

Figure 4.8 Status of self-healing agents and converters in 6 different case studies.

two (for study cases 1-5) and three microgrids (for study case 6) are connected through a dc power exchange link, respectively. The performance of such a system has been evaluated through six study cases, as illustrated schematically in Figure 4.8, and discussed separately in this section. In these studies, the maximum capacity of each microgrid is 70kW and the minimum acceptable frequency limit is 49.8Hz while the nominal frequency is 50Hz. The base power is assumed as 100 kVA while the base dc voltage in the power exchange link is assumed as 1kV.

In these study cases, to replicate non-ideal scenarios, all the power electronic converters are represented by their detailed switching model and the conventional close loop control systems are carefully designed with necessary gain and phase

margins, so that rated power exchange can take place within the network and their stability limits. Each assumed microgrid also consists of two or more power electronic converter based DERs, operating under droop control, and one power electronic converter interfaced with BES. Furthermore, different operating and loading conditions of the microgrids and their BES are considered such as – independent/joint operation of the controllers, transition in controller actions and light/moderate/heavy overloading. All the control actions are carried out using local measurements only and without any data communication among the controllers and converters.

4.2.4.1 Case Study-1 (*Light Overloading*)

To verify the ability of each microgrid to operate independently and addressing the overloading problem, let us consider the network of Figure 4.8a and assume that both microgrids are initially operating at the steady-state condition and under the droop control. In this particular study case, both microgrids will be lightly overloaded, and the situation can be alleviated by their respective BES units. Hence, no external power support is required. The applied events in both microgrids at different time instants are as follows while the simulation results of the microgrids are shown in Figure 4.9.

The BES unit of MG-1 and 2 are initially in discharging mode and respectively providing a power of 0.1 and 0.075 pu. At $t = 0.7$ s, MG-1 becomes overloaded by 15% (see Figure 4.9a); hence, its frequency decreases to 49.7 Hz (see Figure 4.9e). As the frequency has fallen beyond the acceptable limit of 49.8 Hz, MG-1's BFC gets activated after a fixed delay of 0.5 s. The controller determines the amount of overload, $P_{\mathrm{BSC-1}}^{\mathrm{OL}}$, to bring the frequency back to its acceptable limit. The BES unit adjusts its reference power, $P_{\mathrm{BSC-1}}^{\mathrm{ref}}$, and starts to inject the required power to alleviate the overload situation. At $t = 2.5$ s, the BES power level has decreased from 0.1 to 0.075 pu, based on its SoC level, as decided by the MGCC. Thus, the BFC again adjusts the power level to maintain the frequency at 49.8 Hz. At $t = 4$ s, the overloading of MG-1 is removed, and it goes back to normal operating condition. The BFC sets the reference overload power to zero and gets deactivated after a delay of 0.4 s. MG-1 continues to receive 0.075 pu of power from BES as decided by MGCC.

Now, let us consider the scenarios applied in the case of MG-2. MG-2 was initially at the steady-state condition while MG-1 was undergoing the overloading scenarios. As

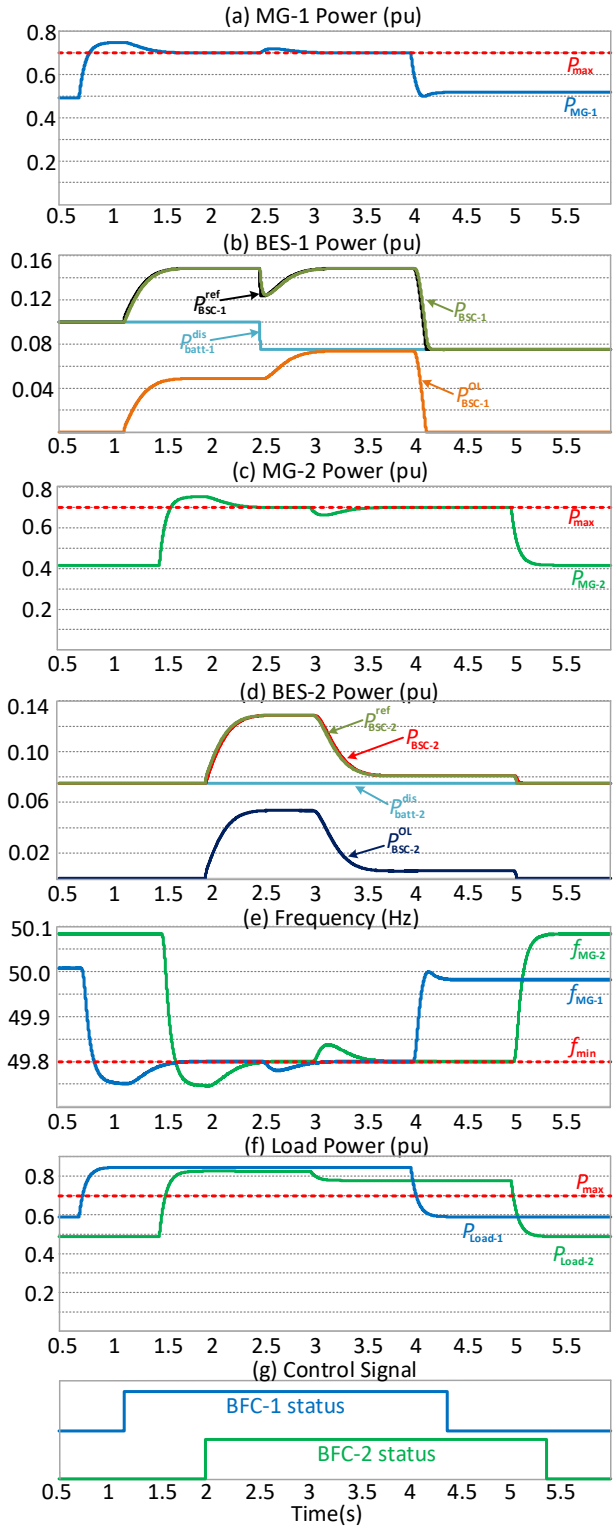

Figure 4.9 Simulation results for light overloading in case study-1.

the ICC and the power exchange link provide complete isolation among the microgrids, any changes in MG-1 does not affect the operation of MG-2, and thus ensures complete autonomy in the operation of the microgrids. At $t = 1.5$ s, 13%

overload is applied in MG-2, and thus frequency goes below 49.8 Hz (See Figure 4.9c and 4.9e). The BFC of MG-2 gets activated after 0.5 s and starts to inject additional power of 0.055 pu to the MG-2 to retain the frequency back to 49.8 Hz. At $t = 3$ s, the overload is reduced by 8%, and hence the new overload level is 5%. Therefore, the BFC reduces the reference power to the new value of 0.005 pu. At $t = 5$ s, the overload is completely removed and the BFC gets deactivated after 0.4 s as the microgrid returns to the normal operation.

4.2.4.2 Case Study-2 (*Moderate Overloading*)

Let us assume, a scenario in which a microgrid is moderately overloaded, but the BES unit does not have enough energy storage to alleviate the overload. At that instant, if the neighbouring microgrid has excess power available, it can supply the required power to the overloaded microgrid through the power exchange link. The schematic of the considered network is shown in Figure. 4.8b while the simulation results are provided in Figure 4.10. Let us assume a scenario in which MG-2 is overloaded by 20% at $t = 0.3$ s, and hence its frequency drops below 49.8 Hz. During this time, the BES of MG-2 is not in operation due to its low stored energy level, i.e., the SoC of the BES unit is below $SOC_{\min}^{\mathrm{ICC}}$. As a result, the BFC remains inactive and the IFC gets activated by sensing the frequency deviation and low level of SoC. First, the IFC will change the mode of operation of ICC from dc-link voltage control to constant PQ control mode. After a preset delay of 0.4 s, the IFC calculates the amount of overload power that needs to be imported from MG-1 to retain the frequency back to 49.8 Hz through the ICC of MG-2. It may be noted that the ICC of MG-1 will continue to operate in maintaining the dc-link voltage of the power exchange link and operates in its nominal condition. A power of 0.2 pu is required to alleviate the overload situation of MG-2 as can be seen from Figure 4.10c, denoted as P_{g2}. The power supplied by MG-1 is slightly higher over 0.2 pu because of the losses in the converter and tie-line as denoted by P_{g1}. At $t = 1.3$ s, an additional 15% load is added to MG-1. Due to the addition of this load, while it was supporting MG-2 to alleviate its overloading, MG-1 also becomes overloaded by 5%. The SoC level of BES in MG-1 is over nominal value and was delivering power of 0.1pu while it was overloaded. Hence, additional power needs to be supplied by the BES and thus the BFC of MG-1 is activated. It determines

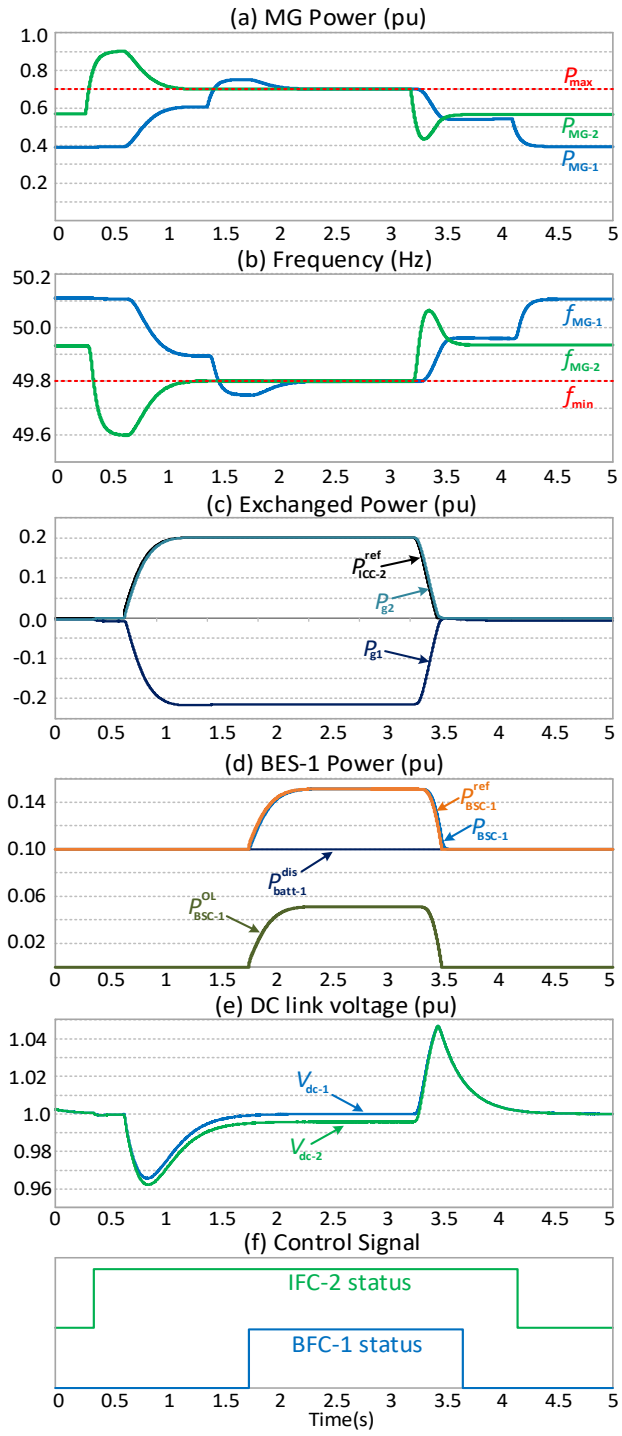

Figure 4.10 Simulation results for moderate overloading in case study-2.

the required overload power to be supplied is 0.05 pu and the total output power of BSC of MG-1 is 0.15 pu, as can be seen from Figure 4.10d. This scenario continues until $t = 3.2$ s at which the overloading of MG-2 is removed and MG-2's frequency increases above the minimum limit. Therefore, MG-2 goes back to the normal operating condition. As MG-1 does not need to support MG-2 anymore, the frequency

of MG-1 also increases above the minimum limit of 49.8 Hz at the same time and MG-1 goes back to its nominal operating condition as soon as MG-2's overload is removed. MG-1 continues to operate nominally with an additional 15% added load until $t = 4.2$ s when the additional load is also removed from MG-1. The respective control signals for activating the self-healing agents are shown in Figure 4.10f. It is to be noted that the IFC is activated for MG-2 as it needed support through the power exchange link while BFC was activated for MG-1 as it is supported by its local BES unit. It may also be noted here that both IFCs must not get activated at the same time in the event of overloading as there will be no converter to regulate the voltage of the power exchange link. This is realised by the ICC detection loop (which is a window detector circuit). The time delay in the deactivation of IFC is greater than BFC as IFC must wait for a longer period to allow the dc-link voltage to settle down and reach the steady-state. When the IFC is deactivated, the control of the corresponding ICC shifts from constant PQ control mode to dc-link voltage control mode.

4.2.4.3 Case Study-3 (*Controller Transition*)

Let us consider the network of Figure 4.8c and assume a scenario in which a microgrid is lightly overloaded, and the situation can be alleviated easily just by the BES unit itself. But if the overloading continues for a long duration of time, the BES's stored energy will be depleted rapidly. As a result, the SoC level is also decreasing in proportion to its stored energy. At some point, the BES will stop supporting the microgrid due to the lack of adequate stored energy. Therefore, a transition in the control action needs to take place, i.e., the IFC should take over in the place of the BFC to alleviate the overload. This transition in control should be done smoothly and without causing any stability issues. The simulation results of this case are provided in Figure. 4.11. Let us assume MG-1 is operating nominally with the BES supplying power of 0.025 pu at an SoC level of 65%. At $t = 0.2$ s, the microgrid is overloaded by 6%. Thus, the BFC gets activated and starts to supply an additional power of 0.06 pu to alleviate the overloading. Hence, the total power provided by the BES unit to the microgrid is 0.085 pu as can be seen in Figure. 4.11d. At $t = 2.35$ s, the SoC of BES in MG-1 goes below the minimum limit of $SoC_{\min}^{\mathrm{ICC}}$, which is assumed to be 55% in this study and hence the BFC gets deactivated as per the developed control logic.

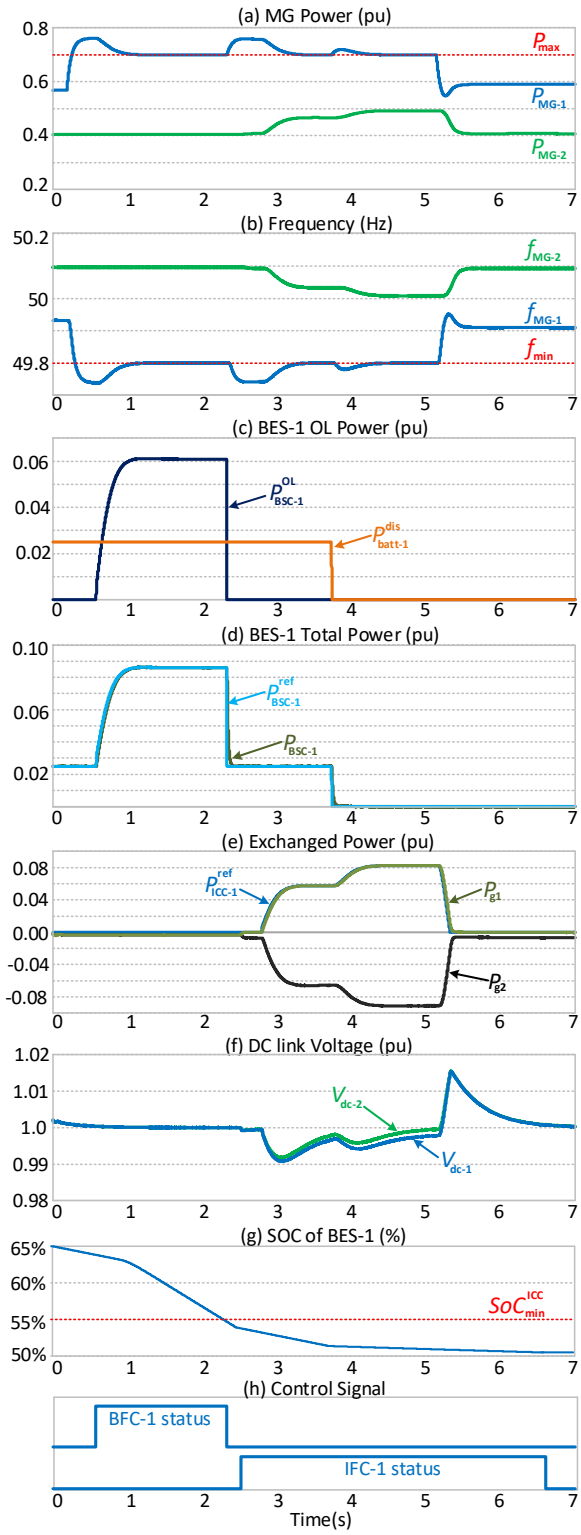

Figure 4.11 Simulation results for controller transition in case study-3.

In this instant, the BES is providing only power of 0.025pu, instead of the required power of 0.085 pu. Hence, MG-1 becomes overloaded again and the frequency falls below 49.8 Hz. It is then sensed by the IFC and therefore, gets activated at $t = 2.5$ s.

The subsequent steps of operation of IFC are the same as it was in the study case-2. IFC enables the ICC to import a power of 0.06 pu from MG-2 to alleviate the overload. This is continued until $t = 3.8$ s at which the BES of MG-1 completely stops supplying power to MG-1 as decided by the MGCC based on its SoC level. Therefore, the IFC adjusts the required power demand to retain the frequency back to 49.8 Hz once again. The overload of MG-1 is removed at $t = 5.2$ s and it goes back to its nominal operation again. The IFC waits for a certain time for the dc-link voltage to settle and then switches back to the dc-link voltage control mode.

4.2.4.4 Case Study-4 (*Heavy Overloading-1*)

To alleviate a heavy overloading situation, the total power may be shared between the local BES and the neighbouring MG. In the event of any overloading, it is expected that the microgrid should first try to alleviate the problem using local BES. If the stored energy of BES or the capacity of the BSC is not enough to address the overload problem, the microgrid should start importing power through ICC. Both BSC and ICC should operate simultaneously to supply the overload power demand. Now, let us consider the network of Figure. 4.8d. Let us assume a scenario where both the microgrids are operating in nominal condition as can be seen in Figure. 4.12. The SoC level of both BESs is at the maximum level. Hence both are supplying rated discharge power of 0.1pu to their respective microgrids. At $t = 0.2$ s, 18% overload has occurred in MG-2, and as a result, the frequency drops drastically below 49.8 Hz. This situation is sensed by BFC and it gets activated at $t = 0.5$ s. At $t = 0.7$ s, the BFC starts to generate the reference power to alleviate the overload situation as can be seen from Figure. 4.12c. Due to heavy overloading, the required power reference produced by the PI controller exceeds the maximum rated capacity of BSC, $P_{\mathrm{BSC}}^{\max}$, which is assumed as 0.2 pu in this study. Hence, the PI controller should freeze (not reset) by setting its input to zero using the multiplexer circuit. Thus, the output of the PI controller will retain the evaluated value which is the maximum power that can be delivered by the BES unit at that SoC level. This is realised by comparing the instantaneous output power of BSC, P_{BSC}, with $P_{\mathrm{BSC}}^{\max}$. The parameter of $P_{\mathrm{BSC}}^{\max}$ can be dynamically varied and evaluated based on the SoC level. In this study case, $P_{\mathrm{BSC}}^{\max}$ is set based on the BSC's maximum capacity, as BES's SoC level is at its maximum level. In any other

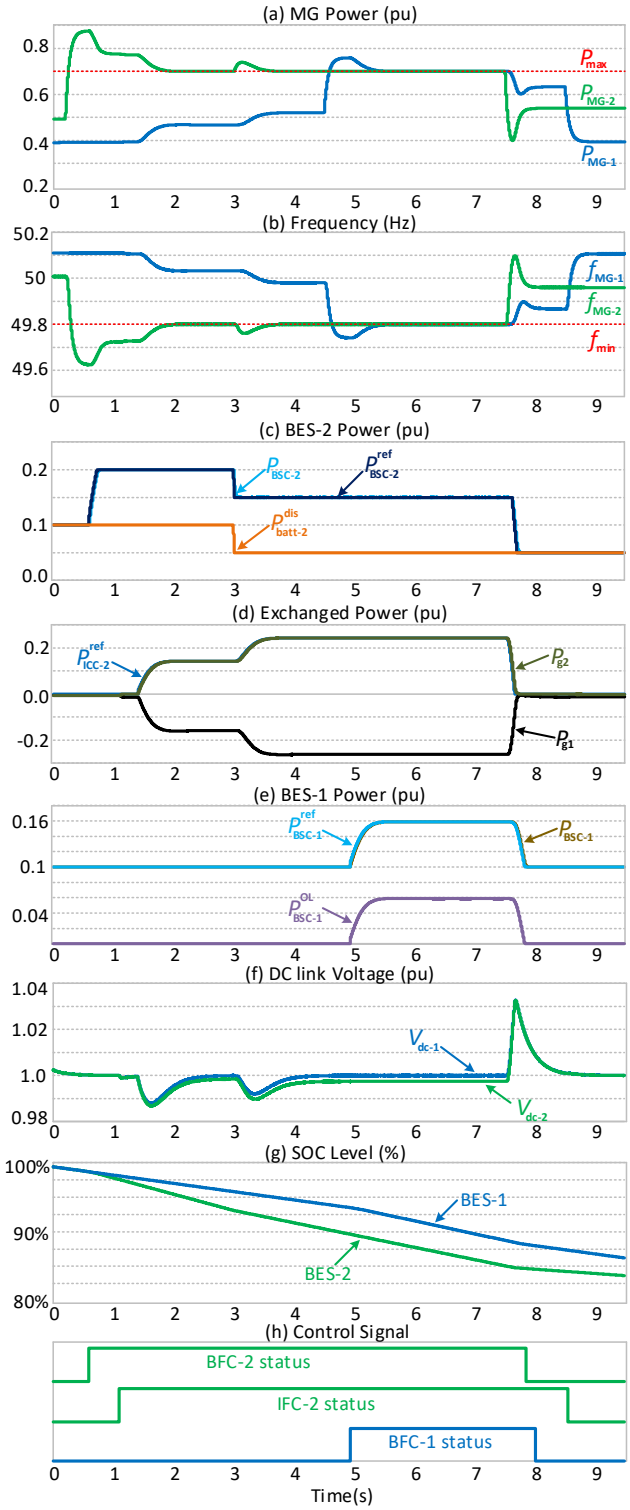

Figure 4.12 Simulation results for heavy overloading- 1 in case study- 4.

scenario, $P_{\mathrm{BSC}}^{\max}$ can be evaluated dynamically based on the BES' SoC level. This means that even though the BSC is capable to handle the required overload power, the SoC level of the BES is insufficient to produce it. Hence, $P_{\mathrm{BSC}}^{\max}$ needs to be updated

dynamically based on its SoC level and such freezing mechanism of PI controller is needed for this purpose. While both BSC and BES reach their maximum power limit of 0.2 pu, the overloading of the microgrid is not alleviated, and hence, the frequency still stays below 49.8Hz, as can be seen from Figure. 4.12b and 4.12c. This situation makes the IFC gets activated at $t = 1.1$ s. The ICC of MG-2 changes its operation from the dc-link voltage control mode to constant PQ mode and starts importing power from MG-1 at $t = 1.5$ s. Thus, the overload of the MG-2 is alleviated with both self-healing agents working simultaneously during which the BSC provides a power of 0.1 pu while the ICC supplies power of 0.12 pu, as can be seen from Figure. 4.12d. Due to the rapid discharge rate of BES-2 (as it is operating at its maximum capacity due to overload), at $t = 3$ s, the MGCC reduces the power from 0.1 to 0.05 pu. Therefore, the IFC increases the ICC's power reference to maintain the frequency at 49.8 Hz. At $t = 4.5$ s, MG-1 becomes overloaded by 6%. The BFC of MG-1 gets activated and alleviates the overload situation. At $t = 7.5$ s, the overloading of MG-2 is removed, and as a result, both microgrids are back to normal operation. It should be noted that all the four converters of both microgrids (i.e., 2 BSCs and 2 ICCs) were active and working in conjunction to alleviate the overload situation. The BFCs of both microgrids were active whereas the IFC of only MG-2 was active (as both IFCs are not allowed to get activated simultaneously). This is realised by the activated control signals, as shown in Figure. 4.12h.

4.2.4.5 Case Study-5 (*Heavy Overloading-2*)

To investigate the efficacy and capability of alleviating the overloading situation in a decentralised manner, another heavy overloading situation is considered. This study verifies that a lightly or moderately overloaded microgrid which is being supported by its BES can support its heavily overloaded neighbouring microgrid through interconnection. The proposed decentralised topology will enable the microgrids to exchange power among themselves during overload situation as long as at least one IFC is inactive. In other words, as long as a microgrid exists that is capable of regulating the voltage of the power exchange link, the exchange of power among them can take place, even though that particular microgrid may be overloaded and being supported by its BES unit. Consider the network of Figure. 4.8e for this study while

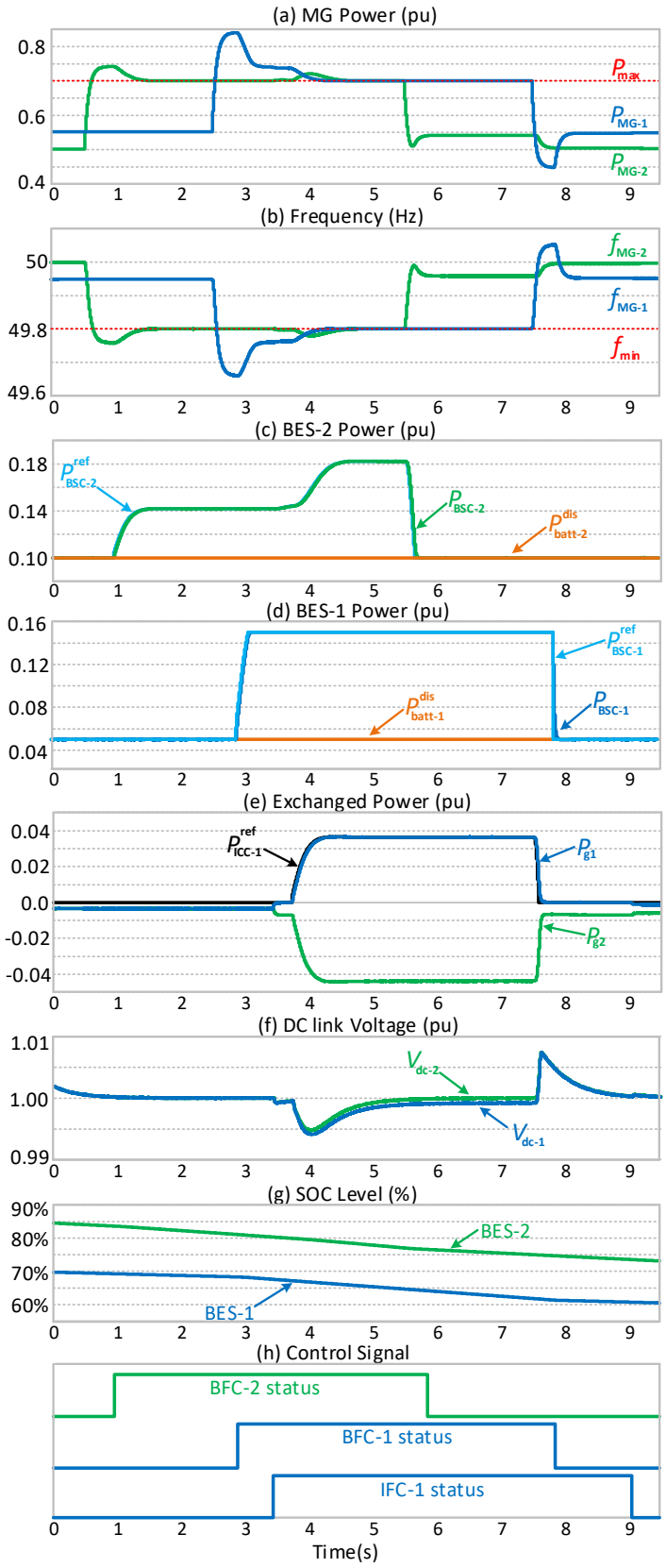

Figure 4.13 Simulation results for heavy overloading- 2 in case study- 5.

Figure. 4.13 illustrates the simulation results. Let us assume that at $t = 0.5$ s, MG-2 is

overloaded by 5%. As a result, the frequency has dropped below 49.8 Hz. BES-2 was supplying power of 0.1pu as decided by the MGCC, at the time of overloading. The drop in frequency level activates the BFC and it adjusts the active power reference for BSC to supply the required overload power to MG-2. Thus, the frequency returns to 49.8 Hz. The situation continues until $t = 2.5$s at which MG-1 becomes overloaded by 14%. At the time of overloading, BES-1 was delivering power of 0.05 pu to the MG. This activates the BFC's associated controller. The SoC of BES-1 is less than 70% at this time as can be seen from Figure. 4.13g, which sets the maximum power that is supplied by BSC, $P_{\mathrm{BSC}}^{\max}$, as 0.15 pu. In this case, the value of $P_{\mathrm{BSC}}^{\max}$ is determined based on the BES' SoC value unlike the previous case, where it was chosen based on the converter's maximum rating. Due to heavy overloading, the output of the PI controller of the BFC will reach its maximum limit of 0.15 pu within a short period of time and freezes, as can be seen from Figure. 4.13d. As the overloading problem is not alleviated, the IFC of MG-1 will get activated at $t = 3.4$ s. Hence, the mode of operation of the ICC of MG-1 changes from the dc-link voltage control to the constant PQ mode. This is a scenario where both microgrids are overloaded (MG-2 is lightly, and MG-1 is heavily overloaded). As the ICC of MG-1 is changed to constant PQ mode, the ICC of MG-2 must remain in the dc-link voltage control mode to regulate the voltage of the power exchange link. It is to be noted that, for a network where more than two microgrids are interconnected to share power, at least one microgrid is needed which is not heavily overloaded and can assign its ICC to regulate the dc-link voltage of the power exchange link. Once, the IFC of MG-1 is activated, it will produce the desired reference to start importing power from MG-2, as can be seen from Figure. 4.13e. As such, the frequency of MG-1 retains back to 49.8 Hz and the overloading is alleviated. At $t = 5.5$ s, the overloading in MG-2 is removed and it goes back to its normal operation mode. However, MG-2 keeps on supporting MG-1, as long as it remains overloaded. At $t = 7.5$ s, the overloading in MG-1 is removed and it also moves back to its normal operation. The corresponding activation control signals for BFCs and IFC of both microgrids are shown in Figure. 4.13h.

4.2.4.6 Case Study- 6 (*Multiple MGs*)

This study case demonstrates the power-sharing amongst multiple microgrids to

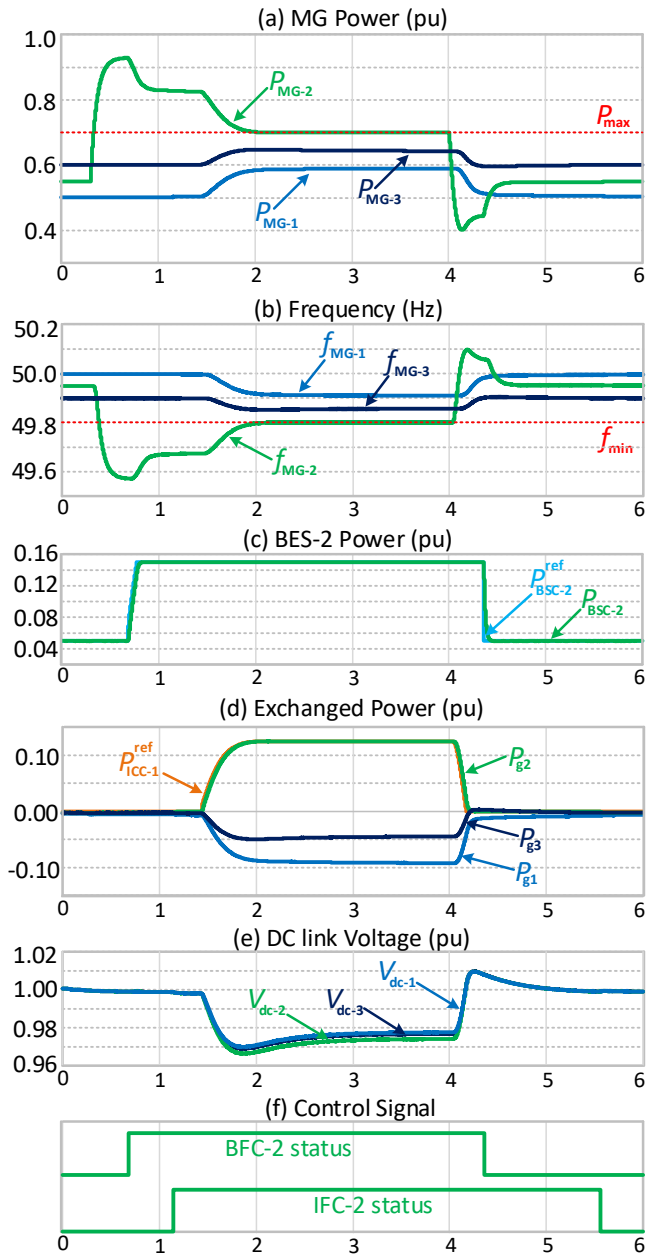

Figure 4.14 Simulation results for Multiple microgrids in case study- 6.

alleviate the overloading situation. Let us consider the network in Figure. 4.8f and assume a scenario in which three microgrids are coupled through the power exchange link. The results of this study are provided in Figure. 4.14. Let us assume that all of the three microgrids are operating in their nominal condition. BES-1, 2 and 3 are supplying respectively a power of 0.1, 0.05 and 0.1 pu to their respective microgrids, as can be seen from Figure. 4.14c. At $t = 0.3$ s, MG-2 is overloaded by 22%, and as a result, the frequency drops below 49.8 Hz. This activates the controller of BFC-2 at $t = 0.6$ s. Based on the SoC level of BES-2, the maximum power that is supplied,

P_{BSC}^{max}, is evaluated as 0.15 pu. As soon as the output power of BSC-2 reaches 0.15 pu, the controller of BFC-2 freezes, as can be seen from Figure. 4.14c. As the frequency of MG-2 is still below 49.8 Hz, IFC-2 will get activated at $t = 1.2$ s, and hence, the mode of operation of ICC-2 changes from the dc-link voltage control to constant PQ mode. At $t = 1.5$ s, both MG-1and MG-3 start supplying power to MG-2 to alleviate the overloading situation with a power ratio of $P_{g1}: P_{g3} = 2: 1$, as determined by their droop coefficients. It is expected that the power shared by MG-1 should be greater than MG-3 as the loading of MG-1 is less than MG-3 (See Figure. 4.14a). The total overload power demand for MG-2 is 0.1245 pu where the supplied power from MG-1 and MG-3 are respectively 0.091 and 0.0458 pu, as can be seen from Figure. 4.14d. To obtain the desired power-sharing, the ratio of droop coefficients of MG-3 and MG-1 is set as $q_{MG-3}: q_{MG-1} = 2: 1$ based on the ratio of their droop coefficients. The excess power supplied by MG-1 and MG-3, in addition to the overload power of MG-2, is to overcome the line and converter losses. At $t = 4$ s, the overloading of MG-2 is removed, and it goes back to its normal operation, and as such, both MG-1 and MG-3 cease to supply power to it. The corresponding control activation signals for BFC-2 and IFC-2 are shown in Figure. 4.14f.

4.3 Comparison in performance of the three topologies

Based on the time domain case studies, comparative performance analysis can be done for all of the three topologies. First, a comparison based on the output power and voltage quality can be done for topology- 1 and 2. It can be seen that both ac topologies can successfully alleviate the overloading or over-generation problems based on the developed control mechanism, however, the power quality is poorer in topology-2 as single-phase instantaneous power is oscillatory in nature. As a result, the dc-link voltage in the back-to-back converter contains a larger ripple in the case of topology-2 as compared to topology- 1. Though the number of components and power lines require for the three-phase link are more, the power quality and performance are superior and produce significantly lower line loss and thus, makes the system more efficient. Hence, the three-phase power exchange link is superior in terms of power and voltage quality as compared to the single-phase link unless a very small amount of power is required to be exchanged within the CMG network through short

interconnecting lines. Moreover, single-phase VSC operating in PQ control mode requires a phase-shifting for dq transformation that somewhat restricts its operating frequency range as the phase shifting filter is operational in one particular frequency (e.g., 50Hz in this case). The employed angle droop control technique is also beneficial for this purpose as the frequency of operation remains fixed. However, if a frequency droop control is used instead of angle droop, the performance of the single-phase VSC will deteriorate in PQ control mode as the power exchange link does not operate at a fixed frequency value in this case. Three-phase VSCs of topology- 1 does not have this problem and can be functional in both angle and frequency droop.

It has been already discussed in section 3.2.1.2 how the problem of synchronization can be overcome in ac interlinking topologies by employing angle droop instead of frequency droop. However, the dc interconnecting link in topology- 3, does not have this problem. This feature can be explained by referring to the time domain simulation results of the case studies of the three topologies. In the dc interconnecting link of topology-3, once a microgrid becomes an HMG from PMG, it can instantly join the other HMGs to support the PMGs within a CMG network, unlike topology-1 and 2. This can be observed from Figure 4.6 and 4.7. At, $t = t_5$ the microgrid's overloading is over, it becomes an FMG from a PMG. Thus, after the preset delay of 0.6s at, $t = t_6$ it becomes an HMG and instantly it joins the other HMG to support the PMG. Whereas, a similar scenario can be noticed at time $t = t_6$ in Figure 4.2 for topology-1 and Figure 4.5 for topology-2, respectively. In both topologies, though microgrid-1 becomes an HMG at this instant, it cannot get connected back to the other HMGs as long as there is an operational PMG in the CMG network. Therefore, the newly recovered HMG must wait until all the PMG(s) become HMG(s) and the exchange of power among the microgrids in the CMG network ceases completely as the synchronization with the interconnecting lines is not possible while the other microgrids are exchanging power. When there is no exchange of power, all the microgrids are at no load and the power exchange lines will operate at the same phase angle and voltage magnitude. Hence, at this situation, the mode of operation can be changed from constant PQ to angle droop control without causing any unwanted power surge or oscillation within the CMG. This can be seen from Figure 4.2 and Figure 4.5, at time instant $t = t_8$ when both the microgrids change their mode of operation from PQ to droop control simultaneously.

4.4 Summary

This chapter has demonstrated the efficacy of the proposed control technique through time-domain simulation studies, in retaining the desired upper and lower frequency limits in autonomous microgrids coupled to a common power exchange link. Such frequency regulation is achieved through proper exchange of power via the interconnecting link where the interconnecting link can be made of three different topologies. Also, it shows a control mechanism to coordinate the power-sharing among the local BES and the neighbouring microgrids in several scenarios. The presented case studies in this chapter assume different scenario and critical operating conditions of the microgrids. The studies also demonstrate that the developed control mechanism can successfully and effectively alleviate all the overloading and overgeneration scenarios through proper MG's frequency regulation and exchange of power without any communication among the microgrids.

Chapter 5 Stability Analysis

This chapter presents the small signal stability analysis of the three proposed power exchange topologies to determine the stability of the system against different operational and network parameters. The study reveals the system stability limits and margins at different operating conditions and its findings help us in selecting the suitable network and design parameters for different topologies to avoid instability.

5.1. Stability Analysis

The stability of the power exchange strategy for all three CMG topologies is evaluated. The small signal stability analysis is performed by varying numerous key design parameters such as the active and reactive power droop coefficients, interconnecting line's impedance, and PMG's power demand. The eigenvalue plots obtained from the stability analysis are shown in Figure 5.1-5.11.

Among all these parameters, the active power droop coefficient, m_{MG}, (for topology-1 and 2) exhibits the most dominating effect over the CMG stability and can drive the system towards instability; whereas the CMG's dynamics and response are affected by the other parameters but have relatively less influence on the system's stability. For topology-3, parametric variations affect the network dynamics, but it is not as dominant as it is in topology-1 and 2 and more importantly, do not lead the system to instability.

5.1.1. Variation of Droop Coefficients

The active power droop coefficient of m_{MG} is changed in steps from its nominal value of $0.002\mathrm{rad/kW}$ for both topology-1 and 2, while the reactive power droop coefficient of n_{MG} is kept constant. The coefficient m_{MG} and n_{MG} are defined in Equation 3.12

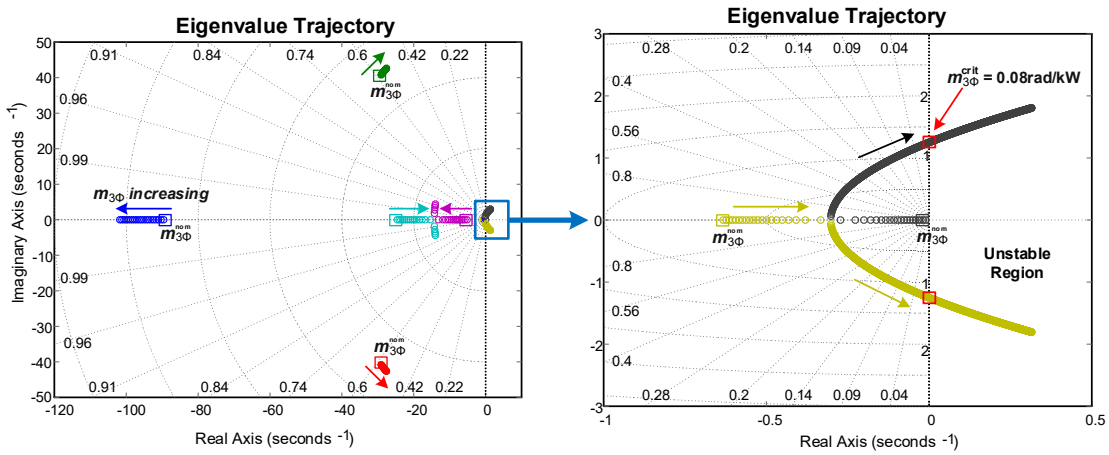

Figure 5.1 CMG Stability analysis for topology-1: Eigenvalue trajectory for variation of droop coefficients $m_{MG}^{3\emptyset}$.

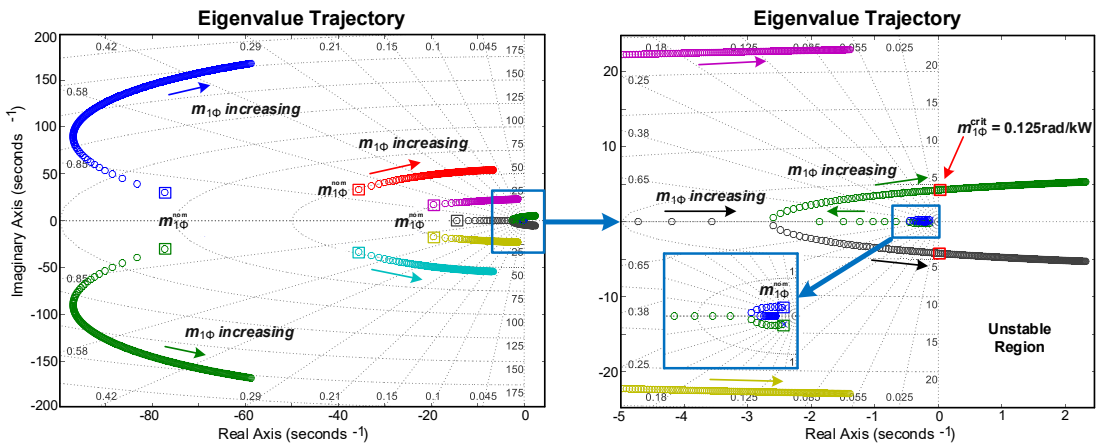

Figure 5.2 CMG Stability analysis for topology-2: Eigenvalue trajectory for variation of droop coefficients $m_{MG}^{1\emptyset}$

and 3.13, respectively. The critical value of $m_{\mathrm{MG}}^{3\emptyset}$ for topology-1 is obtained as $m_{3\emptyset}^{\mathrm{crit}} = 0.08\mathrm{rad/kW}$ which can be seen from Figure 5.1 whereas, the critical value of $m_{\mathrm{MG}}^{1\emptyset}$ for topology-2 is obtained as $m_{1\emptyset}^{\mathrm{crit}} = 0.125\mathrm{rad/kW}$ that can be seen from Figure 5.2. Any further increase in the value of m_{MG} in both topologies will make the CMG unstable. This is also verified by time-domain simulation in PSIM and the critical values are obtained as, $m_{3\emptyset}^{\mathrm{crit}} = 0.076\mathrm{rad/kW}$ and $m_{1\emptyset}^{\mathrm{crit}} = 0.122\mathrm{rad/kW}$ which are almost equal to the values obtained from MATLAB simulation. On the other hand, the variation of n_{MG} for both topology-1 and 2, does not significantly affect the stability of the CMG as the reactive power flowing through the CMG link is very small, and

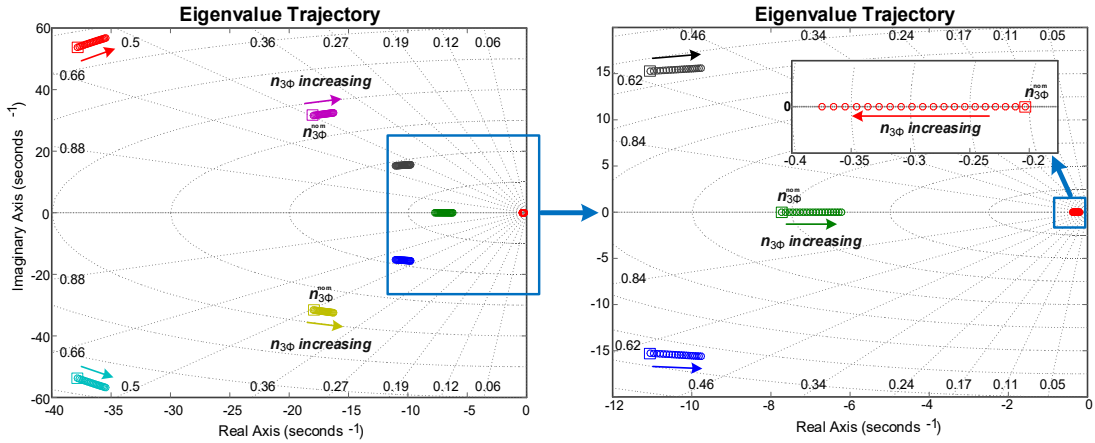

Figure 5.3 CMG Stability analysis for topology-1: Eigenvalue trajectory for variation of droop coefficients $n_{MG}^{3\emptyset}$.

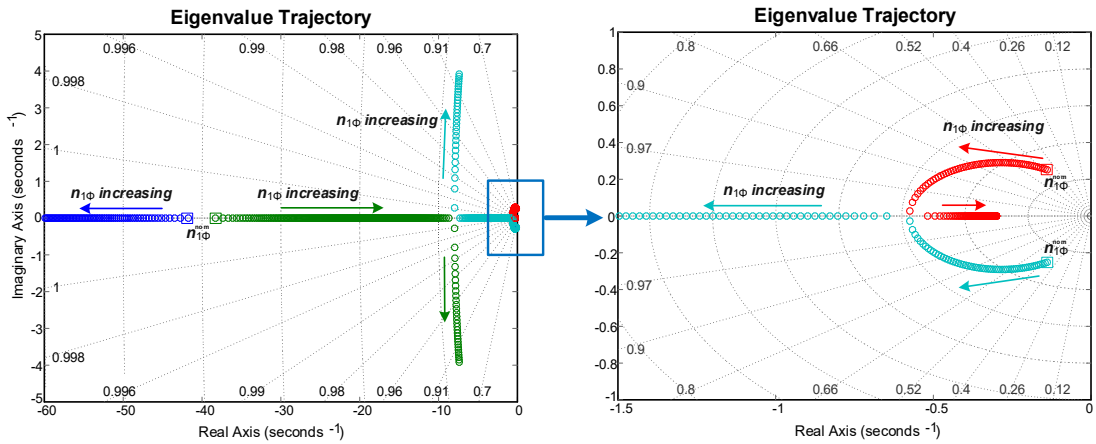

Figure 5.4 CMG Stability analysis for topology-2: Eigenvalue trajectory for variation of droop coefficients $n_{MG}^{1\emptyset}$.

hence the variation of n_{MG} does not have a noticeable effect on the system stability, as seen from Figure 5.3 and Figure 5.4, respectively. The value of n_{MG} was varied from its nominal value of $0.004\mathrm{rad/kVAR}$ up to $0.4\mathrm{rad/kVAR}$ (i.e.,100 times of its nominal value) to obtain the eigenvalue trajectory plots.

At the nominal value of droop coefficients $m_{\mathrm{MG}}^{\mathrm{nom}}$ and $n_{\mathrm{MG}}^{\mathrm{nom}}$, the response of topology-2 is more oscillatory (less damping) compare to the topology-1 which can also be justified from the eigenvalue location for nominal values of droop coefficients as shown in Figure 5.1-5.4 and also from the frequency response plots of Figure 3.10 and Figure 3.18. However, topology-1 is more sensitive to variation of droop coefficients

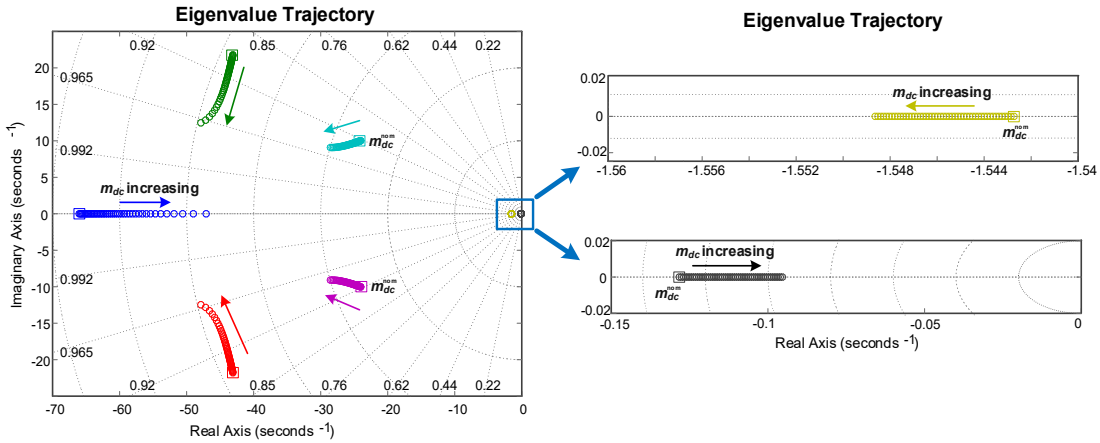

Figure 5.5 CMG Stability analysis for topology-3: Eigenvalue trajectory for variation of droop coefficients $m_{\mathrm{MG}}^{\mathrm{dc}}$

and becomes unstable with a relatively smaller value ($m_{3\emptyset}^{\mathrm{crit}} = 0.08\mathrm{rad/kW}$) as compared to topology-2 ($m_{1\emptyset}^{\mathrm{crit}} = 0.125\mathrm{rad/kW}$). In other words, topology-2 has better tolerance to droop coefficient variations and a larger stability range even though the nominal response is more oscillatory compared to topology-1. If the CMG network requires to operate with a larger value of droop coefficients, topology-2 is more suitable than topology-1. For topology- 3, the eigenvalue trajectory plot is obtained by varying only the active power droop coefficient m_{MG} as the exchange of reactive power is not possible in dc droop control and the associated dc power exchange link. The value of $m_{\mathrm{MG}}^{\mathrm{dc}}$ is incremented from its nominal value of $1V/\mathrm{kW}$ up to $50V/\mathrm{kW}$ to obtain the eigenvalue trajectory plot as shown in Figure 5.5. It can be observed that, increasing the value of $m_{\mathrm{MG}}^{\mathrm{dc}}$ does not make the CMG network unstable like topology-1 and 2 and hence no critical value of $m_{\mathrm{MG}}^{\mathrm{dc}}$ was obtained. However, the response of the dc power exchange link is affected by such variation of m_{MG}. The response of the dc power exchange link becomes over-damped and sluggish as the value of m_{MG} is increased. It can be seen from the eigenvalue plot of Figure 5.5 that, the dominant pole moves further towards the origin as m_{MG} is increased and hence make the system response very slow and thus the dc power exchange links relatively longer time to settle to its steady-state value when power exchange occurs among the microgrids. A smaller value of m_{MG} makes the dc-link respond faster. However, there is a limiting value of m_{MG} that depends on the value of line resistance. To share the desired amount

of power among the microgrids according to their droop ratio, m_{MG} should be large enough as compared to the line resistance, otherwise, the assumption based on which conventional dc droop method is developed does not remain valid, and hence the property of the desired power-sharing among the microgrids according to their droop coefficients is lost. This phenomenon is further discussed in section 6.1 of sensitivity analysis.

5.1.2. Variation of PMG Power

The dynamic response of the CMG is also affected by the amount of power absorbed (overload) from or injected (over-generation) to the CMG network through the PMG. To observe this effect, the PMG power was varied from 0.02pu to 0.15pu for all the three topologies and the corresponding eigenvalues are plotted. This is shown in Figure 5.6-5.8. In all the three topologies, as the PMG power increases, the system damping increases and the response becomes slightly sluggish. In other words, the CMG network performs better when rated power is exchanged among the microgrids forming the CMG. In topology-1, the dominant eigenvalue moves towards the right as the PMG power increases and hence makes the system response sluggish; however, such variation of PMG power level does not lead the system to instability as can be seen from the eigenvalue plot of Figure 5.6. A similar scenario can be observed in topology-2 also, but the dominant eigenvalues in this topology are complex conjugate pair that moves towards left as the PMG power increases and thus the CMG stability remains unaffected as shown in Figure 5.7. Finally, in topology-3, the dominant eigenvalue moves towards the right with PMG power variation and the effect is similar to the effect as discussed for topology-1. The eigenvalue plot for topology-3 is shown in Figure 5.8.

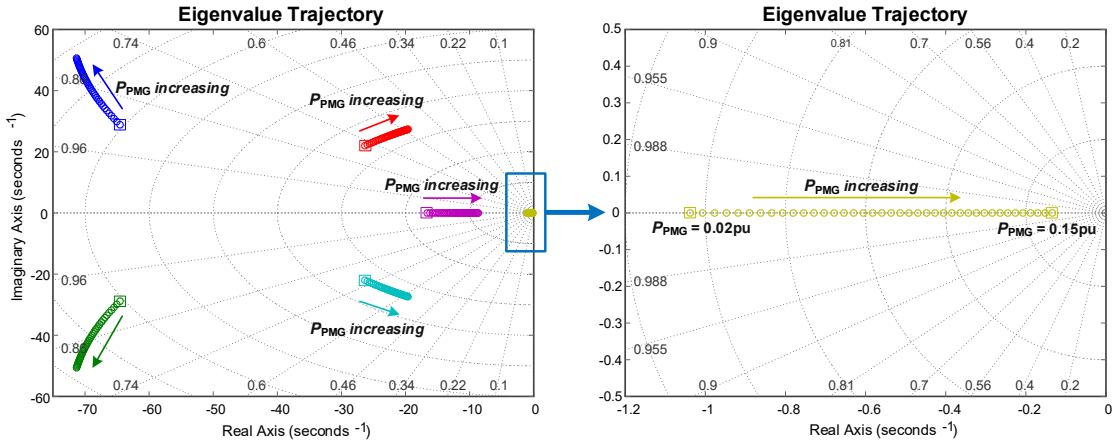

Figure 5.6 CMG Stability analysis for topology-1: Eigenvalue trajectory for PMG Power variation

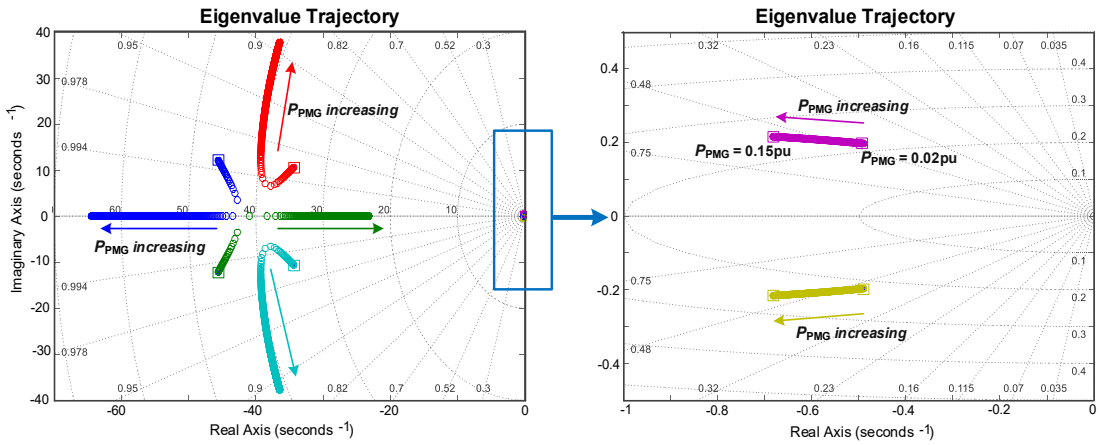

Figure 5.7 CMG Stability analysis for topology-2: Eigenvalue trajectory for PMG Power variation

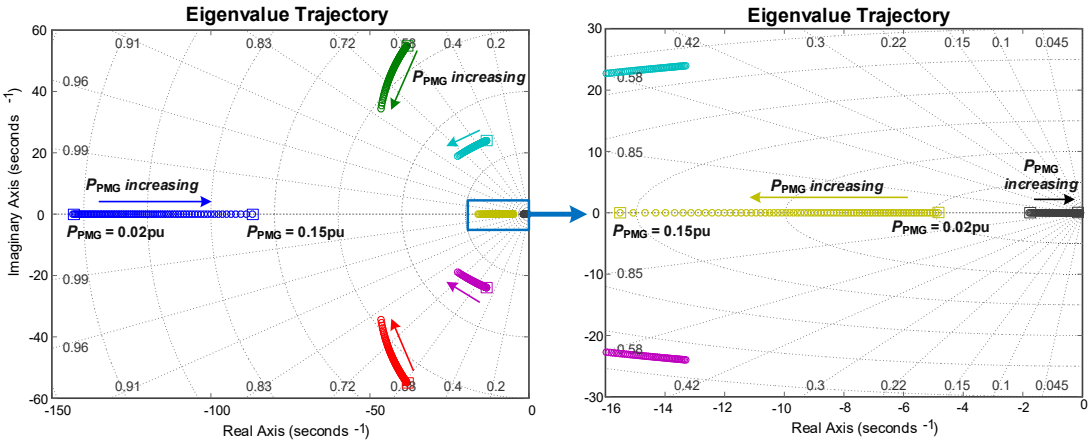

Figure 5.8 CMG Stability analysis for topology-3: Eigenvalue trajectory for PMG Power variation

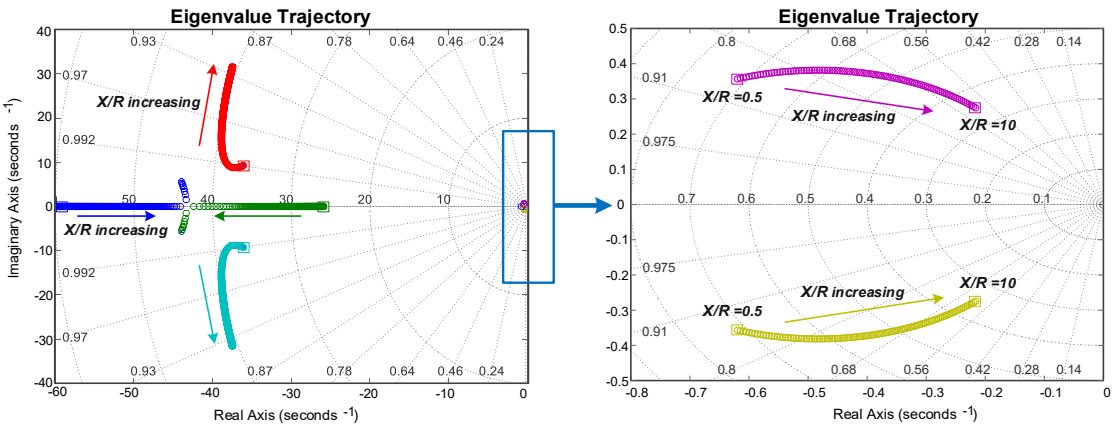

Figure 5.9 CMG Stability analysis for topology-1: Eigenvalue trajectory for line impedance variation.

5.1.3. Variation of Line parameters

The impedance of the line (i.e., line reactance to resistance ratio, termed as X/R) was varied for topology-1 and 2 whereas, the line resistance, R_{line} is varied for the topology- 3, to see the effect on stability. It may be noted here that, as topology- 3 is a dc interconnection link, the power exchange

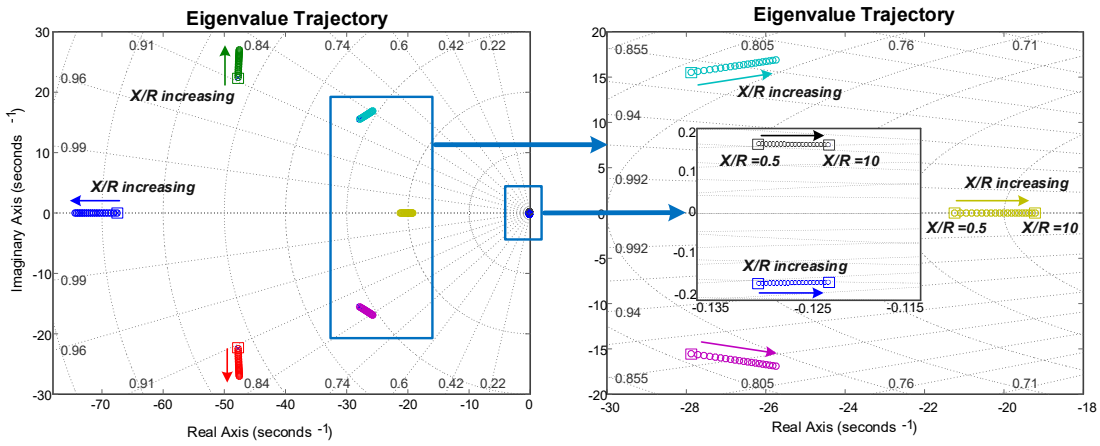

Figure 5.10 CMG Stability analysis for topology-2: Eigenvalue trajectory for line impedance variation.

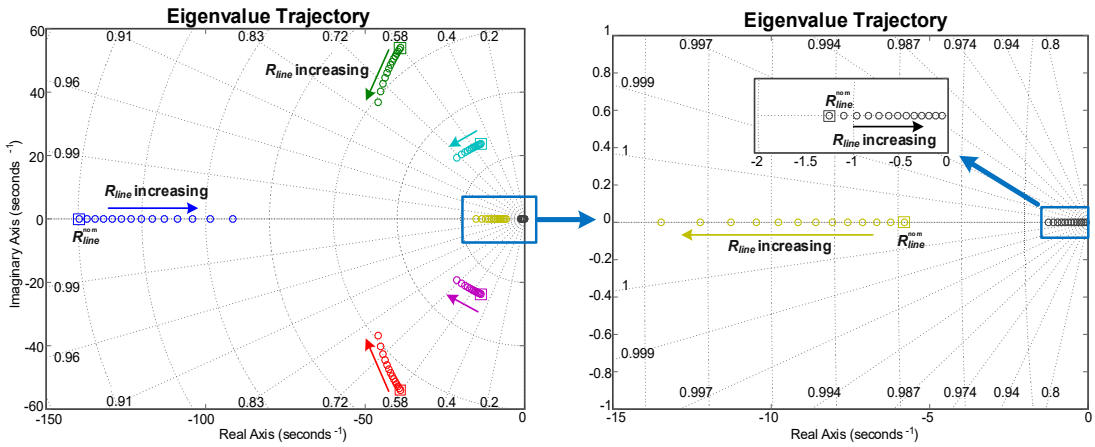

Figure 5.11 CMG Stability analysis for topology-3: Eigenvalue trajectory for line resistance variation.

lines are assumed to be purely resistive with zero inductance. In topology-1 and 2, the X/R ratio is varied from 0.5 to 10 (i.e., line inductance is increased from 0.16mH to 3.2mH while the resistance of the line is held constant at 0.1Ω). The evaluated eigenvalues are shown in Figure 5.9-5.11. It can be observed that increase in X/R ratio i.e., increase in line inductance, reduces the system damping and makes the system response oscillatory as the complex conjugate pair of eigenvalues moves towards the right (see Figure 5.9 and Figure 5.10), whereas in topology-3, the system damping increases and makes the response very sluggish as the dominant eigenvalue moves

further towards the right with increasing value of line resistance (see Figure 5.11). Such increase in line resistance deteriorates the property of power-sharing based on the microgrid's droop coefficient but, does not lead the system towards instability.

5.2. Summary

This chapter has presented the stability analysis of all of the three CMG topologies. The stability of all the CMG topologies was examined for different design and network parametric variations. It has been found that the stability of the CMG is affected by the active power droop coefficient in topology-1 and 2, and hence the critical value of the parameter is evaluated. On the other hand, the reactive power droop coefficient cannot affect the CMG stability and its effect is almost negligible. However, in topology-3, variation of dc droop coefficient does not make the system unstable; but, a large value of dc droop coefficient makes the system highly overdamped. The power injected or consumed by PMG also affects the CMG dynamics. A larger amount of PMG power offers more damping and makes the system response sluggish whereas, a smaller value of PMG power reduces the system damping and makes the response oscillatory as can be seen in all three topologies. Line resistance and reactance reasonably affect the CMG dynamics but not dominating enough to cause instability unless an extremely large value of reactance is used. Finally, based on all the stability results, it can be concluded that three-phase topology is more stable than single-phase topology but less tolerant and more sensitive to parameter variations. On the other hand, dc-link topology appears to be the most stable and robust among all the three topologies.

Chapter 6 Sensitivity Analysis

This chapter presents the sensitivity analyses to demonstrate and validate the performance of the three proposed topologies in terms of several key design and operational factors. Sensitivity analysis reveals the system operation robustness against the variation of some network and design parameters. The findings of this chapter help us in selecting the suitable network parameters for a robust operation. In this study, sensitivity analysis reveals several key design factors that govern and affect the performance of the CMG.

6.1. Sensitivity Analysis

The sensitivity of the power exchange link and employed control strategy for all the three topologies against the design and operational parameters has been analysed. The objective is to determine how the variation of the interconnecting line impedance (i.e., the distance of the microgrids from each other) and the amount of power delivered or absorbed by a PMG affect the power exchange link's performance. The line loss, the amount of power delivered/absorbed from HMGs to PMG, the LSC's voltage and droop angle, the HMG's frequency, dc-link voltage, and finally error in power-sharing based on their droop ratio are evaluated in the sensitivity analysis. The obtained results are shown in Figure 6.1-6.14.

The study is carried out for all three CMG topologies for a scenario where two HMGs are supporting one PMG while sharing the power with a droop ratio of 2:1. The results show that the power-sharing among the HMGs based on their droop ratios is affected to some extent as the impedance of the interconnecting lines (i.e., the distance among the microgrids) is increased in the case of topology-1 and 2. The error in power-sharing stays within the limit due to the employed modified angle droop control technique using virtual inductance which minimizes the error margin. It can be noted here that,

conventional angle droop technique is highly sensitive to the magnitude of the line impedances and for the technique to be accurate and applicable, the line reactance should be several times larger than the resistance, which may not be always feasible for practical CMG networks. Moreover, a larger value of droop coefficients drives the system towards instability. To ensure adequate stability margins, droop coefficients are selected to be small enough, but the sharing of the desired power among the microgrids according to their droop coefficients will be lost. Hence, to ensure the desired power-sharing among the HMGs, the modified angle droop method is employed. One of the main objectives of the sensitivity analysis is to demonstrate the ability to share power among the HMGs operating under the modified angle droop while line impedances are varied, and the ratio of line resistance to reactance is larger than unity.

However, in the case of topology- 3, such error in power-sharing is substantially larger as the conventional dc voltage-power droop control technique is employed. The conventional dc droop method is subjected to a mismatch in power-sharing and experiences an uneven drop in dc-link voltage across the interconnecting link [114, 115]. Different values of resistances of the interconnecting lines (that is governed by the distance among the microgrids forming the CMG) cause this voltage drop and such voltage mismatch is responsible for the loss of the desired power-sharing according to their droop coefficient among the microgrids. This mismatch in the droop voltage and the resulting circulating current can be removed using the virtual resistance method proposed in [115].

6.1.1. Line Parameter Variation

The first analysis is conducted for topology-1 and 2 together to make a comparison between the sensitivity of the three-phase and single-phase ac interconnecting links for variations of the same parameter. The HMG's shared power through the link, LSC's droop angle and voltage, line loss, and error percentage in power-sharing as the impedance varies are shown in Figure 6.1a-6.1h. For both topologies, the sensitivity analysis was carried out considering a situation when one PMG is supported by two HMGs. The nominal line impedance used in the simulation of case studies is used as a reference and all parameters are normalised based on this value. The PMG power

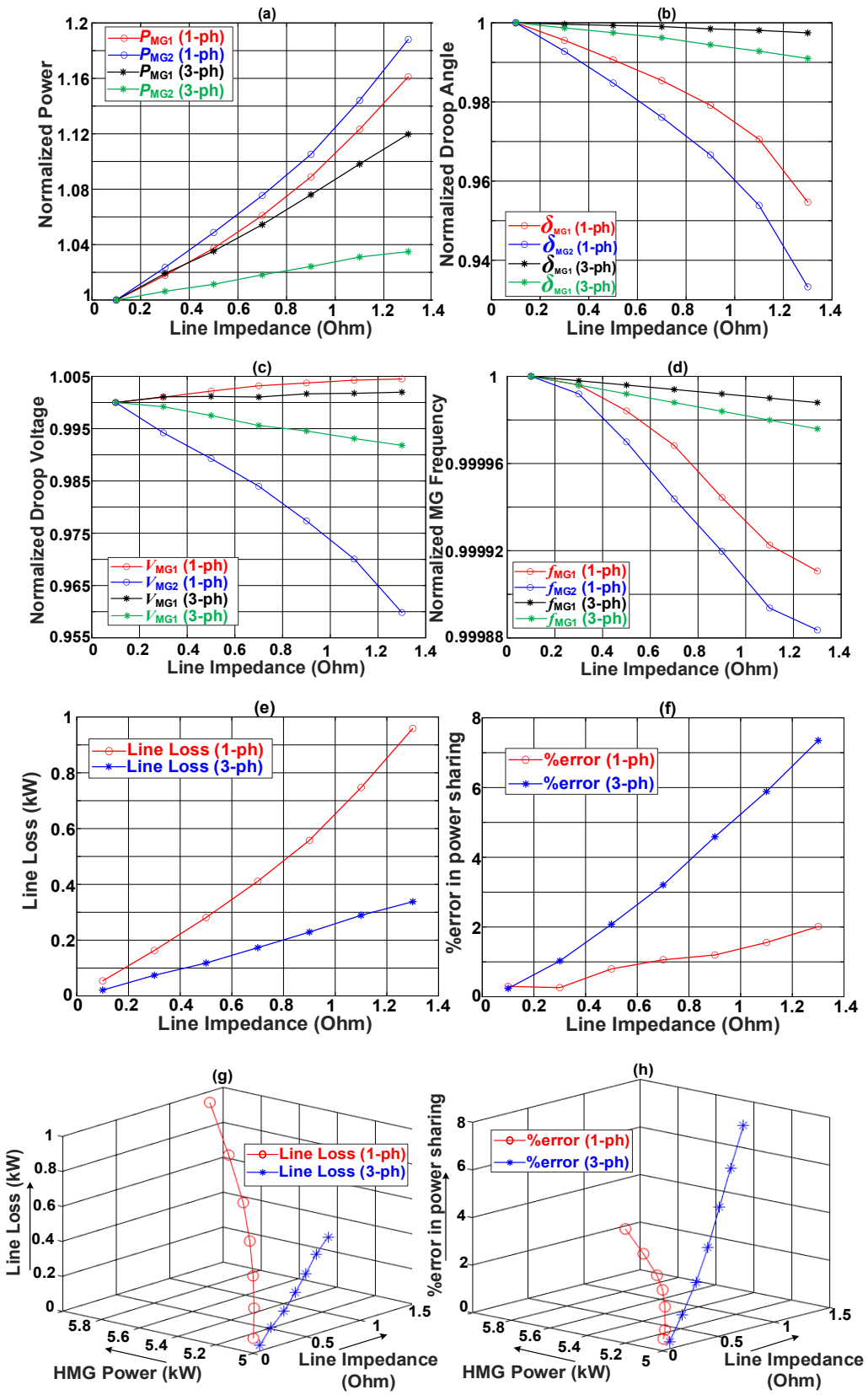

Figure 6.1 Comparative CMG sensitivity analysis of topology-1 and 2 for line impedance variation.

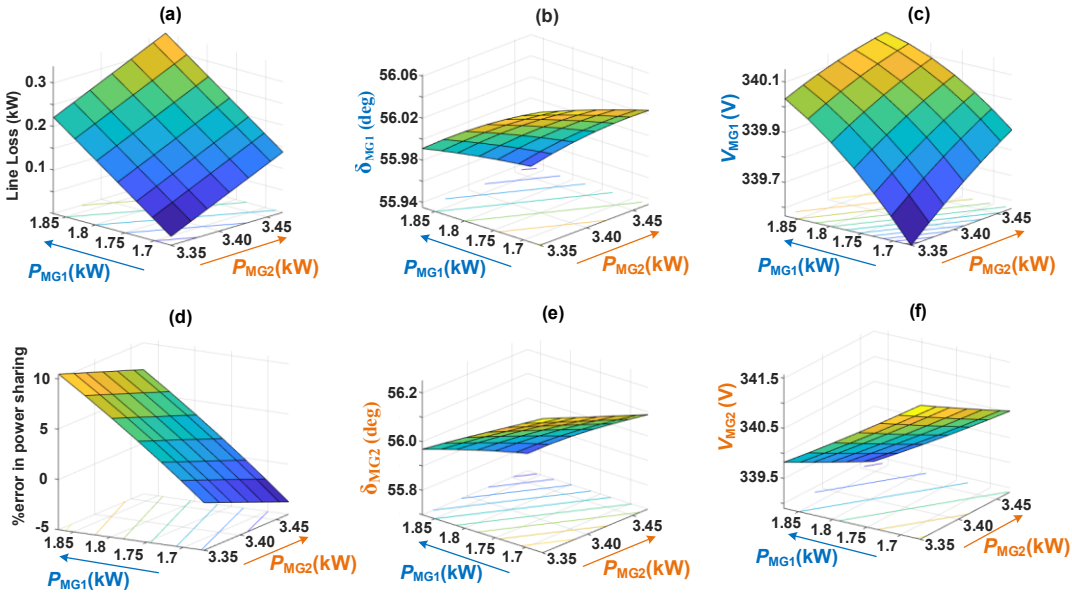

Figure 6.2 Effect of line impedance variation on CMG network for topology-1

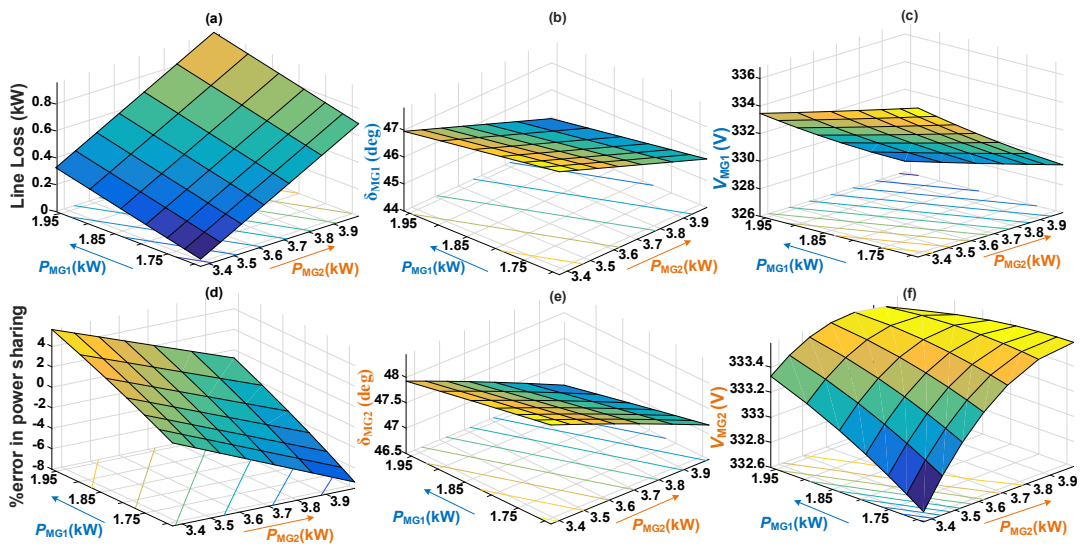

Figure 6.3 Effect of line impedance variation on CMG network for topology-2

demand is assumed to be 5kW. Referring to Figure. 6.1a - 6.1h, it can be seen that the power delivered, and line loss increase as the line impedance is increased. To accommodate the excess power required due to the increase in line loss, the interconnecting line's droop voltage and angle start to drop, according to their droop coefficients. Hence, the frequency of each microgrid also starts to drop as the power delivered by them increases due to increasing line loss. The variations in all parameters are within the acceptable limit though the variations are more prominent in topology-2 as compared to topology-1. Figure. 6.1e to 6.1f show the line loss and the percentage

of error in power-sharing according to their droop ratio, as the line impedance increases. It can be observed from Figure. 6.1e to 6.1h that the line loss in the single-phase link of topology-2 is higher as compared to the three-phase link of topology-1, whereas the error in power-sharing is larger in the three-phase link. The line loss in a three-phase link is less as the current is three times smaller than that of a single-phase link. On the other hand, a single-phase link exhibits better accuracy in power-sharing according to their droop coefficient among the microgrids. The Line loss and error percentage are also shown as a 3D plot with respect to HMG's total power due to line impedance variation in Figure. 6.1g and 6.1h, respectively.

Figure 6.2 and Figure 6.3 show the surface plot of line loss, droop angle, voltage and error percentage in power-sharing as the power delivered by two HMGs is varied due to an increase in the line impedance in topology-1 and topology-2, respectively. It can be observed that the droop angle plots of both HMG follow a similar pattern, whereas the droop voltage plots are not similar. As the impedance of the interconnecting lines is increased, the sharing of desired power, according to their droop coefficients, starts to deviate slightly and produces an error. The reason behind such behaviour is that, as the impedances of the lines become larger, the assumption of droop coefficients being greater than the line reactance does not remain valid any longer, and thus, the property of power-sharing, as the reciprocal of the droop coefficients, is lost. As can be seen from Figure 6.2d, the variation of impedance causes an error of –5 to +10% in topology-1 whereas, the error ranges from –8 to +4% in topology-2, as can be seen from Figure 6.3d. In both topologies, the error stays in an acceptable range because of the implemented modified angle droop, which is an effective way to ensure accurate power-sharing among the microgrids.

The sensitivity analysis for topology-3 due to line resistance variation is shown in Figure 6.4. It can be observed from Figure 6.4a to 6.4d that the line loss and power delivered by each microgrid are increased as the line resistance (i.e., the distance of the microgrids from each other) increases, whereas to accommodate the excess power required due to line loss, the frequency and dc-link voltages start to drop according to their droop coefficients values. The nominal PMG power demand is assumed to be 10kW. As the resistance of the interconnecting lines is increased, the property of power-sharing based on their droop coefficients starts to become erroneous. This is due to the fact that as the resistances of the lines become larger than droop coefficients values, the property of power-sharing as the reciprocal of the droop coefficients, is not

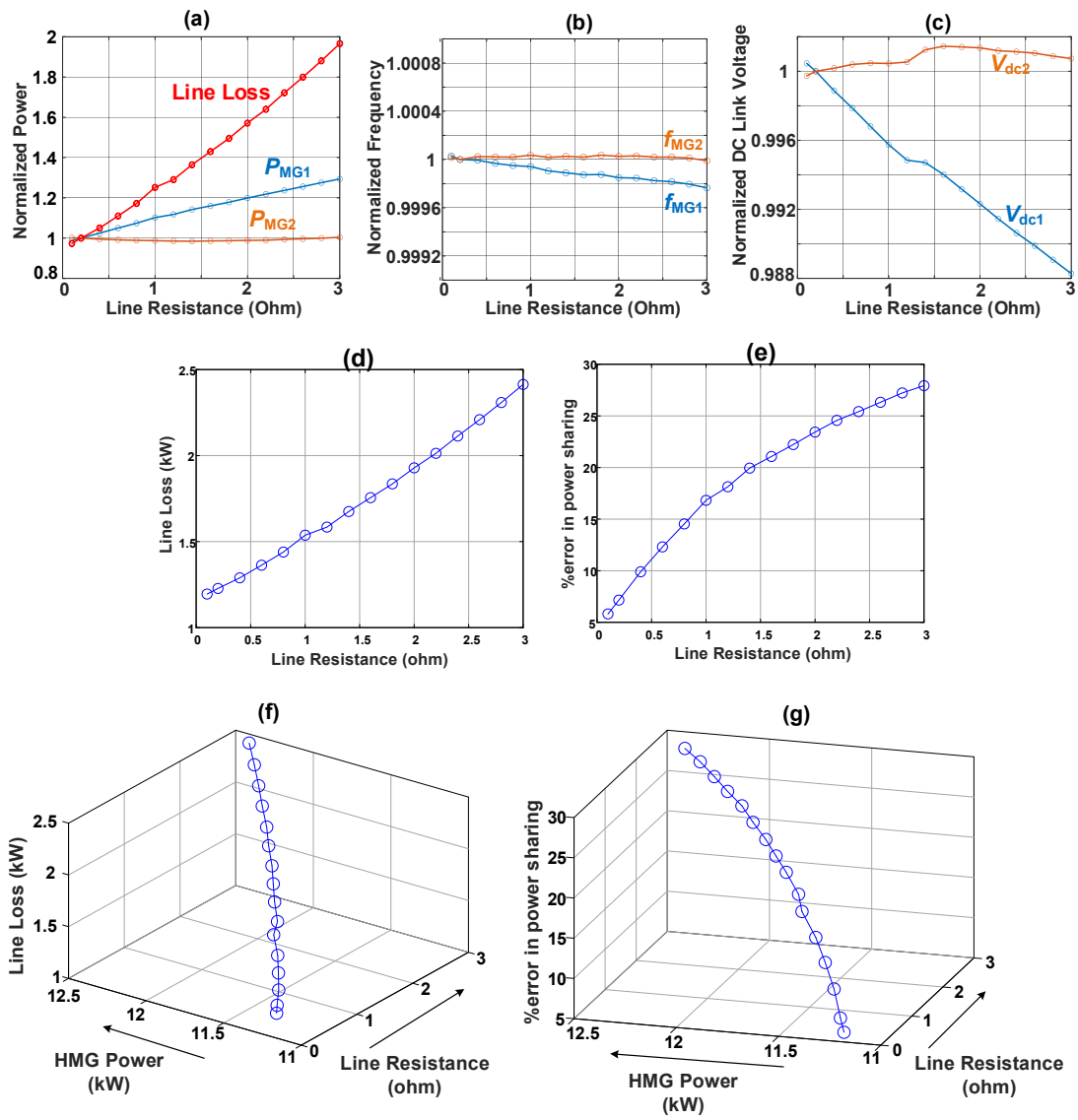

Figure 6.4 CMG sensitivity analysis of topology-3 for line resistance variation

valid any longer. This can be seen in Figure 6.4e. The Line loss and percentage of error are also shown as a 3D plot with respect to total HMG power variation due to the increased line resistance, in Figure 6.4f and 6.4g, respectively. It can be observed from the above analysis that, the error in power-sharing based on the HMG's droop coefficient, is noticeably larger in topology-3 as compared to topology-1 and 2.

Figure 6.5 shows the surface plot for line loss, frequency, the dc-link voltage of each HMG, and the percentage of error in power-sharing as a function of power delivered by both HMGs due to the increase in line resistance. The surface plots of frequency and dc-link voltage of individual HMG follow a similar pattern. From Figure 6.5, it can be observed that the power, frequency and dc-link voltage of microgrid-1 (with larger droop value, provides 33% of the total PMG power demand and line loss) drops

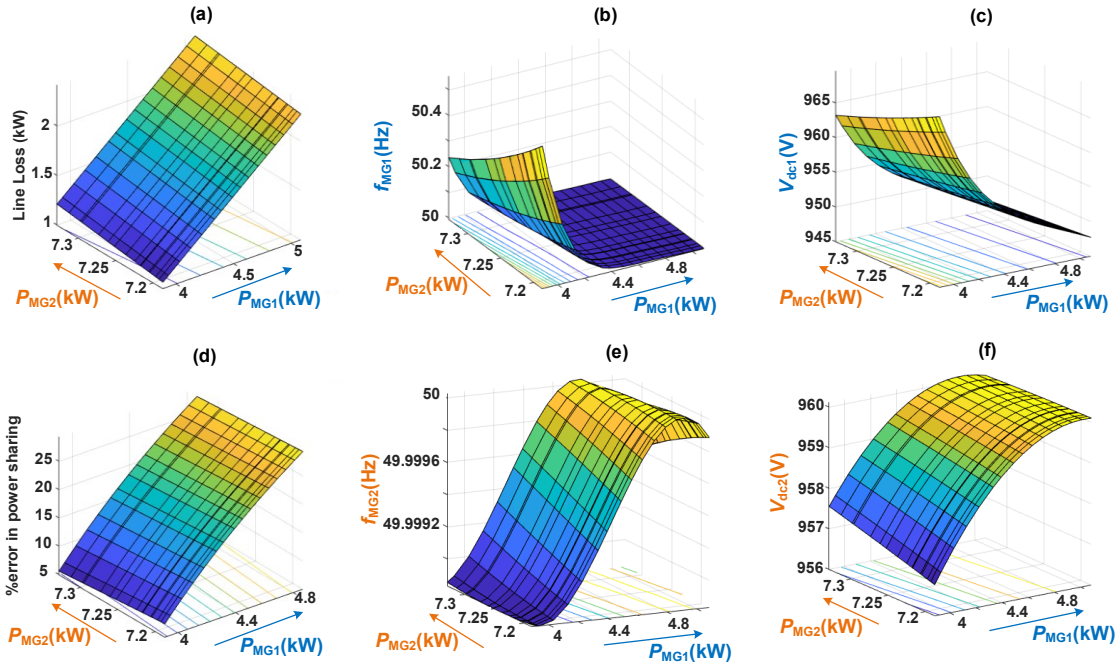

Figure 6.5 Effect of line resistance variation on CMG network for topology-3.

more abruptly where, for microgrid-2 (with a smaller droop value, provides 67% of the total PMG power demand and line loss) the parameters remain fairly constant. This scenario can also be observed from the surface plots.

6.1.2. PMG Power Variation

The second sensitivity analysis was performed by varying the power demand of the PMG in the CMG network. The parameters of CMG in both topology-1 and 2 are shown in Figure 6.6 as the power consumed by the PMG varies from 2 to 10kW. The delivered HMG power, line loss, the HMG's droop angle, voltage, and percentage of error in power-sharing are plotted as a function of the PMG's power demand. The plots are normalised based on a value of 6kW. It can be seen from Figure 6.6 that for both topologies, the power-sharing between the two HMGs remains constant irrespective of the PMG's power demand. Hence, it can be observed in this analysis that, the error in power-sharing as per their droop coefficient is very negligible. In other words, the modified angle droop control-based power-sharing approach is insensitive to the PMG's power variation.

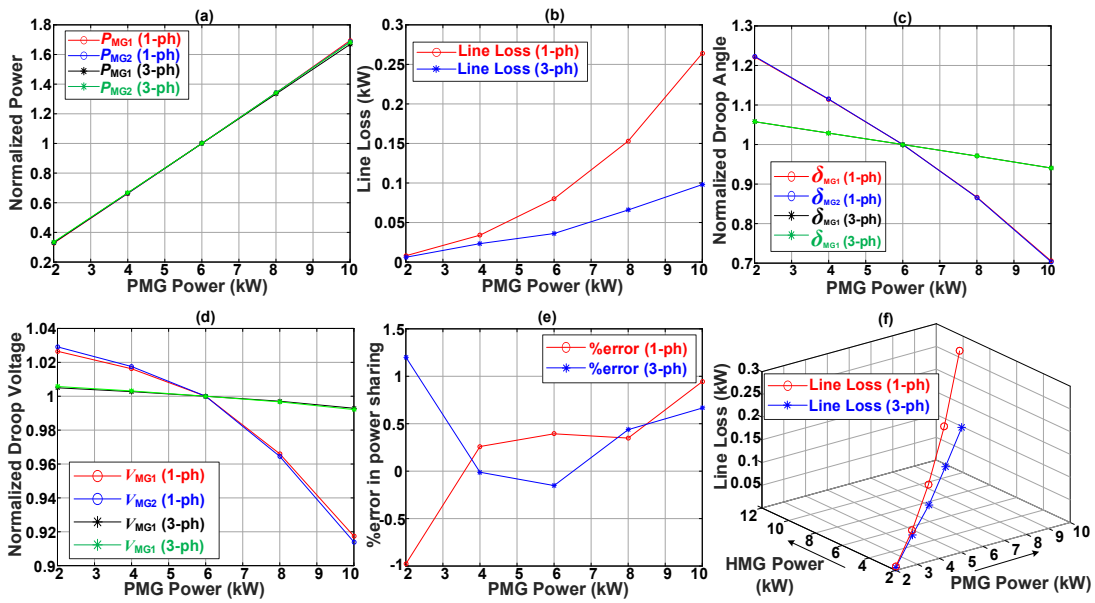

Figure 6.6 Comparative CMG sensitivity analysis of topology-1 and 2 for PMG power variation

Finally, the sensitivity analysis for topology-3 is conducted by varying the PMG's power from 2 to 20kW. Figure 6.7a to 6.7f show the normalised line loss, HMG power, frequency, respective HMG's dc-link voltages, actual line loss, and percentage of error in power-sharing as the PMG's power demand are varied. The values are normalised based on the PMG power demand of 10kW.

Figure 6.7f and Figure 6.7g show the 3D plot for line loss and error percentage in power-sharing as the PMG power demand and the total supplied power of the HMGs are varied. It can be seen from Figure 6.7a and Figure 6.7b that the sharing of power between the two HMGs remains fairly constant irrespective of the PMG's power demand. Hence, the error in power-sharing according to their droop ratio is very negligible when the PMG's power demand varies. Thus, the sharing of power amongst the HMGs is insensitive to the PMG's power demand.

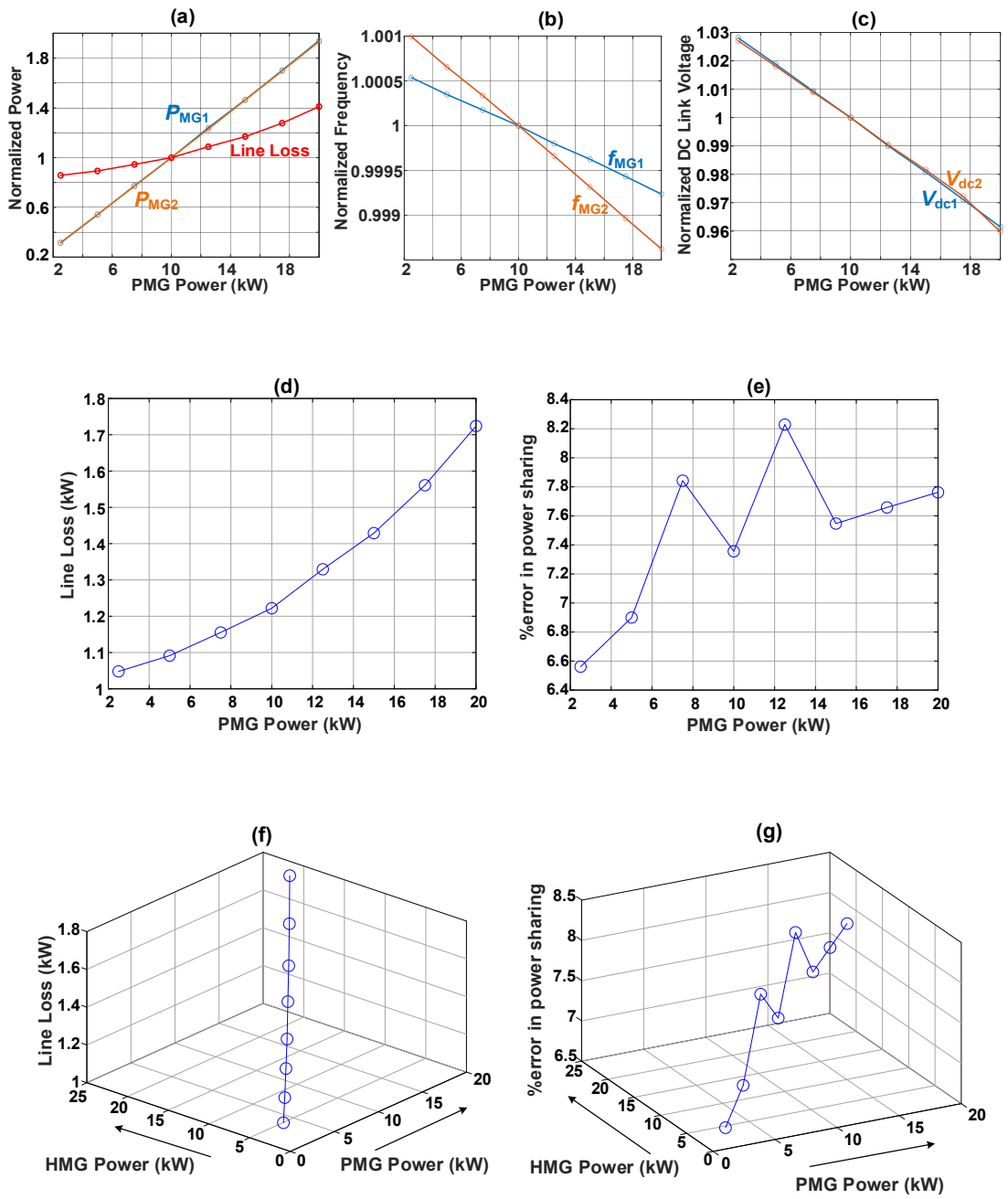

Figure 6.7 Sensitivity analysis of the CMG network in topology-3 with PMG power demand variation.

6.1.3. Number of MG variation in CMG

The third and final sensitivity analysis is conducted to determine the relative stability margin of all the three types of power exchange network by varying the number of

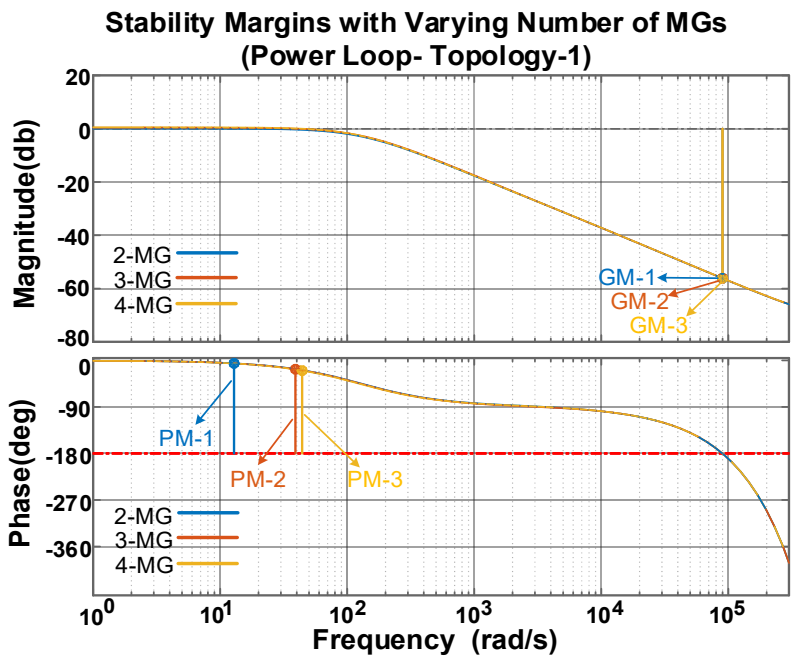

Figure 6.8 Stability margin comparison of the power control loop for topology-1 with varying number of microgrids to form CMG.

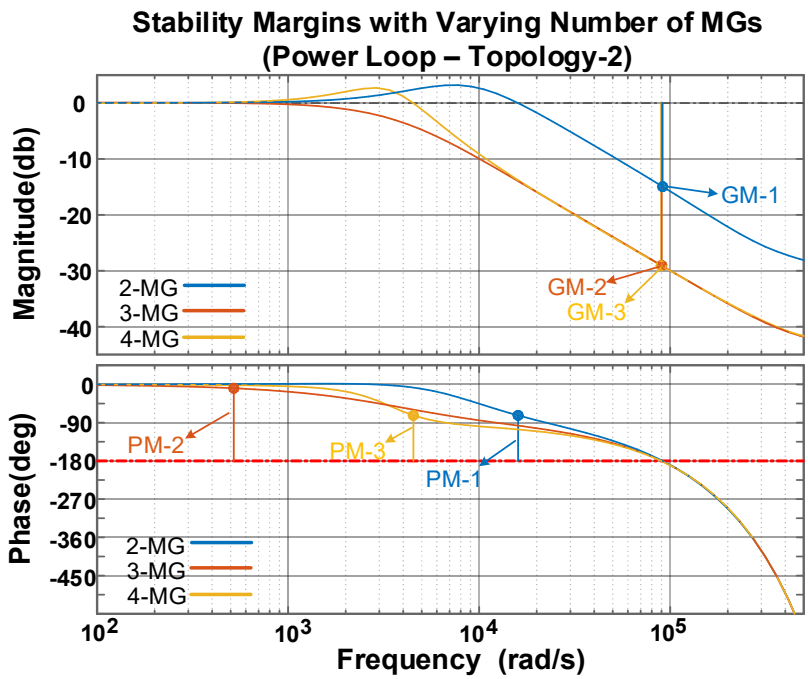

Figure 6.9 Stability margin comparison of the power control loop for topology-2 with varying number of MGs to form CMG.

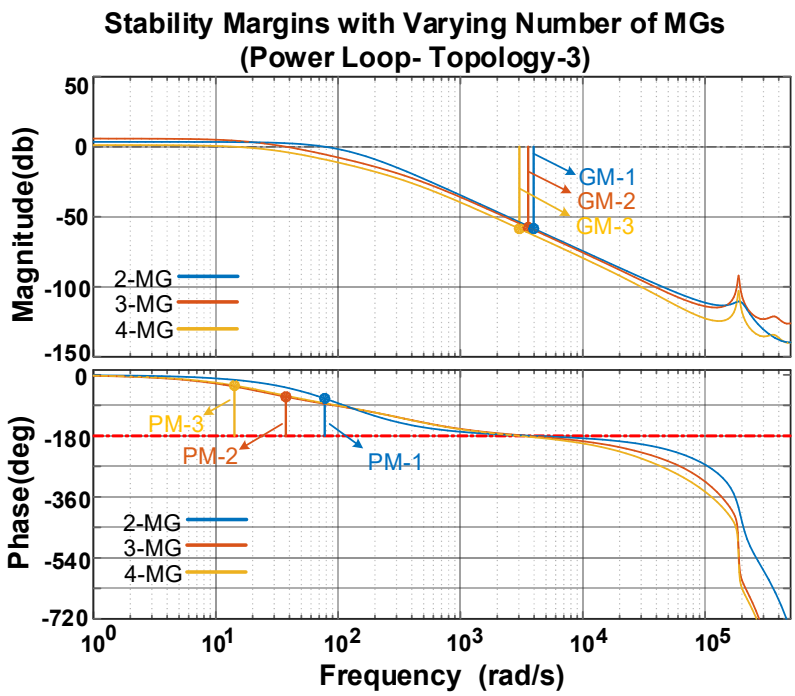

Figure 6.10 Stability margin comparison of the power control loop for topology-3 with varying number of MGs to form CMG.

interconnected microgrids to form the CMG. The two outer most control loops (i.e. power and frequency) of LSCs (all the three topologies) and the dc power exchange link (topology- 3) are examined in this analysis. The frequency responses of the power control loop (Figure 3.6) with varying numbers of microgrids in all the topologies are shown in Figure 6.8 – 6.10 whereas, responses of the frequency control loop (Figure 3.13) are shown in Figure 6.11-6.13, respectively. It can be observed from this analysis that, the number of microgrids participating to form the CMG power exchange network affects the dynamic response of the overall system and thus its gain and phase margin. Even though the effect on gain and phase margin is not too significant but coupling a large number of microgrids to form the CMG may result in a poor dynamic response or in some cases may even make the network unstable. As can be seen from Figure 6.8, the closed-loop phase margin of the power control loop reduces as the number of microgrids in the CMG network is increased in the case of topology- 1. In topology- 2, the phase margin increases for 3 microgrids whereas, it deteriorates when 4 microgrids are connected as can be seen from Figure 6.9. This implies that this topology can offer the optimum phase margin and performance for 3 microgrids.

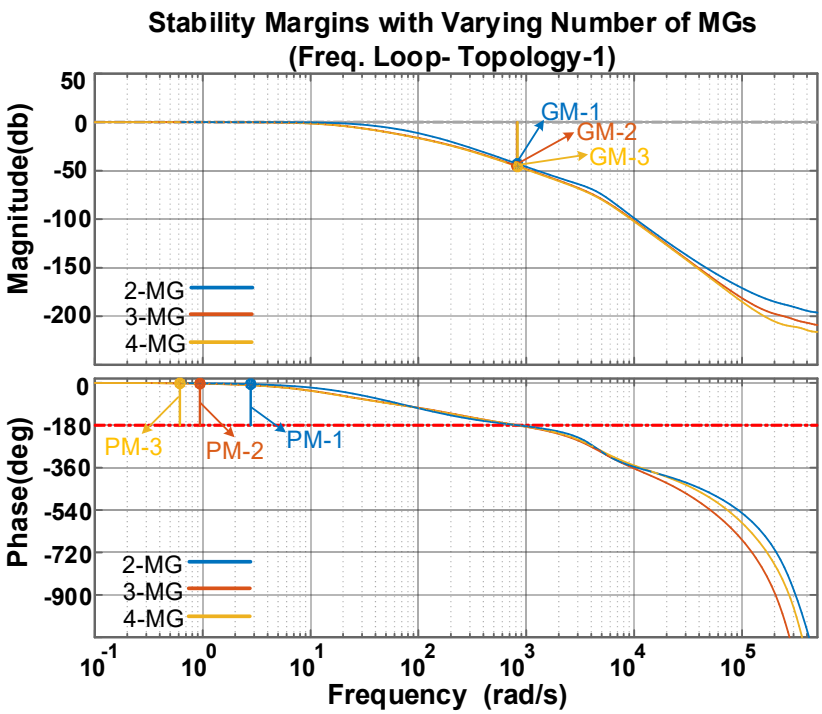

Figure 6.11 Stability margin comparison of the frequency control loop for topology-1 with varying number of MGs to form CMG.

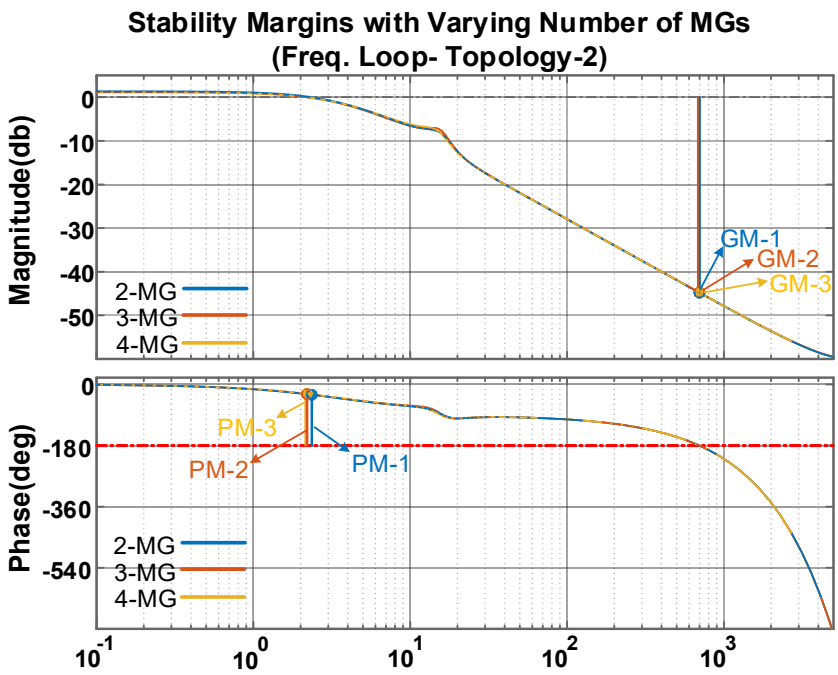

Figure 6.12 Stability margin comparison of the frequency control loop for topology-2 with varying number of MGs to form CMG.

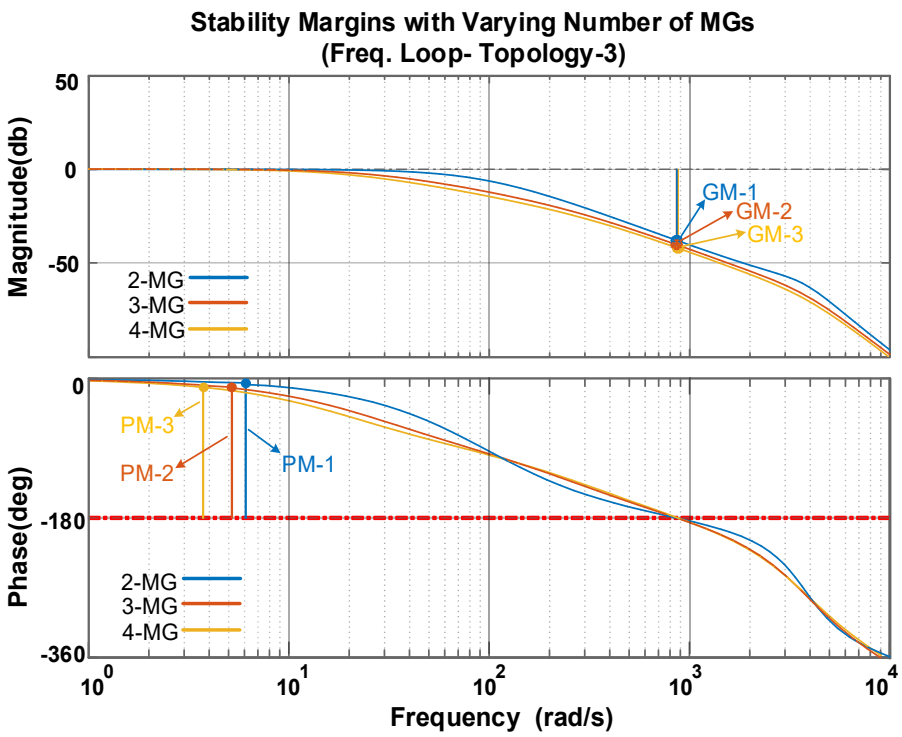

Figure 6.13 Stability margin comparison of the frequency control loop for topology-3 with varying number of MGs to form CMG.

However, the phase margin increases with the increasing number of microgrids in the case of topology- 3 as shown in Figure 6.10, but at the same time, it makes the system response slower. For the frequency loop, the phase margin does not reduce but the crossover frequency shifts towards the left for all the three topologies resulting in a slower dynamic response as can be seen from Figure 6.11-6.13. Topology- 2 is the least sensitive one as the crossover frequency remains almost fixed whereas, topology-1 is the most sensitive one in this case. Overall, this study reveals that, if a large number of microgrids are coupled together to form the CMG, the controllers need to be retuned and redesigned in order to achieve the necessary gain and phase margin of the system.

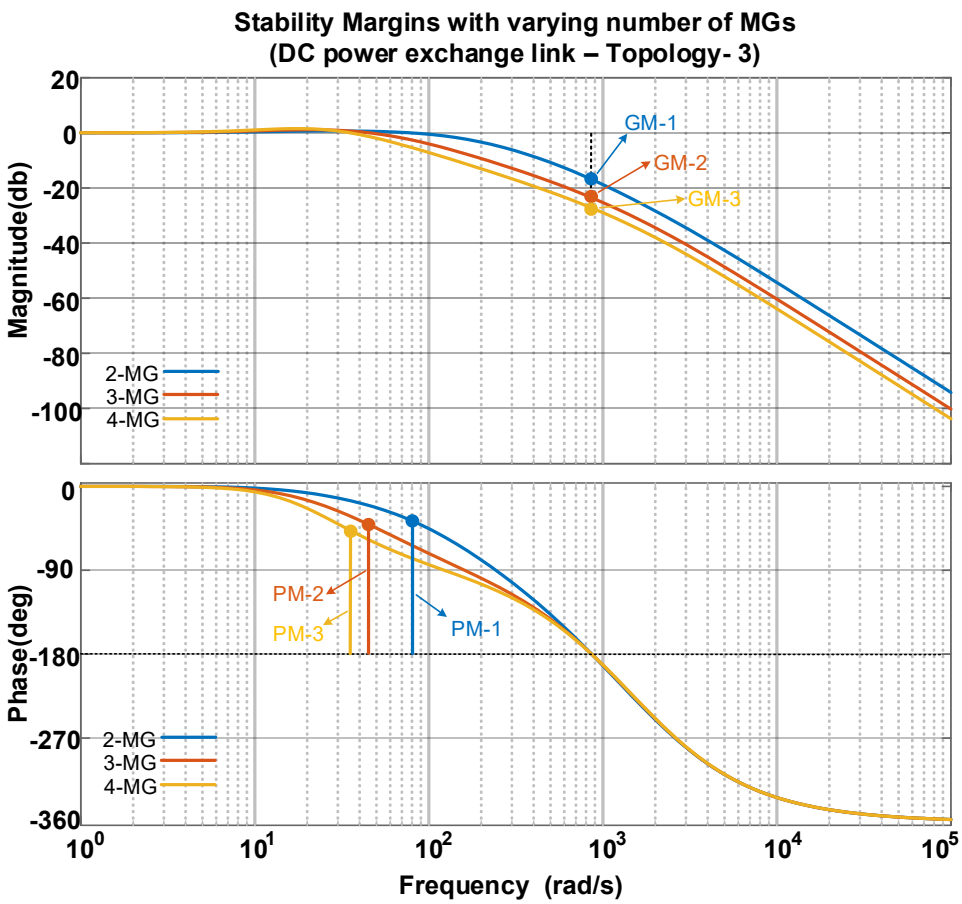

Figure 6.14 Stability margin comparison of the dc power exchange link for topology-3 with varying number of MGs to form CMG.

Finally, it is important to examine the sensitivity of the dc power exchange link as the number of microgrids connected through the power exchange link is varied. It can be seen from Figure 6.14 that, as the number of microgrids is increased within the CMG, the stability margins of the overall interconnected dc power exchange link deteriorates. This is because the equivalent capacitance of the network is increased as more microgrids are added to the link. As a result, the response of the dc-link voltages exhibits larger overshoots and the settling time is increased. In other words, the response of the dc-link becomes slower with larger overshoots and prone to instability. This problem can be addressed by retuning or redesigning the dc-link voltage controller based on the new value of equivalent capacitance of the power exchange link which is determined by the number of microgrids connecting to it. However, such an issue is not encountered in the case of topology-1 and 2 as the back-to-back converter provides isolation between the lines and the dc-link capacitors. As a result,

varying the number of microgrids do not affect the equivalent dc-link capacitance in topology- 1 and 2.

6.2. Summary

This chapter has presented the sensitivity analysis of the three proposed CMG topologies against their different operational parameters. The sensitivity analysis of all the three topologies shows that the minimum power loss has occurred in the case of three-phase topology whereas, the dc topology is capable of exchanging the maximum power and the distance among the microgrids does not affect the exchanged power level. On the other hand, for three-phase and single-phase ac links, line impedance affects the level of power exchange. If the line impedance is very large (i.e., the distance among the microgrids is large) the CMG network will fail to exchange the desired amount of power or the amount of power that can be exchanged via the interconnecting link needs to be limited. Finally, the study shows the error in power-sharing among the HMGs as the line impedance and PMG power demand varies. The error is minimum and also within the acceptable limit, in the ac topologies because of the implemented virtual impedance-based droop method, whereas the error is large and goes beyond the acceptable limit in the case of dc topology.

Chapter 7 Conclusions and recommendations

This chapter summarises the important findings of this thesis. Based on different findings and observations, some recommendations are also made for future researchers.

7.1. Conclusions

A standalone microgrid is an effective approach to electrify remote and isolated communities. It can integrate various renewable-based distributed energy resources along with required energy storages and coordinate them to supply its demand. The uncertainties of load demand and the power generated by the renewable sources cause the overloading and over-generation situations in standalone remote area microgrids Such problems make it difficult to maintain the voltage and frequency within the desirable range and if not alleviated, it may even lead the whole system towards instability.

This thesis reports the newly developed control techniques for power electronic converters used for interconnecting neighbouring autonomously operating microgrids to prevent unacceptable voltage and frequency deviation due to overloading and over-generations. The thesis has analysed and discussed three different approaches to forming a system of interconnected microgrid networks that will facilitate power exchange through a power electronic converter-based interface only when one or more of those microgrids are experiencing either overloading due to lack of adequate power generation or over-generation from its renewable-based sources. The studied topologies provide the necessary isolation of the microgrids so that each microgrid can operate autonomously according to its own internal standards and control techniques while enabling power-sharing amongst them. The control mechanism of each structure is based on a decentralised local frequency monitoring and regulation technique for

the individual microgrids that eliminates the requirement for a centralised control or data communication infrastructure. Also, a suitable framework has been discussed that ensures adequate and proper power-sharing among the microgrids based on droop control mechanism when more than one microgrid will support overloaded or over-generating microgrid(s). Thus, the approach reduces or prevents load-shedding or curtailment of renewable sources when microgrid experiences such overloading or excessive generation. The mechanism includes an approach to realise the desired power-sharing ratio among multiple HMGs and various control techniques to detect the microgrid's status. At the same time, it also determines the required level of active power that needs to be exchanged to support the PMG which will operate in the constant PQ control mode. Such transitions between the various modes of operation of the microgrids are achieved based on measuring the local parameters only. The simulation-based case studies are carried out in PSIM® to validate the efficacy of the discussed approaches in addressing the problems of the unacceptable frequency deviation in the microgrids, following a power excess or shortfall. The studies demonstrate the success of the proposed technique under various loading conditions.

The stability analysis has identified the system parameters that are responsible to affect the dynamics of the CMG network. The stability studies show that the stability of the CMG in topology- 1 and 2, is mostly affected by the active power droop coefficient, while the reactive power droop coefficient does not affect the CMG stability significantly. In topology- 3, a larger value of droop coefficient makes the system highly overdamped but does not drive the system towards instability. The power consumed and injected by a PMG also affects the system dynamics. A larger PMG power provides more damping and makes the system's response relatively slower, whereas a smaller power exhibits smaller system damping and hence response becomes oscillatory. Such phenomena can be seen for all three topologies. The line impedance also affects the CMG dynamics for topology- 1 and 2, but the impact is not too strong to cause instability. However, a larger value of the X/R ratio reduces the system damping and hence makes the system response oscillatory. The variation of line resistance in the case of topology- 3 makes the system overdamped and very sluggish but does not drives the system towards instability.

Finally, the performed sensitivity analysis of the CMG topologies demonstrates an acceptable variation of the different system parameters and quantities with respect to the variation of design and operational factors. Based on the study results, it can be

concluded that the proposed technique offers a considerably robust performance against variations of those parameters. Between topology-1 and 2, the variations are more prominent in topology- 2, whereas smaller variations are observed in the case of topology- 1. Both topology-1 and 2 equally performed in terms of power-sharing whereas the line losses are 3-4 times higher in the case of topology- 2. On the other hand, topology- 3 is robust in terms of PMG power variation but very sensitive for the variation of line resistance. It was observed that, as the line resistance is increased in topology- 3, the property of power-sharing based on desired droop coefficient starts to exhibit errors. The final sensitivity study was performed to observe the effect of varying the number of microgrids to form the CMG and it was found that the stability margins remain within the acceptable limit for all three topologies.

7.2. Recommendations

Based on the findings of this research, the following topics can be recommended as protentional future research avenues:

- This thesis has fully focused on the technical aspects of the proposal and was not aiming at a techno-economic study. A future research can be on evaluating the economic and cost-benefit analysis of all introduced three topologies to select the most cost optimum topology for a given network.
- The methods in this thesis were based on a decentralised approach. Developing a control mechanism for CMGs assuming the presence of a distributed or semi-decentralised controller can be the topic of a future research.

Appendix

The network and controller parameters used in the simulation studies are given in Table A.1.

Table A.1 Technical data of network under consideration

Network	$V_{\text{rated}} = 415\text{V}$, $f_{\text{nom}} = 50\text{Hz}$, $f_{\text{min}} = 49.5\text{Hz}$, $f_{\text{max}} = 50.2\text{Hz}$, $P_{\text{max}} = 100\text{kW}$, $V_{\text{dc}} = 1.5\text{kV}$, $Z_{\text{MG}} = 0.1 + j0.5\Omega$, $Z_{\text{line}} = 0.1 + j0.08\Omega$
DER droop	$m = 0.01\text{Hz/kW}$, $n = 0.1\text{V/kVAR}$
Angle droop	$m_{\text{d}} = 0.002\ \text{rad/kW}$, $n_{\text{d}} = 0.004\text{V/kVAR}$
DC Droop Parameters	$m_{\text{MG}-1} = 2.5\text{V/kW}$, $m_{\text{MG}-2} = 5\text{V/kW}$, $m_{\text{MG}-3} = 5\text{V/kW}$
VSC and filters	$R_{\text{f}} = 0.1\Omega$, $L_{\text{f}} = 2\text{mH}$, $R_{\text{g}}(\text{MSC}) = 0.04\Omega$, $L_g(\text{MSC}) = 1.36\text{mH}$, $R_{\text{g}}(\text{LSC}) = 0.12\Omega$, $L_g(\text{LSC}) = 10\text{mH}$, $C_{\text{f}} = 25\mu\text{F}$, $C_{\text{dc}} = 4700\mu\text{F}$
Linear quadratic regulator gains	$k_1 = 58.63$, $k_2 = 97.18$, $k_3 = 1.2$, $\omega_c = 6283.2\ \text{rad/s}$
PI - PQ controller (MSC)	Proportional Gain, $K_{\text{c}} = 0.628$, Time Constant, $T_{\text{c}} = 0.034$ s, $f_{\text{BW}} = 73.5\text{Hz}$
PI - PQ controller (LSC)	Proportional Gain, $K_{\text{c}} = 0.628$, Time Constant, $T_{\text{c}} = 0.0834$ s, $f_{\text{BW}} = 10\text{Hz}$
Frequency controller	$K_{\text{OL}} = 15\text{k}$, $T_{\text{OL}} = 0.025$ s, $\omega_{\text{OL}} = 314$ rad/s, $K_{\text{OG}} = 20\text{k}$, $T_{\text{OG}} = 0.05$ s, $\omega_{\text{OG}} = 37.7$ krad/s. $K_{\text{PLL}} = 5$, $T_{\text{PLL}} = 0.02$ s
Dc-link voltage controller	$K_{\text{dc}} = 222$, $\omega_{\text{z}} = 2.2\text{rad/s}$, $\omega_{\text{p}} = 1000\text{rad/s}$, $\tau_{\text{dc}} = 392.2\text{ms}$, $P_{\text{so}} = 100\text{kW}$, $V_{\text{d}} = 380\text{V}$

References

[1] R.H. Lasseter, “Microgrids,” IEEE Power Engineering Society Winter Meeting. Conference, vol. 1, pp. 305-308, 2002.

[2] R.H. Lasseter, and P. Piagi, “Microgrid: A conceptual solution,’ IEEE Power Electronics Specialists Conference, vol. 6, pp. 4285-4291. 2004.

[3] Y. Yoldaş, A. Önen, S. M. Muyeen, A. V. Vasilakos, İ. Alan, “Enhancing smart grid with microgrids: Challenges and opportunities”, Renew. Sustain. Energy Rev., vol. 72, pp. 205-214, May 2017.

[4] L. Ali and F. Shahnia, “Determination of an economically-suitable and sustainable standalone power system for an off-grid town in Western Australia,” Renewable Energy, vol. 106, pp.243-254, 2017.

[5] L. Ali and F. Shahnia, “Selection of a suitable standalone power supply system for an off-grid town in Western Australia,” 2016 IEEE 16th International Conference on Environment and Electrical Engineering (EEEIC), 2016, pp. 1-6, doi: 10.1109/EEEIC.2016.7555735.

[6] L. Ali and F. Shahnia, “Impact of annual load growth on selecting the suitable sustainable standalone system for an off-grid town in Western Australia,” 2016 IEEE International Conference on Power System Technology (POWERCON), 2016, pp. 1-5, doi: 10.1109/POWERCON.2016.7754043.

[7] L. Ali, F. Shahnia, A. Arefi, H. Iu and T. Fernando, “Feasibility analysis of a sustainable system for an Australian remote town,” 2017 3rd International Conference on Power Generation Systems and Renewable Energy Technologies (PGSRET), 2017, pp. 118-122, doi: 10.1109/PGSRET.2017.8251812.

[8] J.G. de Matos, F.S.F. de Silva, L.A. de S. Ribeiro, “Power control in ac isolated microgrids with renewable energy sources and energy storage systems,” IEEE Trans. Industrial Electronics, 62(6):3490-3498, 2015

[9] N. Eghtedarpour and E. Farjah, “Power Control and Management in a Hybrid

AC/DC Microgrid," in IEEE Transactions on Smart Grid, vol. 5, no. 3, pp. 1494-1505, May 2014, doi: 10.1109/TSG.2013.2294275.

[10] F. Katiraei and M. R. Iravani, "Power Management Strategies for a Microgrid With Multiple Distributed Generation Units," in IEEE Transactions on Power Systems, vol. 21, no. 4, pp. 1821-1831, Nov. 2006, doi: 10.1109/TPWRS.2006.879260.

[11] R. P. S. Chandrasena, F. Shahnia, A. Ghosh and S. Rajakaruna, "Operation and control of a hybrid AC-DC nanogrid for future community houses," 2014 Australasian Universities Power Engineering Conference (AUPEC), 2014, pp. 1-6, doi: 10.1109/AUPEC.2014.6966617.

[12] R. P. S. Chandrasena, F. Shahnia, S. Rajakaruna and A. Ghosh, "Operation and control of three phase microgrids consisting of single-phase DERs," 2013 IEEE 8th International Conference on Industrial and Information Systems, 2013, pp. 599-604, doi: 10.1109/ICIInfS.2013.6732052.

[13] F. Shahnia, et al. "A three-phase community microgrid comprised of single-phase energy resources with an uneven scattering amongst phases." International Journal of Electrical Power & Energy Systems 84 (2017): 267-283.

[14] M.F. Zia, E. Elbouchikhi and M. Benbouzid, "Microgrids energy management systems: A critical review on methods, solutions, and prospects," Applied energy, vol. 22. 1033-1055, 2018.

[15] R. P. S. Chandrasena, F. Shahnia, S. Rajakaruna and A. Ghosh, "Control, operation and power sharing among parallel converter-interfaced DERs in a microgrid in the presence of unbalanced and harmonic loads," 2013 Australasian Universities Power Engineering Conference (AUPEC), 2013, pp. 1-6, doi: 10.1109/AUPEC.2013.6725382.

[16] S.A. Arefifar, Y.A.R.I. Mohamed, "DG mix, reactive sources and energy storage units for optimizing microgrid reliability and supply security," IEEE Trans. Smart Grid, 5(4):1835-1844, 2014.

[17] F. Nejabatkhah and Y. W. Li, "Overview of Power Management Strategies of Hybrid AC/DC Microgrid," in IEEE Transactions on Power Electronics, vol. 30, no. 12, pp. 7072-7089, Dec. 2015, doi: 10.1109/TPEL.2014.2384999.

[18] M. A. Shoeb, F. Shahnia and G. Shafiullah, "A Multilayer Preventive Control to Regulate Voltage and Frequency in Autonomous Microgrids," 2018 Australasian Universities Power Engineering Conference (AUPEC), 2018, pp.

1-6, doi: 10.1109/AUPEC.2018.8758055.

[19] M. A. Shoeb, F. Shahnia, G. M. Shafiullah and X. Su, "Sensitivity of Prediction Error on the Performance of a Preventive Controller for Microgrids," 2019 IEEE International Conference on Industrial Technology (ICIT), 2019, pp. 1717-1722, doi: 10.1109/ICIT.2019.8755157.

[20] Kani, A. P., et al. "Microgrid control overview." Variability, Scalability and Stability of Microgrid. IET Press, 2019.

[21] M. A. Shoeb, F. Shahnia and G. Shafiullah, "A Two-stage Optimal Generation Units Dispatch for Standalone Microgrids," 2019 9th International Conference on Power and Energy Systems (ICPES), 2019, pp. 1-6, doi: 10.1109/ICPES47639.2019.9105544.

[22] F. Shahnia. "Microgrids and their control." Hybrid Renewable Energy Systems and Microgrids. Academic Press, 2021. 399-462.

[23] M. A Shoeb et al. "Peer-to-peer load allocation using potential field concept for optimal operation of standalone microgrids." IET Generation, Transmission & Distribution (2020).

[24] F. Shahnia, et al. "Application of DSTATCOM for surplus power circulation in MV and LV distribution networks with single-phase distributed energy resources." Electric Power Systems Research 117 (2014): 104-114.

[25] R. Fornarelli, et al. "Selecting an economically suitable and sustainable solution for a renewable energy-powered water desalination system: A rural Australian case study." Desalination 435 (2018): 128-139.

[26] F. Shahnia, M. Moghbel, A. Arefi, G. M. Shafiullah, M. Anda and A. Vahidnia, "Levelized cost of energy and cash flow for a hybrid solar-wind-diesel microgrid on Rottnest island," 2017 Australasian Universities Power Engineering Conference (AUPEC), 2017, pp. 1-6, doi: 10.1109/AUPEC.2017.8282413.

[27] T. Jamal, G. M. Shafiullah, C. Carter, S. M. Ferdous and M. Rahman, "Benefits of Short-term PV Forecasting in a Remote Area Standalone Off-grid Power Supply System," 2018 IEEE Power & Energy Society General Meeting (PESGM), 2018, pp. 1-5, doi: 10.1109/PESGM.2018.8586416..

[28] J. Susanto and F. Shahnia, "Smoothing Batteries for PV-Diesel Microgrids," 2019 IEEE 28th International Symposium on Industrial Electronics (ISIE), 2019, pp. 2609-2614, doi: 10.1109/ISIE.2019.8781461.

[29] M. Moghbel, et al. "Output power fluctuations of distributed photovoltaic

systems across an isolated power system: insights from high-resolution data." IET Renewable Power Generation (2020).

[30] R. P. S. Chandrasena, F. Shahnia, A. Ghosh and S. Rajakaruna, "Secondary control in microgrids for dynamic power sharing and voltage/frequency adjustment," 2014 Australasian Universities Power Engineering Conference (AUPEC), 2014, pp. 1-8, doi: 10.1109/AUPEC.2014.6966619.

[31] E. Pashajavid, F. Shahnia and A. Ghosh, "Overload management of autonomous microgrids," 2015 IEEE 11th International Conference on Power Electronics and Drive Systems, 2015, pp. 73-78, doi: 10.1109/PEDS.2015.7203515.

[32] F. Shahnia. "Hybrid nanogrid systems for future small communities." Sustainable Development in energy systems. Springer, Cham, 2017. 19-38.

[33] E. Pashajavid, F. Shahnia and A. Ghosh, "A decentralized strategy to remedy the power deficiency in remote area microgrids," 2015 50th International Universities Power Engineering Conference (UPEC), 2015, pp. 1-6, doi: 10.1109/UPEC.2015.7339865.

[34] S.M. Ferdous, F. Shahnia, G. Shafiullah, "Power sharing and control strategy for microgrid clusters", 9th International Conference on Power and Energy Systems (ICPES), Perth, 2019.

[35] I.U. Nutkani, P.C. Loh, P. Wang, et al., "Intertied ac–ac microgrids with autonomous power import and export," International Journal of Electrical Power & Energy Systems, vol. 6, pp. 385-393, 2015.

[36] M. Goyal, A. Ghosh and F. Shahnia, "Overload prevention in an autonomous microgrid using battery storage units," 2014 IEEE PES General Meeting | Conference & Exposition, 2014, pp. 1-5, doi: 10.1109/PESGM.2014.6939459.

[37] M. Goyal, A. Ghosh and F. Shahnia, "Distributed battery storage units for overload prevention in an islanded microgrid," 2014 Australasian Universities Power Engineering Conference (AUPEC), 2014, pp. 1-6, doi: 10.1109/AUPEC.2014.6966556.

[38] Q. Zhou, Z. Li, Q. Wu and M. Shahidehpour, "Two-Stage Load Shedding for Secondary Control in Hierarchical Operation of Islanded Microgrids," in IEEE Transactions on Smart Grid, vol. 10, no. 3, pp. 3103-3111, May 2019, doi: 10.1109/TSG.2018.2817738..

[39] Y. Hong, M. Hsiao, Y. Chang, Y. Lee and H. Huang, "Multiscenario

Underfrequency Load Shedding in a Microgrid Consisting of Intermittent Renewables," in IEEE Transactions on Power Delivery, vol. 28, no. 3, pp. 1610-1617, July 2013, doi: 10.1109/TPWRD.2013.2254502.

[40] Y. Hong and M. Nguyen, "Multiobjective Multiscenario Under-Frequency Load Shedding in a Standalone Power System," in IEEE Systems Journal, vol. 14, no. 2, pp. 2759-2769, June 2020, doi: 10.1109/JSYST.2019.2931934.

[41] Z. Guo, R. Xie, Q. Ma, L. Yang, W. Wei and S. Mei, "Impact of Storage and Transmission Line Capacity on the Curtailment of a Remote Renewable Plant: A Multiparametric Programming Method," 2020 10th International Conference on Power and Energy Systems (ICPES), 2020, pp. 489-492, doi: 10.1109/ICPES51309.2020.9349713.

[42] H. Bae, T. Tsuji, T. Oyama and K. Uchida, "Frequency regulation method with congestion management using renewable energy curtailment," 2016 IEEE Power and Energy Society General Meeting (PESGM), 2016, pp. 1-5, doi: 10.1109/PESGM.2016.7741811.

[43] M. Andrychowicz and B. Olek, "Energy storing vs. generation curtailment — The measures for controlling renewable generation," 2017 14th International Conference on the European Energy Market (EEM), 2017, pp. 1-5, doi: 10.1109/EEM.2017.7982004.

[44] M. K. C. Marwali, M. Haili, S. M. Shahidehpour and K. H. Abdul-Rahman, "Short term generation scheduling in photovoltaic-utility grid with battery storage," in IEEE Transactions on Power Systems, vol. 13, no. 3, pp. 1057-1062, Aug. 1998, doi: 10.1109/59.709099.

[45] X. Y. Wang, D. Mahinda Vilathgamuwa and S. S. Choi, "Determination of Battery Storage Capacity in Energy Buffer for Wind Farm," in IEEE Transactions on Energy Conversion, vol. 23, no. 3, pp. 868-878, Sept. 2008, doi: 10.1109/TEC.2008.921556.

[46] Farhad Shahnia, Ali Arefi,"Eigenanalysis-based small signal stability of the system of coupled sustainable microgrids", International Journal of Electrical Power & Energy Systems, Vol. 91, pp. 42-60, 2017.

[47] Z. Zhao, P. Yang, Y. Wang, Z. Xu and J. M. Guerrero, "Dynamic Characteristics Analysis and Stabilization of PV-Based Multiple Microgrid Clusters," in IEEE Transactions on Smart Grid, vol. 10, no. 1, pp. 805-818, Jan. 2019, doi: 10.1109/TSG.2017.2752640..

[48] S. Bahramirad, W. Reder and A. Khodaei, "Reliability-Constrained Optimal Sizing of Energy Storage System in a Microgrid," in IEEE Transactions on Smart Grid, vol. 3, no. 4, pp. 2056-2062, Dec. 2012, doi: 10.1109/TSG.2012.2217991.

[49] S. M. Ferdous, G. M. Shafiullah, F. Shahnia, R. M. Elavarasan and U. Subramaniam, "Dynamic Frequency and Overload Management in Autonomous Coupled Microgrids for Self-Healing and Resiliency Improvement," in IEEE Access, vol. 8, pp. 116796-116811, 2020.

[50] R.H. Lasseter, "Smart distribution: Coupled microgrids," Proceedings of the IEEE, vol. 99, no. 6, pp.1074-1082, 2011.

[51] F. Shahnia. "Interconnected microgrid systems for remote areas" Sustainable Development in Energy Systems. Springer, Cham, 2017. 39-63.

[52] F. Shahnia, et al. "Interconnected autonomous microgrids in smart grids with self-healing capability." Renewable Energy Integration. Springer, Singapore, 2014. 347-381.

[53] F. Shahnia, R. P. S. Chandrasena, S. Rajakaruna and A. Ghosh, "Autonomous operation of multiple interconnected microgrids with self-healing capability," 2013 IEEE Power & Energy Society General Meeting, 2013, pp. 1-5, doi: 10.1109/PESMG.2013.6672794.

[54] M. Goyal, and A. Ghosh, "Microgrids interconnection to support mutually during any contingency," Sustainable Energy, Grids and Networks, vol. 6, pp. 100-108, 2016.

[55] B. John, A. Ghosh, M. Goyal, and F. Zare, "A dc power exchange highway based power flow management for interconnected microgrid clusters," IEEE Systems Journal, vol. 13, no. 3, pp. 3347-3357, 2019.

[56] E. Bullich-Massague, F. Díaz-González, M. Aragüés-Peñalba, et al, "Microgrid clustering architectures," Applied energy, vol. 212, pp. 340-361, 2018.

[57] H. Zou, S. Mao, Y. Wang, F. Zhang, X. Chen and L. Cheng, "A Survey of Energy Management in Interconnected Multi-Microgrids," in IEEE Access, vol. 7, pp. 72158-72169, 2019.

[58] F. Shahnia and A. Ghosh. "Coupling of neighbouring low voltage residential distribution feeders for voltage profile improvement using power electronics converters." IET Generation, Transmission & Distribution 10.2 (2016): 535-547.

[59] E. Pashajavid, F. Shahnia and A. Ghosh, "Overloading conditions management in remote networks by coupling neighbouring microgrids," 2015 50th International Universities Power Engineering Conference (UPEC), 2015, pp. 1-6, doi: 10.1109/UPEC.2015.7339874.

[60] E. Pashajavid, F. Shahnia, and A. Ghosh, "Provisional internal and external power exchange to support remote sustainable microgrids in the course of power deficiency," IET Generation, Transmission & Distribution, vol. 11, no. 1 pp. 246-260, 2017.

[61] I.U. Nutkani, P.C. Loh, and F. Blaabjerg, "Distributed operation of interlinked AC microgrids with dynamic active and reactive power tuning," IEEE Trans. Industry Applications, vol. 49, no. 5, pp. 2188-2196, 2013.

[62] P.C. Loh, D. Li, Y.K. Chai, F. Blaabjerg, "Autonomous operation of hybrid microgrid with ac and dc subgrids," IEEE Trans. Power Electronics, 28(5):2214-2223, 2013.

[63] S. M. Ferdous, F. Shahnia and G. Shafiullah, "Provisional Energy Transaction Management amongst Neighbouring Microgrids through a DC Power Exchange Link," 2019 9th International Conference on Power and Energy Systems (ICPES), 2019, pp. 1-6, doi: 10.1109/ICPES47639.2019.9105555.

[64] S. M. Ferdous, F. Shahnia and G. Shafiullah, "Realizing a System of Coupled Microgrids using a Single-phase AC Power Exchange Link," 2019 9th International Conference on Power and Energy Systems (ICPES), 2019, pp. 1-6, doi: 10.1109/ICPES47639.2019.9105363.

[65] J. Susanto, F. Shahnia, A. Ghosh and S. Rajakaruna, "Interconnected microgrids via back-to-back converters for dynamic frequency support," 2014 Australasian Universities Power Engineering Conference (AUPEC), 2014, pp. 1-6, doi: 10.1109/AUPEC.2014.6966616.

[66] R. Majumder, A. Ghosh, G. Ledwich, F. Zare, "Power management and power flow control with back-to-back converters in a utility connected microgrid," IEEE Trans. Power Systems, 25(2):821-834, 2010.

[67] Z. Wang, B. Chen, J. Wang and C. Chen, "Networked Microgrids for Self-Healing Power Systems," in IEEE Transactions on Smart Grid, vol. 7, no. 1, pp. 310-319, Jan. 2016, doi: 10.1109/TSG.2015.2427513.

[68] Zhaoyu Wang, Bokan Chen, Jianhui Wang, M. Begovic and Chen Chen, "Coordinated energy management of networked Microgrids in distribution

systems," 2015 IEEE Power & Energy Society General Meeting, Denver, CO, USA, 2015, pp. 1-1, doi: 10.1109/PESGM.2015.7286148.

[69] Y. Zhang, L. Xie, and Q. Ding, "Interactive control of coupled microgrids for guaranteed system-wide small signal stability," IEEE Trans. Smart Grid, vol. 7, no. 2, pp. 1088-1096, 2015.

[70] M. Batool, S. M. Islam and F. Shahnia, "Master control unit based power exchange strategy for interconnected microgrids," 2017 Australasian Universities Power Engineering Conference (AUPEC), 2017, pp. 1-6, doi: 10.1109/AUPEC.2017.8282475.

[71] M. Batool, F. Shahnia, and S. M. Islam."Market model for clustered microgrids optimisation including distribution network operations." IET Generation, Transmission & Distribution 13.22 (2019): 5139-5150.

[72] C. M. Colson and M. H. Nehrir, "Comprehensive Real-Time Microgrid Power Management and Control With Distributed Agents," in IEEE Transactions on Smart Grid, vol. 4, no. 1, pp. 617-627, March 2013, doi: 10.1109/TSG.2012.2236368.

[73] F. Shahnia, R.P.S. Chandrasena, S. Rajakaruna, and A. Ghosh, "Primary control level of parallel distributed energy resources converters in system of multiple interconnected autonomous microgrids within self-healing networks," IET Generation, Transmission & Distribution, vol. 8, no. 2, pp. 203-222, 2014.

[74] Y. Zhang and L. Xie, "Online Dynamic Security Assessment of Microgrid Interconnections in Smart Distribution Systems," in IEEE Transactions on Power Systems, vol. 30, no. 6, pp. 3246-3254, Nov. 2015, doi: 10.1109/TPWRS.2014.2374876

[75] S. M. Ferdous, F. Shahnia and G. Shafiullah, "Various Structures and Control Strategies for Provisional Energy Transaction Management in Coupled Microgrid Clusters," 2020 Intermountain Engineering, Technology and Computing (IETC), 2020, pp. 1-6, doi: 10.1109/IETC47856.2020.9249113.

[76] F. Shahnia, et al. "Stability and eigenanalysis of a sustainable remote area microgrid with a transforming structure." Sustainable Energy, Grids and Networks 8 (2016): 37-50.

[77] J. Susanto, F. Shahnia and A. Arefi, "Small signal model load flow initialisation for converter-dominated microgrids," 2016 IEEE International Conference on Power System Technology (POWERCON), 2016, pp. 1-6, doi:

10.1109/POWERCON.2016.7754050.

[78] F. Shahnia, "Eigenvalues and their participation factors for the system of coupled adjacent microgrids," 2016 IEEE 2nd Annual Southern Power Electronics Conference (SPEC), 2016, pp. 1-6, doi: 10.1109/SPEC.2016.7846138.

[79] F. Shahnia, "Stability of a sustainable remote area microgrid," 2016 IEEE Region 10 Conference (TENCON), 2016, pp. 1220-1223, doi: 10.1109/TENCON.2016.7848205.

[80] I. P. Nikolakakos, H. H. Zeineldin, M. S. El-Moursi and N. D. Hatziargyriou, "Stability Evaluation of Interconnected Multi-Inverter Microgrids Through Critical Clusters," in IEEE Transactions on Power Systems, vol. 31, no. 4, pp. 3060-3072, July 2016, doi: 10.1109/TPWRS.2015.2476826.

[81] A. Kunwar, F. Shahnia and R. C. Bansal, "Impact of the Capacity and Number of Inertial and Non-Inertial Distributed Energy Resources Within a Microgrid on its Stability Margins," 2018 IEEE 27th International Symposium on Industrial Electronics (ISIE), 2018, pp. 55-60, doi: 10.1109/ISIE.2018.8433587.

[82] A. Kunwar, F. Shahnia and R. C. Bansal, "Eigenvalue-Oriented Dynamic Stability Examination to Enhance Designing a Microgrid Hosting Clusters of Inertial and Non-Inertial Distributed Generators," in IEEE Transactions on Smart Grid, vol. 11, no. 3, pp. 1942-1955, May 2020, doi: 10.1109/TSG.2019.2945587.

[83] R. Minciardi, R. Sacile, "Optimal control in a cooperative network of smart power grids," IEEE Systems Journal, 6(1):126-133, 2012.

[84] M. A. Shoeb, F. Shahnia and G. M. Shafiullah, "Optimal Coupling of Multiple Microgrid Clusters," 2019 IEEE Innovative Smart Grid Technologies - Asia (ISGT Asia), 2019, pp. 2809-2814, doi: 10.1109/ISGT-Asia.2019.8881386.

[85] M. Batool, S. M. Islam and F. Shahnia, "Power transaction management amongst coupled microgrids in remote areas," 2017 IEEE Innovative Smart Grid Technologies - Asia (ISGT-Asia), 2017, pp. 1-6, doi: 10.1109/ISGT-Asia.2017.8378449.

[86] F. Shahnia, S. Bourbour and A. Ghosh, "Coupling Neighbouring Microgrids for Overload Management Based on Dynamic Multicriteria Decision-Making," in IEEE Transactions on Smart Grid, vol. 8, no. 2, pp. 969-983, March 2017, doi: 10.1109/TSG.2015.2477845.

[87] S. Bourbour, F. Shahnia and A. Ghosh, "Selection of a suitable microgrid to

couple with an overloaded neighbouring microgrid based on decision making," 2015 North American Power Symposium (NAPS), 2015, pp. 1-6, doi: 10.1109/NAPS.2015.7335200.

[88] T. Jamal, T. Urmee, G. Shafiullah and F. Shahnia, "Using Experts" Opinions and Multi-Criteria Decision Analysis to Determine the Weighing of Criteria Employed in Planning Remote Area Microgrids," 2018 International Conference and Utility Exhibition on Green Energy for Sustainable Development (ICUE), 2018, pp. 1-7, doi: 10.23919/ICUE-GESD.2018.8635734.

[89] R. Majumder, "Aggregation of microgrids with DC system," Electric Power Systems Research, vol. 108, pp. 134-143, 2014.

[90] F. Shahnia, and S. Bourbour. "A practical and intelligent technique for coupling multiple neighbouring microgrids at the synchronization stage." Sustainable Energy, Grids and Networks 11 (2017): 13-25.

[91] E. Planas, J. Andreu, J.I. Gárate, I.M. De Alegría, E. Ibarra, "AC and DC technology in microgrids: A review," Renewable and Sustainable Energy Reviews. vol. 43, pp.726-749, 2015

[92] J.J. Justo, F. Mwasilu , J. Lee, and J.W. Jung, "AC-microgrids versus DC-microgrids with distributed energy resources: A review", Renewable and Sustainable Energy Reviews, vol. 24, pp. 387-405, 2013.

[93] S. Beheshtaein, R. Cuzner, M. Savaghebi, and J. M. Guerrero, "Review on microgrids protection," IET Generation, Transmission & Distribution vol. 13, no. 6: pp. 743-759. 2019.

[94] Jung-Won Kim, Hang-Seok Choi and Bo Hyung Cho, "A novel droop method for converter parallel operation," in IEEE Transactions on Power Electronics, vol. 17, no. 1, pp. 25-32, Jan. 2002.

[95] S. Augustine, M. K. Mishra and N. Lakshminarasamma, "Adaptive Droop Control Strategy for Load Sharing and` Circulating Current Minimization in Low-Voltage Standalone DC Microgrid," in IEEE Transactions on Sustainable Energy, vol. 6, no. 1, pp. 132-141, Jan. 2015.

[96] Z. Wang and J. Wang, "Self-Healing Resilient Distribution Systems Based on Sectionalization Into Microgrids," in IEEE Transactions on Power Systems, vol. 30, no. 6, pp. 3139-3149, Nov. 2015, doi: 10.1109/TPWRS.2015.2389753.

[97] S. M. Ferdous, M. A. M. Oninda, G. Sarowar, K. K. Islam and M. A. Hoque, "Non-isolated single stage PFC based LED driver with THD minimization using

Cúk converter," 2016 9th International Conference on Electrical and Computer Engineering (ICECE), 2016, pp. 471-474, doi: 10.1109/ICECE.2016.7853959.

[98] A. Yazdani and R. Iravani, "Voltage-Sourced Converters in Power Systems: Modeling, Control, and Applications", Wiley-Blackwell, 2010.

[99] S. M. Ferdous, P. Garcia, M. A. M. Oninda and M. A. Hoque, "MTPA and Field Weakening Control of Synchronous Reluctance motor," 2016 9th International Conference on Electrical and Computer Engineering (ICECE), Dhaka, Bangladesh, 2016, pp. 598-601, doi: 10.1109/ICECE.2016.7853991.

[100] A. Yazdani, and R. Iravani, "An accurate model for the dc-side voltage control of the neutral point diode clamped converter," IEEE Trans. Power Delivery, vol. 21, no. 1, pp. 185-193, 2005.

[101] S.M. Ferdous, G. Shafiullah, M.A.M. Oninda, et al., "Close loop compensation technique for high performance MPPT using ripple correlation control," 27th Australasian Universities Power Engineering Conference (AUPEC), pp. 1-6, Melbourne, Australia, 2017

[102] T. Hosseinimehr, A. Ghosh, and F. Shahnia, "Cooperative control of battery energy storage systems in microgrids," International Journal of Electrical Power & Energy Systems, vol. 87, pp.109-120, 2017.

[103] T. Hosseinimehr, F. Shahnia, and A. Ghosh, "Power sharing control of batteries within autonomous microgrids based on their state of charge," 25th Australasian Universities Power Engineering Conference (AUPEC), pp. 1-6, Wollongong, Australia, 2015.

[104] T. Hosseinimehr, F. Shahnia, R. P. S. Chandrasena and A. Ghosh, "Different power sharing techniques for converter-interfaced DERs in an autonomous microgrid," 2014 IEEE PES Asia-Pacific Power and Energy Engineering Conference (APPEEC), 2014, pp. 1-6, doi: 10.1109/APPEEC.2014.7066196.

[105] T. Hosseinimehr, F. Shahnia and A. Ghosh, "Dynamic power sharing control among converter-interfaced DERs in an autonomous microgrid," 2015 IEEE Eindhoven PowerTech, 2015, pp. 1-6, doi: 10.1109/PTC.2015.7232566.

[106] S. Bourbour and F. Shahnia, "Impact of the weightings of different criteria in selecting the suitable microgrids when forming a system of coupled microgrids," 2016 IEEE Innovative Smart Grid Technologies - Asia (ISGT-Asia), 2016, pp. 1151-1156, doi: 10.1109/ISGT-Asia.2016.7796548.

[107] S. Bourbour and F. Shahnia, "A suitable mechanism for the interconnection

phase of temporary coupling of adjacent microgrids," 2016 IEEE Innovative Smart Grid Technologies - Asia (ISGT-Asia), 2016, pp. 624-629, doi: 10.1109/ISGT-Asia.2016.7796457.

[108] F. Shahnia and A. Arefi, "Defining the suitable adjacent microgrids to form a temporary system of coupled microgrids," 2016 IEEE Region 10 Conference (TENCON), 2016, pp. 1216-1219, doi: 10.1109/TENCON.2016.7848204.

[109] M. A. Shoeb, F. Shahnia and G. Shafiullah, "A multilayer optimization scheme to retain the voltage and frequency in standalone microgrids," 2017 IEEE Innovative Smart Grid Technologies - Asia (ISGT-Asia), 2017, pp. 1-6, doi: 10.1109/ISGT-Asia.2017.8378465.

[110] M. A. Shoeb, F. Shahnia and G. M. Shafiullah, "A Multilayer and Event-Triggered Voltage and Frequency Management Technique for Microgrid"s Central Controller Considering Operational and Sustainability Aspects," in IEEE Transactions on Smart Grid, vol. 10, no. 5, pp. 5136-5151, Sept. 2019, doi: 10.1109/TSG.2018.2877999.

[111] M. Batool, F. Shahnia and S. M. Islam, "Multi-level supervisory emergency control for operation of remote area microgrid clusters," in Journal of Modern Power Systems and Clean Energy, vol. 7, no. 5, pp. 1210-1228, September 2019, doi: 10.1007/s40565-018-0481-6.

[112] M. Batool, F. Shahnia, and S. M. Islam. "Impact of scaled fitness functions on a floating-point genetic algorithm to optimise the operation of standalone microgrids." IET Renewable Power Generation 13.8 (2019): 1280-1290.

[113] Wen-Yeau Chang, "The state of charge estimating methods for battery: A review," ISRN Applied Mathematics 2013.

[114] S.M. Ferdous, M.A.Shoeb, G. Shafiullah, M.A.M.Oninda, "Parallel resonant converter for battery charging application", 9th International Conference on Power and Energy Systems (ICPES), Perth, 2019

Publications Arising from this Thesis

Journal articles

1) **S.M.Ferdous**, Farhad Shahnia and GM Shafiullah, "Realising a system of coupled microgrid networks using single-phase interconnection lines," *IET Smart Grid*, vol. 4, pp. 346-364, doi.org/10.1049/stg2.12033.
   [Chapter-3 (Art – 3.2.2), Chapter-4 (Art – 4.2.2), Chapter-5 (Art – 5.1), Chapter-6 (Art-6.1)].
2) **S.M.Ferdous**, Farhad Shahnia and GM Shafiullah, "Provisional energy transaction management amongst neighbouring microgrids through a dc power exchange link," *IET Power Electronics*, vol. 13, pp. 4129-4139, doi.org/10.1049/iet-pel.2020.0612.
   [Chapter-3 (Art – 3.2.3), Chapter-4 (Art – 4.2.3), Chapter-5 (Art – 5.1), Chapter-6 (Art-6.1)].
3) **S.M.Ferdous**, GM. Shafiullah, Farhad. Shahnia, R. M. Elavarasan and U. Subramaniam, "Dynamic frequency and overload management in autonomous coupled microgrids for self-healing and resiliency improvement," *IEEE Access*, vol. 8, pp. 116796-116811, 2020, doi: 10.1109/ACCESS.2020.3004185.
   [Chapter -3 (Art – 3.3), Chapter-4 (Art – 4.2.4)].
4) **S.M.Ferdous**, Farhad Shahnia and GM Shafiullah, "Power sharing and control strategy for provisionally coupled microgrid clusters through an isolated power exchange network," submitted to *Energies 2021* on 14-August-2021.
   [Chapter-3 (Art – 3.2.1), Chapter-4 (Art – 4.2.1), Chapter-5 (Art – 5.1), Chapter-6 (Art-6.1)].

Conference paper

5) **S.M.Ferdous**, Farhad Shahnia and GM Shafiullah, "Various Structures and Control Strategies for Provisional Energy Transaction Management in Coupled Microgrid Clusters" 2020 Intermountain Engineering, Technology and Computing (IETC), 2020, pp. 1-6, Orem, UT, USA.
[Chapter-3 (Art – 3.2.1, 3.2.2, 3.2.3), Chapter-4 (Art – 4.2.1, 4.2.2, 4.2.3)].

6) **S.M.Ferdous**, Farhad Shahnia and GM Shafiullah, "Provisional Energy Transaction Management amongst Neighbouring Microgrids through a DC Power Exchange Link," 9th International Conference on Power and Energy Systems (ICPES), pp.1-6, Perth, Australia, Dec 2019.
[Chapter-3 (Art – 3.2.3), Chapter-4 (Art –4.2.3)].

7) **S.M.Ferdous**, Farhad Shahnia and GM Shafiullah "Realizing a System of Coupled Microgrids using a Single-phase AC Power Exchange Link," 9th International Conference on Power and Energy Systems (ICPES), pp.1-6, Perth, Australia, Dec 2019.
[Chapter-3 (Art – 3.2.2), Chapter-4 (Art – 4.2.2)].

8) **S.M.Ferdous**, Farhad Shahnia, and GM Shafiullah, "Power Sharing and Control Strategy for Microgrid Clusters," 9th International Conference on Power and Energy Systems (ICPES), pp.1-6, Perth, Australia, Dec 2019.
[Chapter-3 (Art – 3.2.1), Chapter-4 (Art – 4.2.1)].

Book Chapter

9) **S.M.Ferdous**, Farhad Shahnia, GM Shafiullah, "Interconnected Microgrid Clusters through Various Provisional Power Exchange Links," in *Primary control level of parallel distributed energy resources*, In-press, Wiley-IEEE Press, 2021.
[Chapter-3 (Art – 3.2.2, 3.2.3, 3.2.4), Chapter-4 (Art – 4.2.2, 4.2.3, 4.2.4), Chapter-5, Chapter-6].